Reachability Analysis of Cyber-Physical Systems using Symbolic-Numeric Techniques

by

Aditya Krishna Zutshi

B.E., Manipal University, 2007

M.S., University Colorado, 2011

A thesis submitted to the

Faculty of the Graduate School of the

University of Colorado in partial fulfillment

of the requirements for the degree of

Doctor of Philosophy

Department of Electrical, Computer, and Energy Engineering

2016

This thesis entitled:
Reachability Analysis of Cyber-Physical Systems using Symbolic-Numeric Techniques
written by Aditya Krishna Zutshi
has been approved for the Department of Electrical, Computer, and Energy Engineering

_____
Prof. Sriram Sankaranarayanan

_____
Prof. Fabio Somenzi

_____
Prof. Bor-Yuh Evan Chang

_____
Dr. Jyotirmoy V. Deshmukh

_____
Dr. James Kapinski

Date _____

The final copy of this thesis has been examined by the signatories, and we find that both the content and the form meet acceptable presentation standards of scholarly work in the above mentioned discipline.

Zutshi, Aditya Krishna (Ph.D., Electrical Engineering)

Reachability Analysis of Cyber-Physical Systems using Symbolic-Numeric Techniques

Thesis directed by Prof. Sriram Sankaranarayanan

In this thesis, we address the problem of reachability analysis in cyber-physical systems. These are systems engineered by interfacing computational components with the physical world. They provide partially or fully automated safety-critical services in the form of medical devices, autonomous vehicles, avionics and power systems.

We propose techniques to reason about the reachability of such systems, and provide methods for falsifying their safety properties. We model the cyber component as a software program and the physical component as a hybrid dynamical system. Unlike model based analysis, which uses either a purely symbolic or a numerical approach, we argue in favor of using a combination of the two. We justify this by noting that the software program running on a computer is completely specified and has precise semantics. In contrast, the model of the physical system is only an approximation. Hence, we treat the former as a white box, but treat the latter as a black box.

Using symbolic methods for the cyber components and numerical methods for hybrid systems, we carefully capture the complex behaviors of software programs and circumvent the difficulty in analyzing complex models developed through first principles. To combine the two techniques, we use a Counterexample Guided Abstraction Refinement (CEGAR) framework. Furthermore, we explore learning techniques like regression and piecewise affine modeling to estimate and represent black box hybrid dynamical systems for the purpose of falsification.

We use prototype implementations to demonstrate the effectiveness of presented ideas. Using non-trivial benchmarks, we compare their performance against the state of the art. We also comment on their applicability and discuss ideas for further improvement.

Dedication

To my parents, for their sacrifices, love and encouragement.

To the loving memory of my grandfather.

Acknowledgements

First and foremost, I would like to thank my advisor, Prof. Sriram Sankaranarayanan, without whose encouragement, guidance and support, this thesis would have never taken shape and reached completion. His broad knowledge and the ability to draw connections between seemingly unrelated concepts has been a constant source of inspiration.

I would like to thank the committee members for their valuable feedback and their mentorship which has helped shape not only this thesis, but me as a person. Thanks to Prof. Fabio Somenzi, for introducing me to 'formal methods' through his teachings and for always being available for discussions. Thanks to Prof. Evan Chang for making the CUPLV lab a fun place to work at. I am grateful to Dr. Jyotirmoy Deshmukh for encouraging me to be creative, and Dr. James Kapinski for balancing it and keeping me grounded with real-life examples.

During my first semester, Prof. Aaron Bradley agreed to mentor me and put me on a path to research. I fondly remember his course 'Thinking Concurrently', which I enjoyed like none other. I am indebted to him for his guidance. I am grateful to Dr. Ashish Tiwari for guiding my research career in the very beginning, and for being unreasonably patient at answering my numerous questions.

I would like to thank all past and present members of the CUPLV lab for being amazing friends. Especially, Dr. Aleksandar Chakarov, Dr. Amin Ben Sassi and Yi-Fan Tsai for long discussions and constant support. Thanks to Prof. Ashutosh Trivedi for impromptu discussions and quick feedbacks on my research. I would like to thank Dr. Xin Chen, Hadi Ravanbaksh, Dr. Sergio Mover, Dr. Vris Cheung for interesting discussions over the years.

I am grateful to Prof. Indranil Saha, who has been like an elder brother, providing much needed advice.

I also thank Dr. Nikos Arechiga, Dr. Xioaqing Jin for their friendship and valuable feedback.

Thanks to Dr. Vivek Tiwari, Dr. Rohan Singh and Aditya Bhave for making my years at Boulder memorable.

Thanks to my wife Vidhya, for supporting me through toughest of the times, my parents for their constant love and encouragement, and my brother for providing much needed humor in life.

I am indebted to the ECEE Graduate Program Advisor, Adam Sadoff for answering my countless queries and guiding me effortlessly throughout the years.

I want to mention many others who have influenced this thesis. Discussions with Dr. Bertrand Jeannet, Dr. Peter Schrammel, Prof. Stefan Ratschan, Jan Kuřátko, Prof. Paulo Tabuada, Dr. Hisahiro Ito, Dr. Koichi Ueda, Dr. Ken Butts and Dr. Tomoyuki Kaga have brought in varied perspectives to my research.

Finally, I gratefully acknowledge the support by the US National Science Foundation (NSF) under the award numbers CNS-0953941, CNS-1016994, CPS-1035845 and CNS-1319457 and Toyota Engineering and Manufacturing North America (TEMA).

Contents

Chapter

Tables

Table

Figures

Figure

Chapter 1

Introduction

Digital computers are an essential part of complex engineered systems. In line with Moore's law, computing devices are becoming exponentially smaller, more powerful and cheaper. Their power requirement has also been decreasing. This has not only enabled the design of highly complex digital systems which can successfully carry out increasingly difficult tasks, but also has resulted in the devices pervading our daily lives. Currently, these devices do not perform safety critical functions for the most part, but this is changing as automation is becoming more common for our everyday activities, such as driving and performing complex tasks, in general. As they get smaller they will become part of our daily lives; in the form of implantable medical devices such as pacemakers, artificial pancreas, autonomous cars, smart devices and appliances.

The design of complex systems is prone to errors, and in the domain of safety critical devices, automation surprises can lead to loss of life. The need for their correctness and safety analysis is paramount. In the past, certification of safety was restricted to industrial systems such as large medical machines, cars and infrastructure (railways, aircraft systems, power plants) for which there are established safety regulations and rigorous test procedures. However, the increasing automation has revealed a pressing need for automated analyses. Unfortunately, determining algorithmically all possible behaviors of even simple systems is a hard problem. Manually proving their properties is very resource intensive, if at all feasible.

In this thesis we provide algorithmic techniques to automatically analyze the safety of critical devices capable of making decisions. We define safety by partitioning the state-space of the system into safe and unsafe states. A system is safe if at all times its operation parameters are within a safe (reasonable) range. We propose automatic techniques to analyze the systems for undesirable behaviors. The approaches are more

scalable than the current state of the art and are aimed towards finding functional errors. We conclude by presenting results on their effectiveness and future directions.

1.1 Motivation

In this thesis we are interested in continuous-time dynamical systems that interact with digital systems. These commonly occur in the domain of embedded systems. A digital controller in the form of a software program running on a micro-controller constantly monitors and manipulates a continuous system to ensure stability and performance. Such systems with continuous-time and discrete-time interactions are classified under the domain of hybrid systems. Certain phenomena in the physical world also have a similar flavor when a dynamical system is governed by both continuous and discrete evolution rules. The former is usually modeled by a set of differential equations and the latter using instantaneous actions often called 'impulses' or 'resets'. A classic example is that of a ball thrown from a height which falls under the laws of gravity but also bounces off the ground. The bounce can be modeled as a discrete jump where the velocity v of the ball is instantaneously reset as $v' := -Cv$. These simple systems can exhibit very complex behaviors. Embedded control systems can be modeled similarly, but they have highly complex software representing a 'reset'. These systems also come under the umbrella term of cyber-physical systems (CPS) [1] .

1.2 Safety Properties

The notion of safety properties for hybrid systems is defined over its states. Each state is either labeled as safe or unsafe. The evolution begins with the initial states of the system which must be safe. The safety property captures the following assertion: beginning from a safe state, the system can never reach the unsafe set of states. Thus, the property is violated by an evolution of the system, which begins from an initial state and reaches the unsafe states. A **time bounded** safety property requires the violation to happen within a specified time bound. This is closely tied to the question of general reachability, which tries to find all reachable behaviors of a system.

[1] CPS are not restricted to embedded control systems working in isolation, and a full fledged CPS can also involve a sensor network, distributed computations, network models.

1.3 Current State of the Art

The research in formal methods has resulted in multiple techniques that can guarantee the safety of systems by finding all system behaviors. As an exhaustive enumeration of exact behaviors is not possible, the techniques are divided into two classes. The first, termed as **verification** techniques, assumes the absence of unsafe behaviors and uses over-approximate relaxations to bound all possible behaviors. An exhaustive list of verification techniques is hard to compile, but a few of them are surveyed in [4, 115]. However, there are certain limitations that prevent their deployment and assimilation in industrial practices. They require a precise model of the system, which is seldom available for complex systems. Moreover, the results are valid only on the model and not easily transferable to the underlying system [145]. Apart from theoretical limitations, the methods often suffer from practical limitations preventing them from scaling to large industrial applications.

The other kind of formal approaches are called **falsification** approaches. They assume that a violation of safety exists and try to find it. They often use under-approximations to guide their search [92]. There also exists falsification techniques which do not provide soundness and completeness guarantees, and only provide weak probabilistic completeness. This is the case with techniques based on random exploration; as the exploration progresses, the probability of finding an existing falsification asymptotically converges to 1. These include **sampling based** search using modified motion planning algorithms [23, 25, 41, 53, 94, 134]. Others, use global stochastic optimization methodologies to guide the search for violations using numerical simulations. This is a very general approach which can accommodate black box systems and work with MTL properties [1, 10]. A combination of such techniques with RRT style search has also been explored in [49].

We cover the related work more comprehensively in Chapter 2. We now describe the models for our system under test.

1.4 System Models

We are primarily interested in analyzing embedded control systems modeled as Sampled Data Control Systems (SDCS). An SDCS consists of a controller and a plant which interact at a fixed sampling rate. We

model the controller as a software program, so as to precisely reason about its behaviors. The plant however, is an approximate model, and we use numerical methods for its exploration. We combine the symbolic and the numerical approaches to reason about their composition, an SDCS.

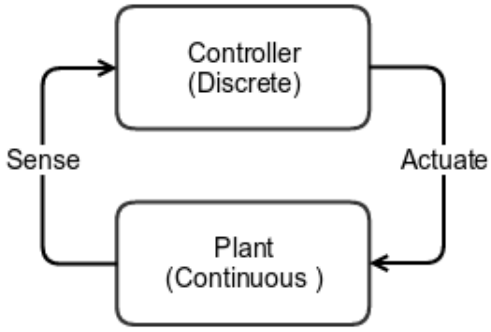

Figure 1.1: Sampled Data Control Systems

1.4.1 Sampled Data Control Systems (SDCS)

An SDCS is a closed loop feedback configuration of a given controller and a plant. The discrete controller periodically 'senses' and 'actuates' the plant in order to maintain certain objectives. Such systems are quite common in the domain of embedded control. Relevant examples include airplane systems featuring fly by wire technology, modern cars with a high degree of controls automation, power plants, intelligent medical devices and of course, robots. Such systems can have additional complexity due to being networked, which leads to the incorporation of highly sophisticated network communication algorithms.

An analysis of such a system must take into account both the controller and the plant together. An isolated study of the controller and the plant, often, has limitations. However, several researchers have explored compositional reasoning in the form of formal assumptions and guarantees [83, 84, 130].

Let us take an example of an SDCS, a digital thermostat controlling the room heater. To maintain the room temperature, the thermostat periodically checks the room temperature and decides to turn on/off the heater. To analyze the behavior of the system, one cannot look at the heater or the thermostat in isolation. Furthermore, to understand the system's non-trivial properties, their mutual interaction mandates their study together, along with the sampling period. Moreover, the thermostat can be a complex piece of software,

connected to the Internet with a rich set of features.

The controllers are decision making logical systems. The plants usually represent physical systems, and are modeled by differential equations. Such models use both abstractions and approximations. For example, representing the thermostat with a finite automaton hides software specific errors, like buffer overflows, out of bounds memory access, and floating point errors. Fortunately, the controller is often completely specified in the form of its implementation (software code). Its semantics are well understood. On the other hand, the plant model is often an approximation of the underlying physical phenomenon. Moreover, the plants modeled from first principles are complex enough to make symbolic analysis prohibitively expensive. We address these issues by (a) introducing numerical techniques for exploring plant behaviors, and (b) using symbolic techniques to explore the controller's behaviors. In the following sections we introduce the models of the plant and the controller.

1.4.2 Plant as a Hybrid System

The class of hybrid systems includes systems that exhibit both continuous dynamics and discrete switching events. Such systems are quite common in the physical world, ranging from the apparently simple bouncing ball to the complex physical systems being controlled by sophisticated software systems. Discrete behaviors in continuous systems can arise due to impacts (collisions) or switching (relays) and hysteresis (memory). Traditionally the field of hybrid systems provides tools like hybrid automata [79] which can, in theory, model embedded control systems. We however, make a distinction and only model the plants using hybrid automata due to practical considerations.

Analysis of hybrid systems is difficult, primarily due to the complex behaviors resulting from the interaction between the continuous and the discrete. Even though mature analysis techniques exist for both discrete transition and continuous dynamical systems, hybrid systems resist a direct approach by such techniques alone. Even low dimensional systems with a few discrete switches can prevent efficient analysis. For example, let us take a simple system of a bouncing ball. The switching in the system arises from the ball hitting the floor. To analyze the behavior of the system, one cannot isolate the continuous dynamics from switchings. To explore the system's non-trivial properties, both classes of behaviors need to be studied

together. This is similar to the case of SDCS as discussed above.

It is required that we highlight an often ignored fact; current formal methods work on mathematical models, and their results are valid only on them. This inherently requires the models of the plants to be very precise. This is problematic due to (a) the difficulty in completely specifying complex dynamical systems, inadvertently leading to unmodeled dynamics and (b) the fact that formal analysis of complex dynamical systems is as yet an unsolved problem.

To tackle both (a) and (b), verification techniques conservatively abstract away details (example, non-determinism). This addresses (a) by capturing unmodeled/uncertain dynamics and (b) by simplifying complex dynamics. As verification tries to certify properties against worst case scenarios, this can often be too conservative. It can insert 'bad behaviors' in the system, thereby rendering it 'unsafe'. In this thesis, we take a different approach. We use numerical falsification techniques to efficiently explore the plant's behaviors with respect to the safety property.

1.4.3 Controller as a Computer Program

We assume the controller to be a program, with clearly defined semantics. With this assumption we justify the usage of symbolic execution [96] to precisely reason about its possible behaviors. We model the program as a control flow graph which is a structural representation of a program capturing all execution paths. We explore its behaviors with respect to each possible execution or path in the graph. This is very useful in practice as we can characterize the coverage quantitatively even when exhaustive coverage fails.

Although not the primary focus of the thesis, such a model also captures common software centric errors such as buffer overflows, out of bound array access and division by zero. Hence, this provides a way to combine our techniques with other software analyses.

1.5 Contributions

The main contributions of this thesis are summarized below.

Exploration techniques based on trajectory segments. We borrow the notion of **multiple shooting** from

the numerical analysis community and use it for falsification. This is similar to the idea of trajectory optimization [24] used in applied optimal controls. We then extend it to implicit abstractions which can be used to efficiently search the state-space of black box system for safety violations.

Symbolic Numerical techniques for falsification of SDCS. We note the distinction between the two different components of SDCS in the form of controller and plant and propose separate analyses for them. We then combine them into a monolithic falsification approach.

Implementation of the tool S3CAM-X. Finally, we implement the above techniques in the tool S3CAM-X which takes in the controller code, the plant description in the form of a numerical simulator and the safety property as a set of unsafe states and returns a trace that violates it. The tool is written in Python and is a prototype demonstrating the effectiveness of the ideas.

Our contributed approaches are designed with scalability and applicability in mind. They use black box plant descriptions and controller code, both readily available. They are light weight, best effort and try to produce results when expensive guaranteed approaches fail.

1.6 Thesis Organization

Chapter 1: [Introduction**]** (this chapter) introduces and motivates the problem and summarizes the contributions of the thesis.

Chapter 2: [Background: System Models and Safety**]** introduces the basic concepts needed to understand this thesis. It also includes a section summarizing the current state of research into the problem of formal verification and falsification of hybrid systems.

Chapter 3: [Segmented Trajectories - A Behavioral Perspective**]** presents the notion of *trajectory segments* to search the state-space of a dynamical system specified as a black box.

Chapter 4: [Implicit Discrete Abstraction of Black Box Dynamical Systems**]** presents discrete abstractions for black box systems appropriate for falsification.

Chapter 5: [Analysis of Sampled Data Control Systems**]** discusses the usage of symbolic execution

in finding behaviors of the control program. This chapter combines the plant analysis (using abstractions) and the symbolic analysis of the controller order to provide a monolithic falsification approach.

Chapter 6: [The Falsification Tool: S3CAM**]** This chapter details the implementation and experimental evaluation of the presented ideas.

Chapter 7: [Relational Modeling for Falsification**]** for black box systems and how it can improve the falsification search.

Chapter 8: [Conclusions**]** Summary and concluding remarks.

1.7 Publications

We include our publications [164] in Chapter 3 and [165] in Chapter 4 and [163] in Chapter 5. The last chapter Chapter 6 includes the results and case studies from the aforementioned publications. The implementation and tools can be found online on GitHub [2] . A work which was referred but not discussed in detail is [166].

[2] `https://github.com/zutshi/`

Chapter 2

Background: System Models and Safety

In this chapter we include the background necessary to understand the rest of the thesis.

2.1 Notation

Let $\mathbb{R}$ denote the set of real numbers. We use $\mathbf{a}, \ldots, \mathbf{z}$ to denote column vectors and $A, \ldots, Z$ to denote matrices. $||\mathbf{x}||_p$ denotes the p-norm of the vector $\mathbf{x}$, and if specified without p, is the Euclidean norm $||\mathbf{x}||_2$. We use norms to quantify the length of vectors, which signify distances in space. A p-norm is also a metric.

Definition 2.1.1 (Metric) For $\mathbf{x}, \mathbf{y} \in \mathbb{R}$, a function $d(\mathbf{x}, \mathbf{y})$ is a metric iff the below conditions are satisfied.

- $d(\mathbf{x}, \mathbf{y}) \geq 0$ (non-negative)
- $d(\mathbf{x}, \mathbf{y}) = 0 \iff \mathbf{x} = \mathbf{y}$ (0 only when $\mathbf{x}$ and $\mathbf{y}$ are the same)
- $d(\mathbf{x}, \mathbf{y}) = d(\mathbf{y}, \mathbf{x})$ (symmetrical)
- $d(\mathbf{x}, \mathbf{z}) \leq d(\mathbf{x}, \mathbf{y}) + d(\mathbf{y}, \mathbf{z})$ (triangle inequality)

2.2 Dynamical Systems

Dynamical systems are mathematical abstractions for capturing evolving phenomenon. They define the rules for the evolution of **states**. The set of states the system can be in, describes the **state-space**, which is typically a manifold in $\mathbb{R}^n$. The state of the system is akin to 'memory' of the past inputs. A dynamical system

can have inputs and outputs, in which case it defines the dependence of its output on its states and inputs. The input models the system's interaction with its environment, and the output represents its observable behavior.

The systems evolving with respect to time are synchronous in nature. They are called continuous-time, if the time varies continuously (and is defined over the reals) or, discrete-time dynamical systems if the time can only take discrete values (and is defined over integers). If their evolution is triggered by **events**, they are called discrete event dynamical systems. We are primarily interested in the combination of continuous-time and discrete event systems: hybrid systems [114].

A gentle introduction to hybrid systems and their analysis can be found in the notes by Branicky [26] and Lygeros [112]. The book by Van der Schaft and Schumacher [158], provides an excellent introduction to hybrid dynamical systems with several academic examples and a detailed overview of early analysis techniques for their verification and control. More recent books [5, 108, 111] discuss modern advances in the control and verification of hybrid systems.

2.2.1 Continuous-time Dynamical Systems

Continuous-time dynamical systems are modeled using differential equations. When the time t can take all values on the real line $t \in \mathbb{R}$, the systems can be modeled using a set of ordinary differential equations (ODEs).

Definition 2.2.1 (Ordinary Differential Equations) A system of ordinary differential equations (ODEs) over states $\mathbf{x} \in X$ on the manifold X is denoted $\dot{\mathbf{x}} = f(\mathbf{x}, t)$, where $f : X \times \mathbb{R} \to \mathbb{R}^n$ is known as a vector field over X. If f is a Lipschitz continuous function then for all $\mathbf{x}_0 \in X$ and time $t \geq 0$, there exists a unique solution $\tau(t)$ such that $\tau(0) = \mathbf{x}_0$ and for all time $t \geq 0$, $\dot{\tau}(t) = f(\tau(t))$.

The vector $f(\mathbf{x}, t)$ represents the **velocity** of $\mathbf{x}$, in other words, the direction and the rate of change of $\mathbf{x}$. Vector fields can be used to visualize the behavior of the continuous systems defined by a set of ordinary differential equations (ODEs). This is achieved by plotting the arrows representing the magnitude and direction of $f(\mathbf{x}, t)$ on a grid of points in the phase space X.

In the rest of the presentation we only consider time invariant systems, where there is no explicit dependence on time. f only depends on $\mathbf{x}$, and will be denoted by $f(\mathbf{x})$ in the rest of the thesis. However, the discussion can be easily extended to time variant systems by introducing time as another state. We now discuss the solution of ODEs.

2.2.1.1 Flows and Trajectories

The behavior of a continuous-time system can also be understood in terms of flows. A flow is a time parameterized differential mapping from a state in the manifold to another state in the manifold, thus defining the evolution rule.

Definition 2.2.2 (Flow) A complete flow $\varphi_t(\mathbf{x})$ of a continuous system defined in $X \subseteq \mathbb{R}$ is a differentiable mapping $\varphi : \mathbb{R} \times X \mapsto X$ such that

- $\varphi_0(\mathbf{x}) = \mathbf{x}$
- $\forall t, \forall s \in \mathbb{R}.\ \ \varphi_t \circ \varphi_s = \varphi_{t+s}$ (Group Property)

The first property presents the identity function φ_0; the case where no time elapses. The second property is known as the group property which implies that under the operation of composition, φ_t is an additive group. Moreover, by substituting $s = -t$, we get $\varphi_{-t} \circ \varphi_t = \varphi_0$. Hence, φ_t is always invertible with its inverse $(\varphi_t)^{-1} = \varphi_{-t}$.

From the above definition, we note that $\varphi_t(\mathbf{x})$ can define the evolution of dynamical systems. As $\varphi_t(\mathbf{x})$ is a differentiable mapping, we can associate it to a time invariant vector field.

$$f(\mathbf{x}) = \frac{d}{dt}\varphi_t(\mathbf{x})$$

Then, the flow describes a family of solutions of the ODE $\dot{x} = f(\mathbf{x})$ as a function of $\mathbf{x}$. If $\mathbf{x}$ is fixed to an initial state $\mathbf{x}_0$, then $\varphi_t(\mathbf{x}_0)$ defines a curve in X as a function of time t. This is also known as the trajectory of the system. Such a solution of the ODEs from a fixed initial state $\mathbf{x}_0$ is often computed in practice to solve the initial value problem (IVP). The group property also implies that two trajectories must not intersect.

Definition 2.2.3 (Time Trajectory) Given the flow of the system φ_t, we define the time trajectory of length $T \geq 0$ beginning from state $\mathbf{x}_0$ as the set $\{\varphi_t(\mathbf{x}_0) \mid 0 \leq t < T\}$. We denote this by $\varphi_{[0,T)}(\mathbf{x}_0)$.

The ODEs are linear when $f(\mathbf{x})$ is a linear map on $\mathbf{x}$, expressed using a matrix A and a constant bias vector $\mathbf{b}$.

$$\dot{x} = f(\mathbf{x}) = Ax + \mathbf{b}$$

Their solution can be expressed using the matrix exponential e^{tA} as

$$\varphi_t(\mathbf{x}) = e^{tA}\mathbf{x} + A^{-1}(I - e^{tA})\mathbf{b}$$

Linear ODEs have been studied extensively in the field of classical dynamical systems and there exist a multitude of analytical methods for reasoning about their various properties. On the other hand, there do not exist direct methods for analysis of general non-linear systems. Instead, the theory of linear systems can be used to locally assess their behavior by the process of **linearization**.

Non-linear ODEs, in general, need not have a closed form solution. In most cases, a computer algorithm can numerically solve (simulate) the system, thereby generating a finite number of trajectories. These can be used to observe the approximation of its behavior. It must be noted that simulation algorithms use some form of discretization, thus involving finite sampling and quantization of states and time. The numerical solution includes the dynamics of the simulation algorithm which can non-trivially affect the precision. In this thesis, we assume the availability

2.2.2 Discrete Event Systems

Discrete event systems are used to model discrete systems like decision making logical processes. We model them using discrete transition systems, a popular model in computer science for modeling software systems [1] . As an aside, they provide a behavioral modeling formalism, unlike finite automata, which are a structural modeling formalism.

A transition system defines the transitions between states of the system. The states can either take continuous or discrete values and evolve as specified by the transition rules. These rules can incorporate

[1] Another popular modeling formalism is petri nets [124, 133].

non-deterministic behavior in order to model uncertain systems. Transition systems are well studied [119] and mature tools exist for their analysis of reachability and termination.

Definition 2.2.4 (Discrete Transition System) is a tuple $\langle L, \mathcal{V}, \mathcal{T}, l_0, \Theta \rangle$ wherein, L is a finite set of **discrete locations**, $\mathcal{V} : (v_1, \ldots, v_n)$ is a set of variables, $\mathcal{T}$ is a set of discrete transitions, $l_0 \in L$ is the initial location, and $\Theta[\mathcal{V}]$ is an assertion capturing the initial values for $\mathcal{V}$. Each transition $\tau \in \mathcal{T}$ is of the form $\langle l, l', \rho_\tau \rangle$, wherein l is the pre-state of the transition and l' is the post-state. The relation $\rho_\tau[v, v'] \subseteq v \times v$, represents the transition relation over current state variables v and next state variables v'.

2.2.3 Hybrid Dynamical Systems

Essentially, we are interested in systems that evolve using a combination of continuous-time dynamics and discrete transitions. We model them using Hybrid Automata which was proposed by Henzinger [79]. Several other models also exist in literature, namely, impulsive differential equations or inclusions, switching systems and the set valued maps proposed in [73].

2.2.3.1 Hybrid Automata

Hybrid automata can be informally described as a finite state automata with each location augmented with differential equations and invariants. We use an extended version with inputs and provide a brief description of its syntax and semantics. More details on this model are available in [79].

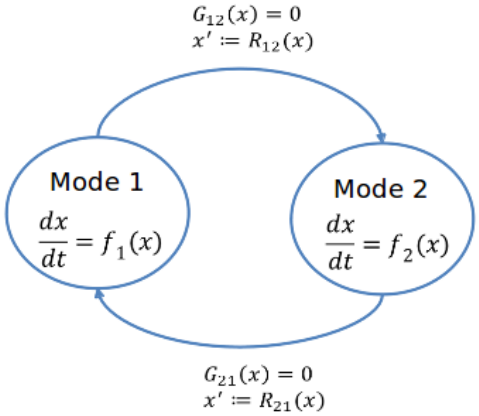

Figure 2.1: Hybrid Automata

Definition 2.2.5 (Extended Hybrid Automata) An extended hybrid automata is completely specified by the tuple $\mathcal{A} : \langle X, \mathcal{U}, \mathcal{Q}, \mathcal{F}, \mathcal{I}, \mathcal{G}, \mathcal{R}, \mathcal{T}, X_0, q_0 \rangle$, wherein,

- $X \subseteq \mathbb{R}^n$ is the n-dimensional continuous state-space, with X_0 being the initial set of states.
- $\mathcal{U} \subseteq \mathbb{R}^m$ denotes the m-dimensional input space.
- $\mathcal{Q}$ is a finite set of discrete modes and $q_0 \in \mathcal{Q}$ is the initial mode.
- $\mathcal{F}$ maps each discrete mode $q \in \mathcal{Q}$ to an ODE $\dot{\mathbf{x}} = F_q(\mathbf{x}, \mathbf{u})$, where $\mathbf{x} \in X$ and $\mathbf{u} \in \mathcal{U}$.
- $\mathcal{I}$ maps each discrete mode $q \in \mathcal{Q}$ to a mode invariant $\mathcal{I}(q) \subseteq \mathbb{R}^n$.
- $\mathcal{G}$ is a set of predicates over X.
- $\mathcal{R}$ is a set of relations mapping X to X.
- $\mathcal{T} \subseteq \mathcal{Q} \times \mathcal{G} \times \mathcal{R} \times \mathcal{Q}$, is a finite set of transitions. A transition $\delta : (q, g_\delta, r_\delta, q') \in \mathcal{T}$, takes the system from mode q to q', when the **guard predicate** $g_\delta \in \mathcal{G}$ is satisfied. Upon taking the jump, the continuous variables are reset according to the **reset map**, $r_\delta \in \mathcal{R}$. The transition relation for δ is defined as $\rho_\delta(\mathbf{x}, \mathbf{x}') : \ g_\delta(\mathbf{x}) \ \wedge \ r_\delta(\mathbf{x}, \mathbf{x}')$.
- The set of hybrid states is denoted by $\mathcal{X} \subseteq \mathcal{Q} \times X \times \mathcal{U}$.

Linear/Affine Hybrid Automaton (LHA) LHA [79] are a subset of hybrid automata which have only linear continuous dynamics, and all constraints and mappings are expressible as linear expressions.

Definition 2.2.6 (Affine Hybrid Automata) A hybrid automata is **affine** iff (a) for each discrete mode q, the dynamics are of the form $\dot{\mathbf{x}} = A_q\mathbf{x} + B_q\mathbf{u} + \mathbf{b}_q$, (b) the predicate over the initial condition X_0 and guard predicates g_δ for each transition $\delta \in \mathcal{T}$, are linear arithmetic formulae, and (c) the reset maps r_δ are affine.

Understanding the semantics. A state of the hybrid automaton is a tuple $(q, \mathbf{x}, \mathbf{u}) \in \mathcal{X}$ wherein $\mathbf{x} \in \mathcal{I}(q)$. The input is set at the beginning of the sampling period τ_s and is held constant throughout the period. Between two sampling instants, the state evolves over time by interleaving two actions: **continuous flows** and **jumps**.

- A **continuous flow** from $(q, \mathbf{x}, \mathbf{u})$ to $(q, \mathbf{x}', \mathbf{u})$ in time $t \geq 0$, denoted by $\varphi^q_{[0,t)} : (q, \mathbf{x}, \mathbf{u}) \rightsquigarrow_t (q, \mathbf{x}', \mathbf{u})$, wherein $\forall\ s \in [0, t)$. $\varphi^q_s \in \mathcal{I}(q)$.

- A **jump** from $(q, \mathbf{x}, \mathbf{u})$ to $(q', \mathbf{x}', \mathbf{u}')$ is due to a discrete transition $\delta : (q, g_\delta, r_\delta, q') \in \Delta$, denoted $(q, \mathbf{x}) \xrightarrow{\delta} (q', \mathbf{x}')$. The jump is taken when (a) $\mathbf{x}$ satisfies g_δ, (b) $\mathbf{x}' = r_\delta(\mathbf{x})$ and (c) $\mathbf{x}'$ satisfies $\mathcal{I}(q')$. Jumps are considered instantaneous, i.e, no time is assumed to elapse during a jump.

For a given hybrid automata $\mathcal{A}$, we can define a relation $\mathcal{H}^{\mathcal{A}}_t$, which is the counterpart of the flow φ_t in the continuous domain. It is a relation that maps a hybrid state $\mathcal{X}$ to a set of $\mathcal{X}$ reachable in some time t through a combination of continuous flows and jumps. Unlike φ_t, which gives a unique solution, $\mathcal{H}^{\mathcal{A}}_t$ need not be unique due to non-determinism in a hybrid automaton.

Definition 2.2.7 (Hybrid Trajectory) A trajectory of the hybrid automaton is an infinite sequence of continuous trajectories alternating with jumps

$$\mathcal{H}^{\mathcal{A}}_t : \varphi^{q_1}_{[t_0,t_1)}(\mathbf{x}_0) \xrightarrow{\delta_1} \varphi^{q_2}_{[t_1,t_2)}(\mathbf{x}_1) \xrightarrow{\delta_2} \dots$$

such that the conditions for **continuous flows** and **jumps** are satisfied.

Time Bounded Trajectories . A trajectory of a hybrid automata beginning from an initial state $(q_0, \mathbf{x}_0, \mathbf{u}) \in \mathcal{X}_0$ can be expressed as $\{\mathcal{X}' | \mathcal{H}^{\mathcal{A}}_t(\mathcal{X}_0, \mathcal{X}')\}$. A time bounded finite trajectory of time length T is the same but with an added restriction on t, $\{\mathcal{X}' | t \in [0, T] \wedge \mathcal{H}^{\mathcal{A}}_t(\mathcal{X}_0, \mathcal{X}')\}$.

Non-determinism. Apart from a mix of continuous and discrete dynamics, inputs, and time dependant dynamics, hybrid automata inherently have non-deterministic switching. This is due to the 'may' semantics of a transition. When a guard is satisfied, the system may take the transition, but it is not forced to do so. This gives rise to multiple branching behaviors where one branch continues evolving according to the continuous evolution while the other takes the enabled transition. It should be noted that non-deterministic switching can also be modeled by a non-deterministic input signal. Additionally, non-determinism can be removed by (a) designing all the invariants and guards to have zero measure intersections, or (b) by using urgent transitions [80].

2.3 Sampled Data Control System (SDCS)

SDCS are feedback control systems, with a discrete controller that periodically senses the state of a continuous physical plant, and actuates it by computing and setting its control inputs (commands). The three important elements in this systems are the plant, the controller and the sampling period, and all three equally affect the SDCS' safety, stability and performance. The control design is classically done assuming a continuous-time interaction with the plant, and the sampling period is heuristically decided a posteriori. The choice of sampling period is as crucial as control design; a small sampling time can place infeasible constraints on the scheduling policy, whereas large sampling times can cause instabilities or safety violations and deteriorate performance.

The controller is usually implemented as a software program, and has known and precise semantics. We model it as an infinite state transition system program for program analysis like symbolic execution. The plant, being a physical dynamical system, can either be modeled as a white box using hybrid automata, or, as a black box.

At each sampling period, the controller senses the state of the plant and performs controller actions that may include (a) setting control input signals for the plant, and (b) 'commanding' the plant to execute a controlled discrete transition, resulting in an instantaneous jump and a mode change in the plant. We group both (a) and (b) as control inputs.

Definition 2.3.1 (Sampled Data Control System (SDCS)) An (SDCS) consists of two components, as illustrated in Figure 5.4. (a) A plant model P described by two functions SIM and g as in Definition 5.5.1, and (b) a controller implementation C described by a program whose semantics are described by a function ρ as in Definition 5.5.2. Finally, the closed-loop parallel composition assumes that the function SIM is always called with $\tau = \tau_s$, i.e., the controller sampling period.

In practice, sampled data control systems include A/D (analog-to-digital) and D/A converters for interfacing between the analog plant and the digital controller. Errors are often introduced due to the presence of measurement noise and the quantization of the A/D and D/A converters. Though we omit exogenous

disturbances for the sake of simplicity of presentation, our implementation allows for bounded controller disturbances, and searches over the disturbance-space during the falsification process.

Throughout our work, we ignore the time taken by the controller to execute and assume its computation to be instantaneous. This is justified as sampling periods are usually much larger than the execution time of the controller. If necessary, the assumption can be done away with, by introducing a fixed time for the controller's execution. For symbolic approaches, this can usually be relaxed to a bounded interval.

2.4 Black Box Models

The last section described the models used for white box modeling of dynamical systems. In practice, a completely specified and well defined model is often unavailable. Instead, black box behavioral models are popularly used to **numerically simulate** the behaviors of the systems. We might also choose to ignore the white box model when available, relying only on the simulator to avoid the complexity of the model.

2.4.1 Plant Behavioral Model

We now present the assumptions and restrictions when modeling black box dynamical system. We assume the underlying system S to be a deterministic hybrid system driven by external inputs $\mathbf{u}$. The system definition is supplied as an opaque function which computes the state transformations under the interface

$$\mathbf{x}' = \text{SIM}_S(\mathbf{x}, \mathbf{u}, t).$$

SIM takes in a system state $\mathbf{x}$ at time s and returns the system's next state at time $s + t$, where t is some selected time step. From the function signature, one can infer the implicit requirement of complete state visibility. We drop the subscript S whenever the system under consideration is non-ambiguous. The definition of SIM can be easily augmented to return outputs if necessary.

We now present our assumptions on the under lying system. As the case with ODEs, we assume existence and uniqueness of trajectories over a finite time horizon $[0, T]$. This can be guaranteed by Lipschitz continuity of the vector field in each hybrid mode and ruling away issues such as finite escape times [120]. In practice, these assumptions do not pose significant restrictions for the type of problems that we wish to

address. We assume full observability of the system state and assume the simulator to be the 'absolute truth', ignoring any numerical errors.

Let $\mathcal{X} \subseteq \mathcal{Q} \times \mathbb{R}^n$ be the (infinite) set of hybrid states of given system S, and $\mathcal{U}$ be the set of input signals to S of the form $[0, T] \to \mathbb{R}^k$ for some given time horizon T. The behavior of the system can then be summarized by a family of relations $\overset{t,u}{\rightsquigarrow} \subseteq \mathcal{X} \times \mathcal{X}$, parameterized by time $t \geq 0$ and input signal $u \in \mathcal{U}$ defined over time $[0, T]$. We use the notation $\mathbf{x} \overset{t,u}{\rightsquigarrow} \mathbf{x}'$ to denote $(\mathbf{x}, \mathbf{x}') \in \overset{t,u}{\rightsquigarrow}$. These relations can be computed using the SIM function as $\mathbf{x}' = \text{SIM}_S(\mathbf{x}, u, t) \iff \mathbf{x} \overset{t,u}{\rightsquigarrow} \mathbf{x}'$, and satisfy the following basic properties:

- **Identity:** Each state is reachable from itself in 0 time under any input, $\forall u : \mathbf{x} \overset{0,u}{\rightsquigarrow} \mathbf{x}$.
- **Forward Determinism:** For each $\mathbf{x} \in \mathcal{X}$, $t \geq 0$, and input $u \in \mathcal{U}$, there is a unique $\mathbf{x}' \in \mathcal{X}$ such that $\mathbf{x} \overset{t,u}{\rightsquigarrow} \mathbf{x}'$.
- **Causality:** For each $\mathbf{x} \in \mathcal{X}$, time $t \geq 0$, and for every inputs $u_1, u_2 \in \mathcal{U}$, if $u_1(s) = u_2(s)$ for $0 \leq s \leq t$ and $\mathbf{x} \overset{t,u_1}{\rightsquigarrow} \mathbf{x}'$ then $\mathbf{x} \overset{t,u_2}{\rightsquigarrow} \mathbf{x}'$.
- **Semi-group Property:** For each $\mathbf{x}, \mathbf{x}', \mathbf{x}'' \in \mathcal{X}$ and every $t_1, t_2 \geq 0$ and signals $u_1, u_2 \in \mathcal{U}$, if $\mathbf{x} \overset{t_1,u_1}{\rightsquigarrow} \mathbf{x}'$ and $\mathbf{x}' \overset{t_2,u_2}{\rightsquigarrow} \mathbf{x}''$ then $\mathbf{x} \overset{t_1+t_2,u_1;u_2}{\rightsquigarrow} \mathbf{x}''$. Here we define $u_1; u_2$ as the composed signal $u(t)$ with $u(t) = u_1(t)$ for $t \in [0, t_1)$ and $u(t) = u_2(t - t_1)$ for $t \in [t_1, t_1 + t_2)$

The trajectory of such a black box model specified by its SIM function is the same as the trajectory of the underlying system. A trajectory of time length $[0, T)$ from a given state $\mathbf{x}_i$ under the input $\mathbf{u}_i$ is defined as $\{\mathbf{x}'_i | t \in [0, T) \wedge \mathbf{x}_i \overset{t_i,u_i}{\rightsquigarrow} \mathbf{x}'_i\}$. We now need a notion of distances to quantify the closeness of two states. This notion can also be lifted to behaviors.

Distances Between States. Let $d : \mathcal{X} \times \mathcal{X} \to \mathbb{R}_{\geq 0} \cup \{\infty\}$ be a **metric** over the state-space X of a system. Common metrics over continuous state-spaces include the L_1, L_2, L_∞ metrics. Usually metrics are available for purely continuous state-spaces. However, for hybrid systems, the state-space requires us to define a metric d that compares two hybrid states $(q, \mathbf{x})$ and $(q', \mathbf{x}')$ belonging to different modes. The difficulties involved in designing a hybrid metric are discussed by Nghiem et al. [128]. Our approach side-steps this difficulty. Let

$\hat{d}$ be a metric defined over $\mathbb{R}^n$. Its **lifting** over a hybrid state-space $\mathcal{X} : \mathcal{Q} \times \mathbb{R}^n$ is defined as:

$$d((\ell_1, \mathbf{x}_1), (\ell_2, \mathbf{x}_2)) = \begin{cases} \hat{d}(\mathbf{x}_1, \mathbf{x}_2), & \text{if } \ell_1 = \ell_2 \\ \infty, & \text{otherwise} \end{cases}$$

It is easy to verify that d is a metric, provided $\hat{d}$ is a metric and $\hat{d}(\mathbf{x}_1, \mathbf{x}_2)$ is finite for all pairs of continuous states $\mathbf{x}_1, \mathbf{x}_2$.

2.4.2 Controller

We only work with the white box model of the controller, but present a behavioral model for completeness. It also aids in clarifying the overall model of the SDCS.

The controller is a full state feedback controller, and operates by being able to sense the complete plant state. This eases up the presentation, but by no means is restrictive as we have assumed full state observability for the plant. The controller samples the plant states $\mathbf{x}$ at the beginning of a sampling period, and updates its internal states s and computes the control input $\mathbf{u}$.

Definition 2.4.1 (Controller's Behavioral Model) A controller is specified in terms of its input space X, its internal state-space $\mathcal{S}$, and the controller sampling period τ_s. Its semantics are provided by a function $\rho : X \times \mathcal{S} \mapsto \mathcal{U} \times \mathcal{S}$, where the function $\rho(\mathbf{x}, s)$ maps the controller input $\mathbf{x}$ (which is the plant's state at time t) and internal state s (at time t) to $(s', \mathbf{u})$, where s' and $\mathbf{u}$ are the updated control state and the input to the plant at time $t + \tau_s$, respectively.

In the above definition, the controller's input space is in fact just the plant's state-space. However, in general the controller can also have disturbance inputs along with parameters. The techniques we introduce can be extended to accommodate them.

2.5 Behavioral Model of SDCS

As stated earlier, the parallel composition of the plant and a controller constitutes an SDCS, as shown in Fig. 5.4.

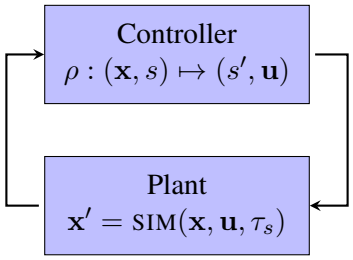

Figure 2.2: SDCS with sampling period τ_s.

Definition 2.5.1 (Sampled Data Control System: Behavioral Model) A behavioral model of an SDCS consists of (a) a behavioral plant model P described by SIM_P, (b) a controller described by a computer program whose semantics are defined by a function ρ, and, (c) sampling time period τ_s.

SDCS Semantics. The state of the SDCS is given by $(\mathbf{x}, s, \mathbf{u})$ where $\mathbf{x} \in \mathcal{X}$, $\mathbf{u} \in \mathcal{U}$ and $s \in \mathcal{S}$, which denotes the internal state of the controller. Let $\mathbf{x}_0$ be the initial plant state at $t = 0$, s_0 be the initial controller state and u_0 be the initial plant input or controller output. Given a controller sampling period τ_s, the operational semantics of the closed-loop SDCS model can be described as a countable sequence of plant and controller moves as follows:

$$(\mathbf{x}_0, s_0, \mathbf{u}_0) \rightsquigarrow_{\mathcal{P}} (\mathbf{x}_1, s_0, \mathbf{u}_0) \rightarrow_{\mathcal{C}} (\mathbf{x}_1, s_1, \mathbf{u}_1) \rightsquigarrow_{\mathcal{P}} (\mathbf{x}_2, s_1, \mathbf{u}_1) \rightarrow_{\mathcal{C}} (\mathbf{x}_2, s_2, \mathbf{u}_2) \cdots$$

In each of the above states, the index i denotes the real time $i\tau_s$. The closed-loop model interleaves two types of moves:

- **Plant Moves:** $(\mathbf{x}_i, s_i, \mathbf{u}_i) \rightsquigarrow_{\mathcal{P}} (\mathbf{x}_{i+1}, s_i, \mathbf{u}_i)$, where $\mathbf{x}_i \overset{\tau, \mathbf{u}_i}{\rightsquigarrow} \mathbf{x}_{i+1}$ is the next state of the plant after time τ_s has elapsed under input $\mathbf{u}_i$. The move has no effect on the controller state, or the control input.

- **Control Moves:** $(\mathbf{x}_{i+1}, s_i, \mathbf{u}_i) \rightarrow_{\mathcal{C}} (\mathbf{x}_{i+1}, s_{i+1}, \mathbf{u}_{i+1})$ describes a move by the controller that denotes an instantaneous execution of the control program to yield $(s_{i+1}, \mathbf{u}_{i+1}) = \rho(\mathbf{x}_{i+1}, s_i)$. As a reminder, no time is assumed to elapse during this computation.

2.6 Reachability Properties

The reachability problem is a fundamental question relevant in different contexts and asks if a given system can reach certain states from a set of given initial states. It is a common problem for discrete transition systems, continuous and hybrid dynamical systems, and several different methodologies have been proposed to address it. Solving this problem is equivalent to verifying or falsifying a safety property. We define a safety property as an assertion, which states that a specified set of states: termed 'unsafe' states, are unreachable.

Definition 2.6.1 (Safety Property) Given a hybrid system S, its initial states $\mathcal{X}_0$, and an unsafe set of states $\mathcal{X}_f$, we want to solve the decision problem $\exists t, \mathcal{X}, \mathcal{X}'.t \geq 0 \wedge \mathcal{X} \in \mathcal{X}_0 \wedge \mathcal{X}' \in \mathcal{X}_f \wedge \mathcal{H}_t^{\mathcal{A}}(\mathcal{X}, \mathcal{X}')$.

The reachability problem is undecidable for general systems [82], and decidable only for cases where the system dynamics are trivial and of very little practical interest. However, the problem gets somewhat tractable by viewing verification and falsification separately. In the past, many sound but incomplete procedures including but not limited to [6, 9, 32, 64, 65, 81, 147, 148] have been put forth to tackle only the verification problem, i.e., the decision procedure that answers either 'verified' or 'don't know'. There have also been a few falsification procedures [10,23,42,49,55,91], but they usually do not rely on under-approximations and are best effort approaches. Falsification procedures, when successful, provide a 'counter-example' as a certificate. This is but a trajectory of the system beginning from the initial set and terminating in the unsafe set.

Time-Bounded Safety Problem. In our work we reason about reachability in bounded time. We try to answer if a set of states $\mathcal{X}_f$ is unreachable from the initial state $\mathcal{X}_0$ for the given time horizon T. In the rest of this thesis, we put forth several time bounded falsification approaches.

2.7 Related Work

Verification and falsification have the common goal of ruling out errors in a system. The former is focused on establishing an assertion, while the latter searches for counter-examples to the assertions. They are similar, but the complexity of the problem divides the approaches into two separate camps. Most approaches

in both camps use relaxations, which makes them complementary in practice. They maintain soundness but forgo completeness towards their respective problem. Hence, if a verification procedure fails, the system could still be safe and if the falsification fails, the system could still be unsafe. When they succeed, we can be assured of their results.

In contrast, there exist several falsification techniques which use numerical simulations. They trade off both soundness and completeness for efficiency and scalability. The techniques proposed in this thesis are of a similar nature.

2.7.1 Verification

The process of verification assumes the validity of the assertion and tries to ascertain it. We now discuss several broad ideas which are commonly used for verification. An overview about verification is also provided in [4].

Discrete Abstractions have been widely employed for verifying safety properties of hybrid systems [7, 156]. As the name suggests, they discretize the continuous dynamics such that soundness against their temporal properties is preserved. The abstractions must be tuned so that they are neither too coarse, nor too fine. This can be automated using Counter-Example Guided Abstraction (CEGAR) refinement [7, 34]. Another technique used in conjunction with discrete abstractions is hybridization. It simplifies the systems behavior by splitting its domain into smaller regions and over-approximating the dynamics for each small region by simpler expressions (like differential inclusions). Usually the hybridization is done over space [11, 40, 81].

Relational Abstractions Relational abstractions have been used to summarize behaviors of hybrid automatons [123, 149] and SDCS [166]. They can be either constructed as time-less or timed depending upon the properties of interest. The idea is to abstract away the dynamics of the system by reachability relations which associate the system states to their reachable states. The abstraction results in a transition system, which can be analyzed using the many available model checkers.

Reach-Set Computation: Flowpipe Construction Numerical simulations have been successfully used to understand behaviors (testing) of the system, but, they alone can never exhaustively enumerate all behaviors.

In hybrid systems, numerical issues and non-robust semantics exacerbate this. Similarly, for complex models, it is unclear when they have been sufficiently tested. Ideally, instead of testing by sampling the search space, we would like to 'simulate' an entire set of conditions. Similar to numerical integration techniques, reach-set computation does exactly this by over estimating the set of states reachable at every step through time. Many techniques differing by their choice of set representations have been proposed in the past like the ones based on ellipsoids [104], zonotopes [71], template polyhedra [147], support functions [74] and Taylor models [19, 20, 31]. Another class of approaches are based on level set methods [121], solutions of Hamilton Jacobi formulations [122] and viability theory [13]. Some tools implementing these ideas include [15, 16, 32, 66, 105, 126, 157].

Logic and theorem Proving Approaches from automatic theorem proving have also had some success in the verification of hybrid systems. Barrier Certificates [140], similar to level sets of Lyapunov functions were proposed to establish a separation based on the continuous dynamics between the safe and the unsafe states of the system. This has been extended in [135] and followed up by a theorem proving engine KeYmaera [137]. The publication [136] summarizes these approaches.

Constraint Solvers. Constraint solvers like Yices [52], Z3 [44], HySAT [63, 85] and its successor iSAT, and dReal [68] are usually used by analysis procedures to check assertions. They cannot directly work with hybrid systems because most do not have decision theories for ODEs. An exception is dReal which uses interval constraint propagation to provide a δ-sat procedure for ODEs [69]. It has a bounded model checker dReach that can check reachability properties for hybrid automata.

2.7.2 Falsification

Falsification is complementary to verification, and attempts to find a violation/witness/counter-example/error trajectory to the safety property. Such a violation if found, is as a proof of an error in the system. Such a trajectory defines the exact initial states, parameters, and inputs required to reach the bad states from the initial states. If found, it can help in debugging the system under test. A process of falsification is commonly carried out in practice, as testing. Specifically, random testing using numerical simulations, where multiple runs of the system/model is observed until the testing budget is exhausted. Even though it is

often the best way to tackle highly complex systems, random exploration often performs poorly with respect to coverage. The coverage of the state-space (and hence the behaviors) can be highly non-uniform, leaving critical errors hidden.

Several approaches have been put forth to address these issues. Some strengthen the simulation based testing (a) sample based incremental search. A few provide a more rigorous search using notions of (b) bisimilarity and state-space coverage. The approaches grouped under (a) usually cannot conclude the absence of errors, but some use a notion of coverage to quantitatively measure the exploration and provide confidence. The group (b) approaches can rule out errors, but are usually harder to apply and not scalable. Some approaches also use under-approximations [2] . We now describe them briefly.

2.7.2.1 Sampling Based Searches

These assume the presence of an error and use best effort global search mechanisms to iteratively converge to an error trace. They are not complete, but in general, do offer the notion of probabilistic completeness. Informally, this means that (under certain assumptions) if an error trace exists, then the probability of finding it converges to 1 as the search progresses.

Motion Planning. Techniques from robotic motion planning have been used in the past to find falsifications in hybrid systems [106, 107]. These methods rely on variations of Rapidly exploring Random Trees (RRTs) to iteratively grow from the initial state set towards the final state set (or vice versa and some times employ bi-directional trees). Using a suitable metric for distance and a sampling scheme, simulations are used to find an error trajectory of the system. Recent advances in the context of falsification in hybrid systems include using a combination of sophisticated heuristics to maximize the exploration of reachable state-space (coverage), and biasing of the tree towards the goal using robust satisfaction measures over partial traces [23, 39, 49, 94, 125, 134]. Even though RRTs have been widely successful in planning, they face difficulties when searching for trajectories in the presence of differential constraints with a highly constrained reachable space (as is the case with under-actuated systems).

Robustness-Guided Falsification. Several techniques have been proposed based on optimizing some

[2] Unlike over-approximate abstractions, under-approximations are harder to build, and very few techniques exist in literature [92].

metric on trajectories. [2, 56–60, 127]. Robustness metrics for trajectories have been defined for Metric Temporal Logic (MTL [99]) by Fainekos et al. [58] and for Signal Temporal Logic (STL [116]) by Donze et al [46]. The robustness-guided falsification proposed by Fainekos et al. associates each trajectory with a **robustness metric** that measures how close a given trajectory is to a violation. Falsification is achieved by using a global optimization techniques (such as simulated annealing and cross-entropy) to minimize the robustness [1]. A value less than 0 signifies a violation. This approach is implemented in the tool S-Taliro for falsifying MTL properties for Simulink/Stateflow diagrams [10]. Donze et al. have implemented Breach to find violations of STL formulas [47]. Such techniques have an obvious advantage over the symbolic techniques and can potentially deal with black box dynamics. However, they can be quite erratic due to heavy dependence on the definition of cost and the optimization (global) technique used. Getting trapped in local minima is very common in practice. Also, they often do not leverage the structural information of the problems.

2.7.2.2 Systematic Testing

Test Generation Using Bisimulation Functions. Efficient test generation and coverage is very common in the field of computer software. Hybrid systems resist such kind of an approach because of the potential presence of infinite behaviors. Using a bisimulation metric 'similar' behaviors can be grouped together potentially resulting in a finite number of them. Unfortunately, with sufficiently complex systems, one can end up with infinite groups. The notion of δ-bisimulation functions [72], which are relaxations of classical bisimulation functions, has been used in [90] to achieve the above. Also, it assumes a bisimulation function, which is hard to find. Such techniques can also be used for verification as they eventually enumerate all possible behaviors from the initial set.

Systematic Simulations. Systematic simulations [38, 48, 93] are quite similar to the above test generation technique, but do not require bisimulation functions. They still are symbolic and use sensitivity information and the notion of continuity of system behaviors. Hence, this can work well with continuous systems, but its harder to extend to hybrid systems.

2.7.3 Closed Loop Analysis Techniques

Given the difficulty of analyzing the components of a SDCS independently, few techniques exist for their closed loop analysis. The first one was proposed by Lerda et al. [109, 110], where model checking [35] of the software was combined with simulation-based systematic exploration of the physical system. Later, Majumdar et al. [113] proposed a verification mechanism by combining an over-approximating reach set computation engine for the plant with the symbolic execution of the controller program. It restricted the plant dynamics to be only linear. Moreover, the combined symbolic approaches are not as scalable as numerical approaches.

Chapter 3

Segmented Trajectories - A Behavioral Perspective

3.1 Introduction

Trajectories of dynamical systems provide a natural way of thinking about their behaviors over time. They can be used to define dynamical systems [160, 161]. For complex systems, numerical methods can serve as a tool for exploring behaviors. Plots of trajectories, called phase portraits are often used to study qualitative behaviors and topological features. For arbitrary systems, they are constructed by plotting trajectories (using numerical integration) in the state-space with different initial conditions. In theory, if we can generate 'enough' trajectories by uniform sampling, we can reveal 'all' behaviors of a continuous-time (and Lipschitz continuous) dynamical system. In practice, such an approach suffers form the curse of dimensionality and cannot scale with increasing number of dimensions. The number of samples and trajectories required can be exponential in high dimensional spaces.

In this chapter, we introduce trajectory based notions **trajectory segments** and **segmented trajectories** for efficient exploration of trajectory space. Trajectory segments are finite time trajectories of the system which can begin from any state in the state-space. Segmented trajectories are a sequence of trajectory segments. Clearly, the segmented trajectories are not real trajectories of the system as there exist gaps between the end points of trajectory segments. To re-state the goal of this thesis, we are interested in searching for trajectories violating safety properties of a hybrid system. We show how an off-the-shelf generic optimization routine can be used to 'splice' together the individual trajectory segments of the segmented trajectory of a hybrid automaton by minimizing the gaps between them. In the next few sections, we introduce trajectory segments and present one approach which utilizes them to find falsifications in hybrid automata.

3.2 Trajectory Segments

Before we formalize trajectory segments for hybrid systems modeled as hybrid automaton and black boxes, let us take the example of a bouncing ball.

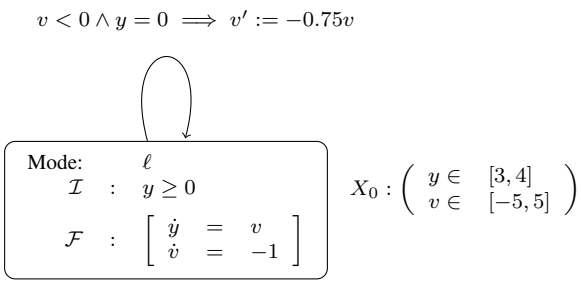

Figure 3.1: Hybrid automaton for a bouncing ball with initial set X_0.

Example 3.2.1 (Bouncing Ball) The model of a ball, bouncing vertically in a gravitational field is given by a hybrid automaton in Fig. 3.2. The ball is thrown from vertical positions $3 \leq y \leq 4$ with a velocity $-5 \leq v \leq 5$. It rises/falls continuously in time and bounces at the instant $y = 0$, and reverses its velocity [1] .

We visualize the behaviors of the system in the phase space y vs v and against the time axis using three different methods. The plots at the top (a) and (b) in Fig. 3.2 are the flowpipes over-approximating all possible reachable set of states from the initial conditions. They were generated using the tool FLOW* [32]. The middle plots are the familiar (c) phase portrait and the (d) time trajectory plot, where the initial conditions are sampled uniformly randomly from X_0 and simulated numerically. Compare these with the last two plots (e) and (f) where trajectory segments were used to discover the behaviors of the system all over the space. They were created by sampling different pairs of values for (y, v) and (t, y) and simulating for $2s$ each. The initial state conditions are not respected and the continuity of trajectories is ignored. This results in segmented trajectories which are not part of the phase portrait. Intuitively, we explore 'more' of the state-space with the same number of simulations.

[1] The model has Zeno behaviors which we avoid by using a fixed time horizon. A detailed discussion is outside the scope of this thesis.

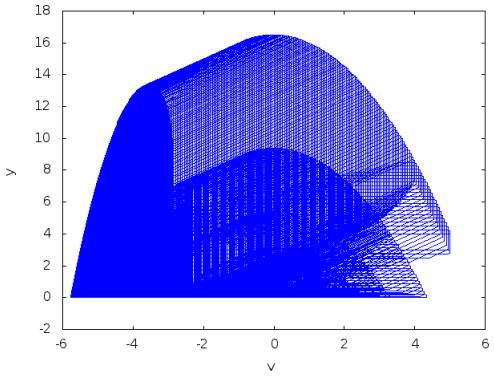

(a) Flowpipe: y vs v

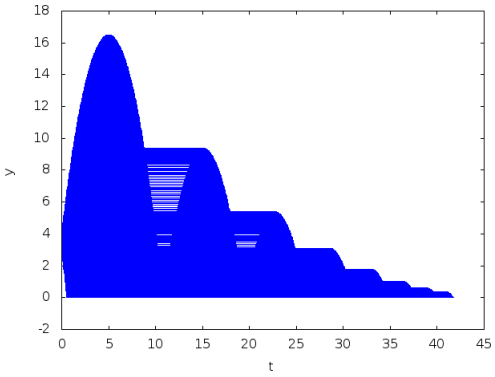

(b) Flowpipe: y vs t

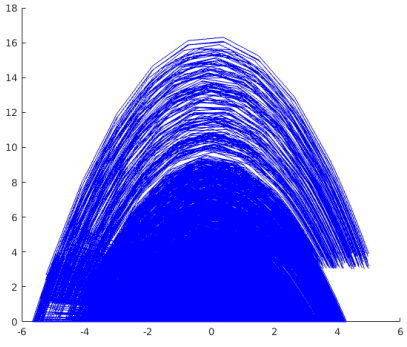

(c) Simulations: y vs v

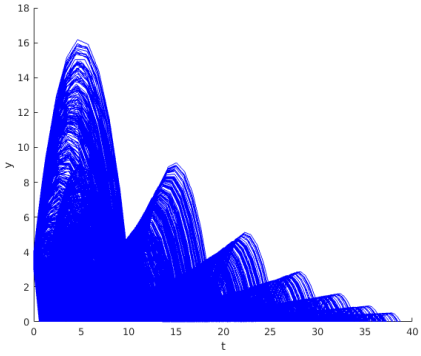

(d) Simulations: y vs t

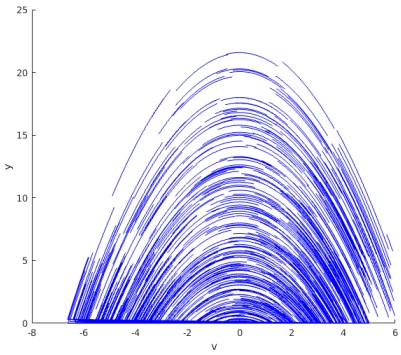

(e) Trajectory segments: y vs v

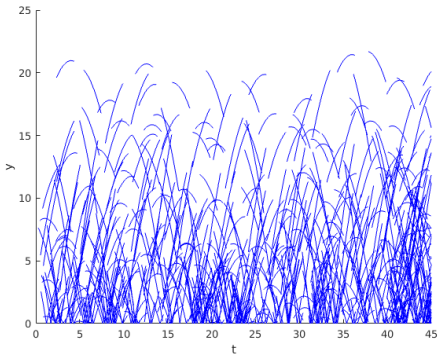

(f) Trajectory segments: y vs t

Figure 3.2: Comparison of state-space exploration using flowpipes, simulations and trajectory segments.

We now formalize segmented trajectories for hybrid systems modeled using hybrid automata and discuss their applicability in the falsification problem. We show how an optimization tool can be used as a falsification tool by reformulating the reachability problem into a minimization problem. Recall the definition of a trajectory of a hybrid automata $\mathcal{A}$.

$$\mathcal{H}_t^{\mathcal{A}} : \varphi^{q_1}_{[t_0,t_1)}(\mathbf{x}_0) \xrightarrow{\delta_1} \varphi^{q_2}_{[t_1,t_2)}(\mathbf{x}_1) \xrightarrow{\delta_2} \dots$$

A finite time trajectory of $\mathcal{A}$ can be expanded as follows [2] : A finite trajectory of a hybrid automaton beginning from $(q_0, \mathbf{x}_0)$ and ending at $(q_0, \mathbf{x}'_N)$ can be expanded as follows.

$$(q_0, \mathbf{x}_0) \rightsquigarrow_{\tau_0} (q_0, \mathbf{x}'_0) \xrightarrow{\delta_0} (q_1, \mathbf{x}_1) \rightsquigarrow_{\tau_1} (q_1, \mathbf{x}'_1) \xrightarrow{\delta_1} \cdots \xrightarrow{\delta_N} (q_N, \mathbf{x}_N) \rightsquigarrow_{\tau_N} (q_N, \mathbf{x}'_N)$$

We now define a basic element of the above trajectory, a trajectory segment. A trajectory of the system can be thought of as a composition of multiple trajectory segments. The segment is completely contained inside the mode invariant [3] .

Definition 3.2.1 (Trajectory Segment) A trajectory segment in mode q of time length τ is a continuous flow of the system denoted by $\pi^q_\tau : \varphi^q_{[0,\tau)}$. Its starting state is denoted as $\mathbf{x} = start(\pi^q_\tau)$ and the terminating state as $\mathbf{x}' = end(\pi^q_\tau)$.

Every state on the trajectory segment satisfies the differential constraints and the invariant constraints of its mode. $\forall\, t \in [0, \tau).\ \pi^q_\tau \in \mathcal{I}(q)$. A trajectory segment can be completely specified by its start state, mode, and time length (x_i, τ_i, q_i). A sequence of trajectory segments: **segmented trajectory** is akin to a trajectory with some caveats.

Definition 3.2.2 (Segmented Trajectories) A segmented trajectory $\mathbf{S}_\pi$ is a sequence of $N+1$ trajectory segments $\mathbf{S}_\pi = \langle \pi^{q_0}_{\tau_0}, \pi^{q_1}_{\tau_1}, \cdots, \pi^{q_N}_{\tau_N} \rangle$.

Clearly, due to the presence of gaps between consecutive pairs of trajectory segments $(\pi^{q_i}_{\tau_i}, \pi^{q_{i+1}}_{\tau_{i+1}})$, $\mathbf{S}_\pi$ is not necessarily a trajectory of the system. We now define a notion of distance between two trajectory

[2] To simplify the presentation, we drop the inputs.

[3] This can be relaxed, as discussed towards the end.

segments using the definitions of distance and metric from Chapter 2.

$$d(\pi_{\tau_0}^{q_0}, \pi_{\tau_1}^{q_1}) = \begin{cases} \hat{d}(end(\pi_{\tau_0}^{q_0}), start(\pi_{\tau_1}^{q_1})), & \text{if } q_0 = q_1 \\ \hat{d}(r_\delta(end(\pi_{\tau_0}^{q_0}), start(\pi_{\tau_1}^{q_1})), & \text{otherwise} \end{cases}$$

where r_δ is a transition from mode q_0 to q_1. For the case when the two π are in different modes, the distance is different along different transitions. Using the notion of distance, we can quantify the closeness of a segmented trajectory to a system trajectory. We do this by associating a cost to it, which is the summation of all the distances between consecutive trajectory segments.

Definition 3.2.3 (Cost of a Segmented Trajectory) The cost of a segmented trajectory $\mathbf{S}_\pi$ is given by the expression:

$$\textsc{Cost}(\mathbf{S}_\pi) : \sum_{j=0}^{N-1} d(\pi_{\tau_j}^{q_j}, \pi_{\tau_{j+1}}^{q_{j+1}})$$

where $\pi_{\tau_j}^{q_j}$ and $\pi_{\tau_{j+1}}^{q_{j+1}}$ are consecutive trajectory segments.

A segmented trajectory is a system trajectory, if there are no gaps between the consecutive trajectory segments.

Definition 3.2.4 (System Trajectory in Terms of a Segmented Trajectory) The segmented trajectory $\mathbf{S}_\pi$ is a system trajectory when

- Cost of the segmented trajectory is 0, i.e., $\textsc{Cost}(\mathbf{S}_\pi) = 0$
- The transition guards are satisfied whenever a transition is taken, i.e., $\forall(\pi_{\tau_0}^{q_0}, \pi_{\tau_1}^{q_1}).q_0 \neq q_1 \implies end(\pi_{\tau_1}^{q_1}) \in g_\delta$, where δ is a transition from q_0 to q_1.

Definition 3.2.5 (Abstract Segmented Counter-example) Given a safety property specifying unsafe set $(q_f, \mathbf{x}_f) \in \mathcal{X}_f$, and the initial states of the system $(q_0, \mathbf{x}_0) \in \mathcal{X}_0$, we can now define a time bounded T abstract segmented counter-example of the system as

$$\mathbf{S}_\pi = \left\langle \pi_{\tau_0}^{q_0}, \pi_{\tau_1}^{q_1}, \cdots, \pi_{\tau_N}^{q_f} \right\rangle$$

where $\sum_{i=0}^{N} \tau = T$, and $(q_0, start(\pi_{\tau_0}^{q_0})) \in \mathcal{X}_0$, $(q_f, end(\pi_{\tau_N}^{q_f})) \in \mathcal{X}_f$.

Given a space of segmented trajectories, we want to search for a concrete counter-example of the system. Such a counter-example satisfies two conditions (a) it is a trajectory of the system, and (b) is also an abstract segmented counter-example. Using the above definitions, we reformulate the reachability problem for finding a witness to a safety property as an optimization problem. The result is a non-linear, non-convex optimization problem.

3.3 Trajectory Splicing using Optimization

We informally state the problem now. Given a hybrid automaton description of a system, and a time bounded safety property, our procedure tries to produce a trace that violates the property. If such a trace does not exist, our procedure might never terminate unless a budget is specified. Even if a violation exists, there is no guarantee that we can find it. However, for the case of LHA we can even compute the gradients, which as we show later using an off-the-shelf optimization routine, can result in a very efficient approach.

The search for a falsification is the search for a hybrid trajectory of the system starting from a given initial state and terminating in the set of unsafe states. Due to the involvement of discrete switching, the search has a combinatorial aspect, and falsification search can be viewed in two parts: (a) the search for a discrete mode and transition sequence, (b) a continuous trace for every mode in the sequence satisfying the mode dynamics and invariants, with the end points on the switching surfaces and obeying respective updates. We relax this aspect for our first optimization based splicing by assuming a given transition sequence, and search for the continuous states and dwell times [4] .

The input to our approach consists of a hybrid automaton along with a sequence of discrete modes and transitions $q_0 \xrightarrow{\delta_1} q_1 \ldots \xrightarrow{\delta_N} q_N$, the first of which ($q_0$) contains the initial region (set of initial conditions), and the last of which (q_N) contains the unsafe region. Our approach attempts to find an actual system trajectory satisfying this discrete mode sequence. This is achieved by viewing the gaps between the trajectory segments as a cost function and attempting to find segments that minimize this function. As a result, standard numerical optimization techniques are used to iteratively narrow these gaps using gradient information from a sensitivity analysis of the system trajectories in each mode. If the optimal cost (sum of gaps between

[4] A discrete mode sequence can be obtained in several ways [164].

segments) is zero, our approach yields a concrete trajectory of the system exhibiting a violation. Often, in practice, a very small gap (10^{-5} or less) suffices to observe a falsification.

3.3.1 Problem Setup

Assume that $\mathcal{A}$ is a hybrid automaton with initial states $(q_0, \mathbf{x}_0) \in \mathcal{X}$ and let $(q_f, \mathbf{x}_f) \in \mathcal{X}_f$ represent an unsafe set. We assume that we are given an abstract counter-example C that is simply a sequence of modes and transitions:

$$C : \langle q_0, \delta_0, q_1, \delta_1, \cdots, \delta_{N-1}, q_N \rangle \tag{3.1}$$

wherein $q_N = q_f$. Our goal is to find a concrete counter-example to this property.

$$(q_0, \mathbf{x}_0) \rightsquigarrow_{\tau_0} (q_0, \mathbf{y}_0) \xrightarrow{\delta_0} \cdots \xrightarrow{\delta_{N-1}} (q_N, \mathbf{x}_N) \rightsquigarrow_{\tau_N} (q_N, \mathbf{y}_N) \tag{3.2}$$

This paves the way to set up an optimization problem, where the cost of the segmented trajectory needs to be minimized to 0. If successful, the minimizers define a segmented trajectory which is actually a concrete violating trace of the system. Otherwise, the cost is strictly positive indicating that no such trajectory exists.

$$\min_{\mathbf{x}_0, \tau_0, \ldots, x_N, \tau_N} \textsc{Cost}(\mathbf{S}_\pi) = \textsc{Cost}(\langle \pi^{q_0}_{\tau_0}, \pi^{q_1}_{\tau_1}, \cdots, \pi^{q_f}_{\tau_N} \rangle) \text{ s.t.} \tag{3.3}$$

$$\tau_{\min} \leq \tau_i \leq \tau_{\max} \tag{3.4}$$

$$\mathbf{S}_\pi \in \{\text{set of all system trajectories}\} \tag{3.5}$$

$$\mathbf{S}_\pi \in \{\text{set of all abstract segmented counterexamples}\} \tag{3.6}$$

Figure 3.3: The optimization problem.

Fig. 3.3 states the optimization problem of minimizing the cost function over a set of segmented trajectories for a given C. The objective function represents the total cost of the segmented trajectory S by summing the gaps between all consecutive trajectory segments $\pi^{q_i}_{\tau_i}, \pi^{q_{i+1}}_{\tau_{i+1}}$. If the dwell times for each mode $\tau_0, \ldots, \tau_N$ are given, then they can be encoded as (3.4), where $\tau_{\min} \geq 0$. $\mathbf{S}_\pi$ must be a system trajectory, and should satisfy the guard constraints when a transition is involved (3.5). Also, it must satisfy the requirements of a segmented counter-example, i.e., the initial state of the trajectory must be in the initial set, and the final

state must be in the unsafe set (3.6). Every point of the trajectory segment must satisfy the respective mode's invariant and differential constraints. We discuss several relaxations in [164].

This complex optimization problem, is in general non-linear and non-convex. However, if initialized properly, it can be solved using numerical solvers such as the `fmincon` optimization function available in Matlab®. To do so, we may numerically approximate the FLOW function using standard ODE solvers. Also, standard sensitivity analysis can be used to compute derivatives $\nabla \mathbf{y}_i$ (w.r.t. $\mathbf{x}_i$) and $\partial \mathbf{y}_i / \partial \tau_i$. This enables the use of gradient-descent and quasi-Newton methods to solve the problem. Furthermore, such a technique places relatively few restrictions on the nature of the automaton $\mathcal{A}$ and the property.

3.3.2 Splitting the Optimization Problem

Let us now look at the practical feasibility of the problem. As noted earlier, it is non-linear and non-convex in nature, and in general, not very amenable to efficient optimization. Using off-the-shelf optimization routines is convenient, but does not remedy the inherent inefficiency. Specifically, the size of the optimization problem in terms of the number of decision variables and constraints, depends linearly on the number of state variables in $\mathcal{A}$ and the length of the counter-example sequence. The latter, can be problematic, if the specified sequence is long. This is undesirable, because we are interested in finding 'deep' counter-examples, which are hard to find using conventional testing. To remedy this, we exploit the structure of the problem to propose a decomposition scheme.

The problem of trajectory optimization has a special constraint structure. A trajectory segment's constraint expression involves only its nearest neighbor and is independent of other segments. This can be noticed as a block diagonal constraint matrix, and gives us a natural way of partitioning and parallelizing the problem. Essentially, each sub-problem considers only one trajectory segment at a time, and fixes its two neighboring segments. It now tries to satisfy the constraint of the segment while trying to extend both the start and the end points towards the previous and the subsequent segment, respectively. This concludes an iteration, with the next iteration beginning with the new segments. The procedure converges when the cost is minimized to 0. It can be shown that if a local minima is reached, it corresponds to the local minima of the original problem.

We partition the optimization problem into smaller sub-problems $P_0, \ldots, P_N$ corresponding to the segments $\pi_0, \ldots, \pi_N$. Specifically, problem P_j is allowed to modify the starting point $\mathbf{x}_j$ and the dwell time τ_j of segment π_j, while fixing the decisions for every other segment to their current value. In effect, we optimize the cost of each segment one at a time rather than all together. This reduces the size of each sub-problem P_i to involve just $(\mathbf{x}_i, \tau_i)$, and is thus independent of the length of the counter-example N. The decomposed problem when solved iteratively for its constituent sub-problems converges to a (local) minimum of the original problem, if the optimization of each of its sub-problem converges. The details are discussed in our presentation [164].

3.3.3 Evaluation on Navigation Benchmark

We implemented the splicing approach in Matlab® using the `fmincon` optimization routine with SQP. The abstract counter-example was obtained by intelligently enumerating all likely mode/transition sequences up to a given length. For each mode sequence, an optimization problem was initialized by using random simulations in each mode of the sequence; which may not be feasible to begin with. As the optimization problems are independent, they can be run in parallel.

The gradients of the objective function and constraints were supplied to `fmincon` in order to improve the speed of convergence. For all practical purposes, a violation is concluded within a small tolerance (10^{-3}) for the cost. The found counter-examples are confirmed by simulating from the initial condition.

Navigation Benchmark. The NAV benchmarks are commonly used to evaluate hybrid system verification tools [61]. These benchmarks model a particle traveling on a 2 dimensional grid of cells. The continuous dynamics of each cell are described by set of affine ODEs. A transition is taken when the particle crosses over from one cell to its neighbor. All instances of the benchmark designate an initial set of states and an error cell. To test our approach we focus on the 'NAV-30' instance which has $25 \times 25 = 625$ cells or discrete modes and roughly 2500 transitions. To make the falsification more challenging, we modify the initial set of states to $X_0 : \ x \in [4, 5], y \in [21, 22], v_x \in [-1, 1], v_y \in [-1, 1]$. We carefully choose safety properties P, Q, R and S which are very hard to violate using only unguided uniform random testing, wherein each safety property is simply a cell in the grid. The cells P, Q, R and S are detailed in Table 3.1. The properties

along with $10,000$ random simulations (assuming uniform distribution on the initial conditions) are shown in Fig. 3.4. The cells P, Q, R were not reachable, although S was reached 10 times. Our optimization scheme could discover the violations within seconds.

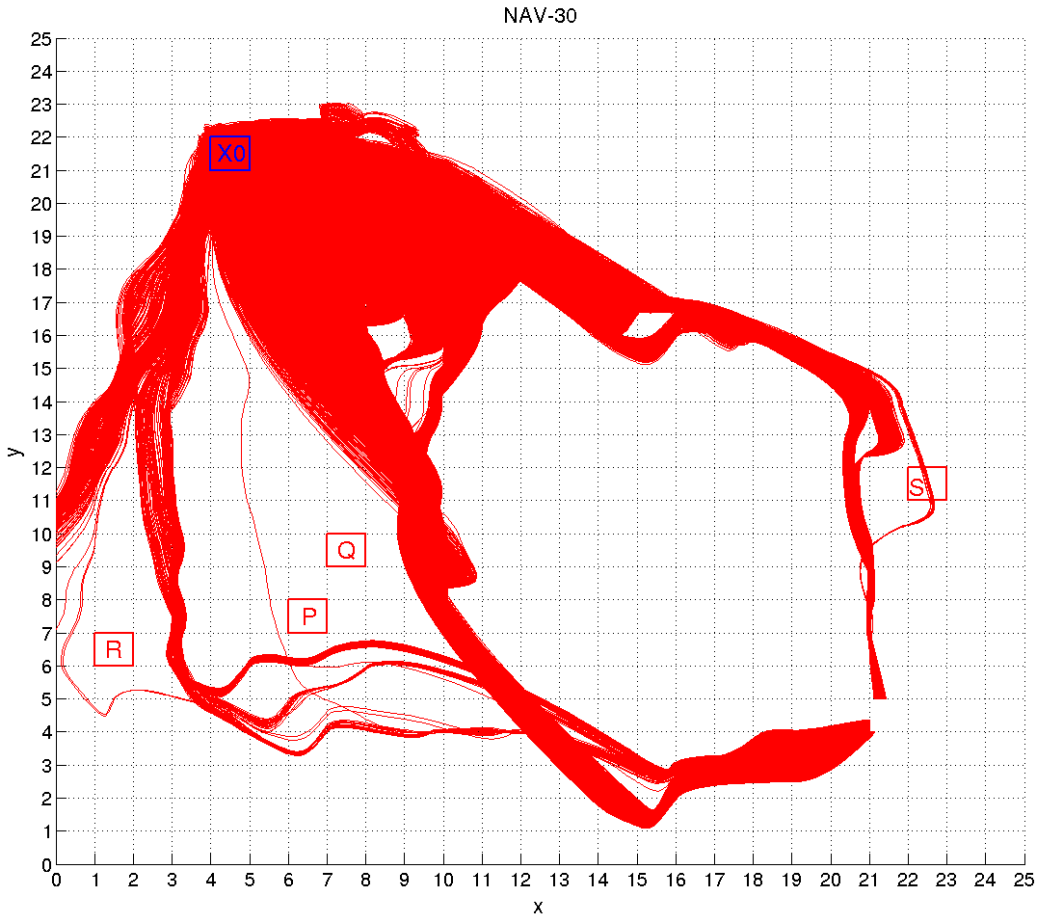

Figure 3.4: 10,000 Simulations and the target cells P, Q, R and S.

Table 3.1: Experimental Results: NAV - 30

Property	Direct	Decomp.(Iters.)
P: $x \in [6,7], y \in [7,8]$	0.3	290 (848)
Q: $x \in [7,8], y \in [9,10]$	0.5	113 (341)
R: $x \in [1,2], y \in [6,7]$	3	285 (704)
S: $x \in [22,23], y \in [11,12]$	8	1721 (2680)

Table 3.1 summarizes the benchmarking of two optimization schemes on the NAV-30 benchmark. The direct formulation is noted as **Direct**, and the decomposed per mode formulation as **Decomp.**. The timings and costs are averaged over 5 runs with different random seeds. Each falsification instance considers multiple mode sequences, but the table reports only the results over sequences that led to error trajectories. Unsuccessful mode sequences could be readily differentiated as they yielded final costs orders of magnitudes (10^4x) greater than successful ones.

The results also suggest that the direct optimization outperforms the decomposed method. This is mainly due to the large number of iterations required by the decomposed method to achieve convergence. A small number of gradient descent iterations sufficed to distinguish a plausible mode sequence from a spurious one, suggesting a fast heuristic for detecting such sequences. We posit that the efficacy of the decomposed scheme can be improved by reducing iterations and may perform better on counter-examples with long mode sequences (this merits further investigation).

Further results can be found in our publication [164] wherein we compare our approach with unguided testing using uniform random sampling and the robustness guided stochastic optimization (implemented by S-Taliro).

3.4 Related Work

One of the benefits of splitting a trajectory into smaller ones lies in better numerical performance of a search method. Another one comes in the form of a performance speedup by employing parallel algorithms to generate trajectory segments simultaneously. Depending upon the problem, the improvement can be superlinear. We briefly mention some of the problems where a trajectory segment like notion has been used both qualitatively and quantitatively. These include the qualitative analysis of dynamical systems, solving boundary value problems, searching for the optimal control strategy and fast motion planning.

3.4.1 Qualitative Exploration of Non-Linear Dynamical Systems

Global behaviors of non-linear dynamical systems are hard to characterize. To study them, cell-to-cell mapping was introduced by Hsu [86] for discrete-time dynamical systems and then extended to continuous-

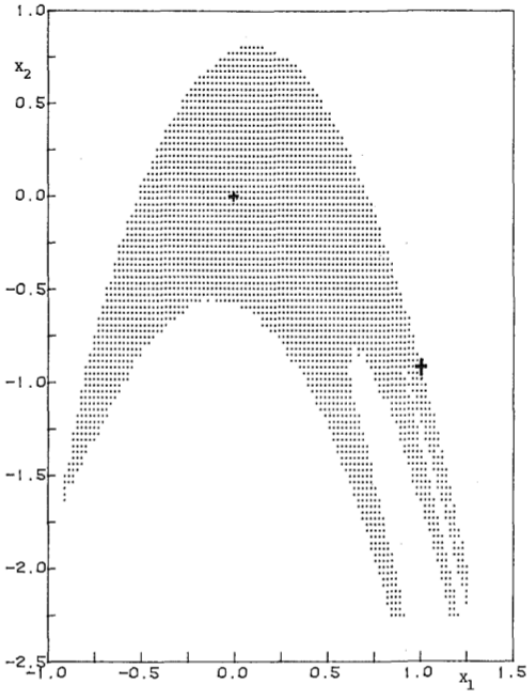

Figure 3.5: Cell-to-Cell mapping (sourced from [87]).

time. Their methodology involves discretizing the state-space uniformly into cells (hyper-cubes) and using its center as the representative discrete state. For every cell, its center is used as the initial state to carry out a single step simulation and compute the next state or the reachable cell. This process highlights the phase portrait with topological features like equilibria, their domain of attraction and periodicity in the system. Algorithms were also introduced to find attractors and limit sets by using an iterative process. The Fig. 3.4.1 taken from [87] illustrates the approach by revealing the domain of attraction for the spiral point $(0, 0)$ for the 2-dim discrete system $x_1(n+1) = (1-\sigma)x_2(n) + (2-2\sigma+\sigma^2)x_1^2(n)$ and $x_2(n+1) = (\sigma-1)x_1(n)$.

3.4.2 Reachability as a Boundary Value Problem

Initial value problems (IVPs) for differential equations have been widely studied. Given a set of ODEs, and initial conditions, one needs to find the solution, either analytically or numerically. As closed form solutions are not commonly available in analytical form, numerical integration is often the preferred solution.

A boundary value problem (BVP) is similar, but instead of specifying the complete set of initial conditions, it partially specifies both initial and final conditions. The general form of a BVP for first order ODEs is shown below.

$$\dot{\mathbf{x}} = f(\mathbf{x})$$

$$g(\mathbf{x}(a), \mathbf{x}(b)) = 0$$

The function $\mathbf{g} = (g_1, \ldots, g_n)$ is a vector of n non-linear functions specifying n boundary conditions. This is similar to the problem of falsification, however, the systems have hybrid dynamics and the boundary conditions are specified by set valued functions. Detailed discussions and solutions for BVPs can be found in the classical text [12].

We are primarily interested in two numerical methods for solving BVPs: **Single shooting** and **Multiple**

Shooting. We describe them briefly in the context of falsification (Fig. 3.6).

$$\begin{aligned} \dot{\mathbf{x}} &= f(\mathbf{x}) \\ \mathbf{x}(0) &\in X_0 \ \text{ (initial conditions)} \\ \mathbf{x}(\tau) &\in X_f \ \text{ (boundary conditions)} \end{aligned} \tag{3.7}$$

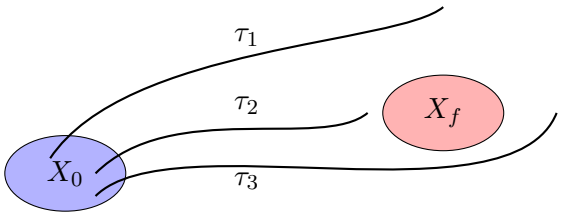

(a) Single shooting

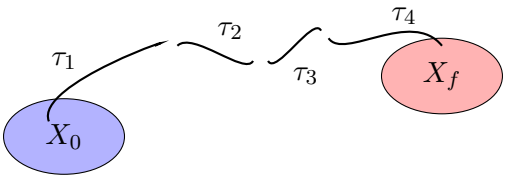

(b) Multiple shooting

Figure 3.6: Comparison between single and multiple shooting methods.

Single Shooting. One of the simplest methods to solve BVPs, single shooting searches for the set of initial condition which when integrated, will satisfy the boundary conditions. For (3.7), it needs to find $\mathbf{x}_0 \in X_0$ such that $\mathbf{x}(\tau) \in X_f$. Finding $\mathbf{x}(\tau)$ involves the solution of an IVP. One way to attack this problem is by changing the constraints to cost and formulating the below optimization problem using a notion of a set based distance $d(.)$.

$$\begin{aligned} \min_{\mathbf{x}_0, \tau} \ & d(\mathbf{x}_0, X_0) + d(\mathbf{x}_f, X_f) \\ s.t. \ & \mathbf{x}_f = \varphi_\tau(\mathbf{x}_0) \end{aligned} \tag{3.8}$$

For a choice of $\mathbf{x}_0$, the system can be numerically integrated to find $\mathbf{x}_f$, thus satisfying the flow constraint. In general, this can be a poorly conditioned optimization problem.

Multiple Shooting Multiple shooting splits the trajectory into several small trajectories (trajectory segments), splitting the interval of integration into small chunks. It then searches for segments which can be spliced up to form a solution. A formulation similar to (3.8) can be used with the additional constraint: the ends of the segments must be continuous.

3.4.3 Trajectory optimization

The problem of finding falsifying trajectories is closely related to optimal control. The distinction lies in the cost functions that are traditionally studied in optimal control problems. Often, the cost functions used exhibits the Bellman optimality principle that allows for a dynamic programming solution. However, work on optimal control has also considered more general **trajectory optimization** problems [76] that define cost functions over the trajectories of a continuous system subject to constraints. A standard approach to trajectory optimization reformulates the problem as a non-linear optimization, and uses numerical optimization techniques [21, 22]. One commonly used technique, 'direct multiple shooting', divides the time domain into segments and solves the control problem for each segment [24]. The key differences arise from the actual application domains: optimal control problems typically consider non autonomous continuous systems, whereas our work addresses falsification of hybrid systems.

3.5 Summary

From the results, we can see that searching over multiple trajectory segments is advantageous for hybrid trajectories. Using gradient information, we can exploit the continuous sensitivity to initial conditions for each mode. Likewise, the use of trajectory segments separated by different discrete modes allows us to naturally handle the discontinuities that arise through discrete transitions.

This is in contrast to single shooting approaches (like S-Taliro), which use global optimizers, often without any gradient information. They have to rely on heuristics to escape regions of state-space with discontinuities. In the case of controllers with complex Boolean conditions over the continuous state variables, or discrete states (representing operating modes), optimizers can often get trapped in regions lacking any gradient information to suggest a search-direction. Another weakness of the existing falsification tools, is the

reliance on a ‘good’ distance metric quantifying the ‘nearness’ to the unsafe states. This is challenging to define in the presence of discrete states and requires a deep understanding of the model structure [127].

However, for the case of non-linear hybrid systems, our proposed approach is sensitive to the underlying dynamics and its performance is not consistent. Moreover, it can also be very sensitive to the initial conditions used by the optimization and can give inconsistent results for the same benchmark. This is expected, as the solvers can get trapped in local minima for non-convex problems. The convergence is also slow due to missing gradient information. Secondly our approach relies on a known mode sequence. There has been work to address these deficiencies by combining the splicing approach with global optimization [102], and also on building a custom optimization engine by leveraging the amenable properties of multiple shooting using SQP [103]. Unfortunately, global optimization is often inconsistent (with hard to tune system dependant parameters). Moreover, hybrid automaton models are often unavailable in practice. Hence, we need a procedure which can reliably work with complex, partially/completely unknown dynamics. The next chapter, presents one such approach.

Chapter 4

Implicit Discrete Abstraction of Black Box Dynamical Systems

CEGAR based verification of hybrid systems usually involves symbolic techniques to build abstractions. These can be explored using model checking tools [8]. In this chapter, we propose grid based abstractions for falsifying safety properties. Previous approaches like that of Ratschan and She, have used similar abstractions, constructed using a rectangular tiling of the state-space [141] (also made available as the tool HSOLVER [142]). Their work combines symbolic search over a grid-based state-space abstraction, and refines using constraint propagation, to prune away unreachable states. We explore a similar abstraction to **falsify** rather than prove properties. This enables us to make some key relaxations.

4.1 Overview

In the previous chapter we used optimization to search for a violation in the trajectory space using trajectory segments. We now discuss an alternative approach which still uses trajectory segments, but under the framework of discrete abstractions [1] . We show how trajectory segments are paths in an abstraction. They can be discovered on demand to find abstract counter-examples, and on refinement can yield violations of safety properties.

Discrete abstractions [8] are often used to analyze the reachability and even stability [50, 138, 139] of hybrid dynamical systems. When used for verification of properties, the abstractions must be sound and capture all behaviors. This requires exhaustiveness for which over-approximation is used. It is also computationally expensive. For the purpose of falsification however, such requirements can be relaxed. We

[1] Chapter 2 provides an introduction of discrete abstractions necessary to understand the presented approach.

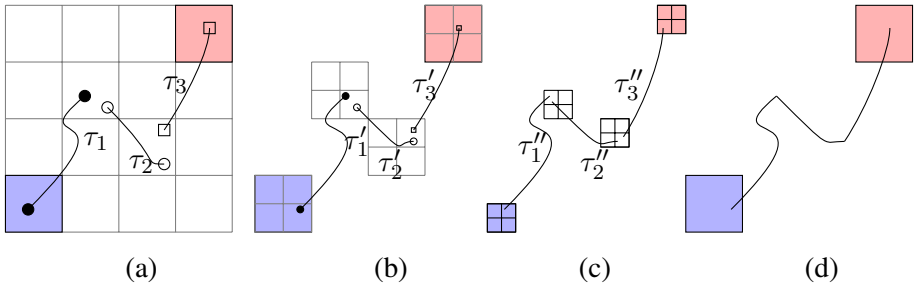

Figure 4.1: An illustration of our approach: (a) segmented trajectory reaching unsafe states (red) starting from initial states (blue), (b) refining an abstract counterexample and narrowing the inter-segment gap, (c) further narrowing the gap by refinement, and (d) a concrete trajectory with no gaps.

use sound but implicit abstractions, and explore them on the fly to find abstract counter-examples. However, knowing such an abstraction is equivalent to solving the reachability problem in the first place. Therefore, we use heuristics to guide us.

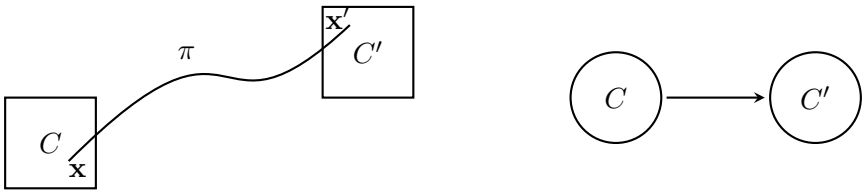

Figure 4.2: (a) A π provides witness to the forward relation between abstract states C and C' which is (b) encoded as an edge between two nodes.

We use a grid-based abstraction to discretize the phase space into cells. Each cell abstracts away the underlying continuous states, and this mapping can be viewed as a quantization function. The relations between cells can be found using trajectory segments which can be generated on demand using the SIM function. This is illustrated by the trajectory segment π with end points $\mathbf{x} \in C$ and $\mathbf{x}' \in C'$ in Fig. 4.2. The relations, like the underlying trajectory segments are time parameterized.

Definition 4.1.1 (Segmented Trajectories) A segmented trajectory $\mathbf{S}_\pi$ is a finite sequence $\langle \pi_1, \ldots, \pi_k \rangle$ of trajectory segments, wherein each trajectory segment π_i is a system trajectory $\mathbf{x}_i \xrightarrow{t_i, u_i} \mathbf{x}_i'$.

We represent the abstraction as a directed graph. Each cell corresponds to a node and a discovered relation is an edge between the two cells with the direction of the edge indicating the direction of the trajectory.

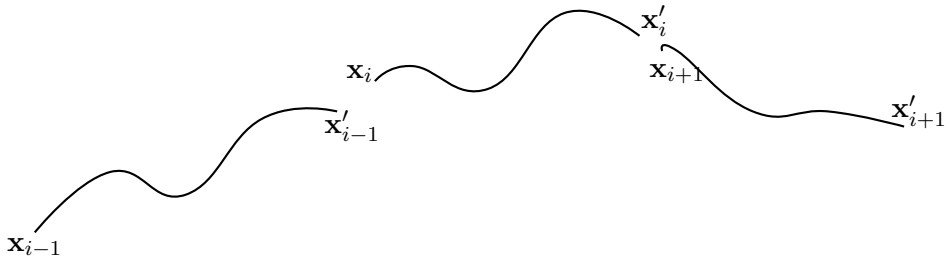

Figure 4.3: Segmented Trajectory.

Using these ideas we capture finite behaviors of a black box system and interpret them as abstract paths. In the rest of the chapter, we show how an abstract path can (potentially) be refined to find a concrete counter-example. Informally, the abstraction is refined by reducing the grid size, narrowing the maximum possible gaps between the trajectory segment at every step (to 0 in the limit).

Note that, for an arbitrary black box dynamical system, an infinite number of simulations are needed to completely build the abstraction. This is not possible in practice, and hence, our approach can only be *best effort* in nature. It does however, provide weak probabilistic completeness. It can discover any **robust** trajectory of the system given enough budget. As we do not assume to know the closed form dynamics of the system, our results are only true against the given SIM function. This is often acceptable in practice.

4.2 Abstractions

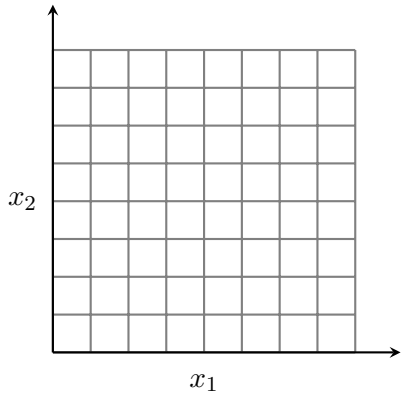

Figure 4.4: Grid abstraction

We now define the quantization function and show how it realizes an implicit tiling based abstraction.

Definition 4.2.1 (Quantization) An ϵ-precise quantization function $Q_\epsilon(\mathbf{x})$ truncates the least significant bits of its arguments such that

$$Q_\epsilon(\mathbf{x}) = (\epsilon) \left\lfloor \frac{1}{\epsilon}\mathbf{x} \right\rfloor .$$

Looking closely, we can see that the quantization function results in a partition of the argument space. For example, given a scalar $x \in \mathbb{R}$, the output of the 1-precise quantization function is always an integer $Q_1(x) \in \mathbb{Z}$. We now illustrate this using an example.

Example 4.2.1 Let us take 0.1-precise quantization given by $Q_{0.1}(x)$. It maps all x into cells of size 0.1 units, evenly distributing the $\mathbb{R}^2$ space. For instance, $\forall x \in [3.5, 3.6)$. $Q_{0.1}(x) = 3.5$. This is visualized in Fig. 4.4.

From the above, we can infer that the quantization function Q_ϵ with $\epsilon > 0$, grids a continuous state-space into discrete states of size ϵ units. We now define this grid as an ϵ-tiling on the state-space.

Definition 4.2.2 (ϵ-tilings) Formally, a tiling $\mathcal{C} : \{C_1, \ldots, C_j, \ldots\}$ is a finite or countably infinite family of closed and bounded subsets C_j of $\mathcal{X}$ called **cells**. A quantization function can be used to define such a tiling implicitly with the below properties.

(1) The tiling covers the entire state-space, i.e., $\bigcup_{C_i \in \mathcal{C}} C_i = \mathcal{X}$.

(2) Two cells are non-overlapping, i.e., $C_i \cap C_j = \emptyset,$ for $i \neq j$.

(3) For every cell $C_i \in \mathcal{C}$, the (L_∞) distance between two states is upper bounded by ϵ, i.e., $\forall\, C_i \in \mathcal{C}.\, \forall\, \mathbf{x}_i \in C_i.\, \exists\, \mathbf{y}_i \in C_i.\, d(\mathbf{x}_i, \mathbf{y}_i) \leq \epsilon$.

In other words, the cells are abstract states, and the quantization function $Q_\epsilon : \mathbf{x} \mapsto C$ maps the system's concrete continuous state $\mathbf{x}$ to its abstract state: its containing cell, such that $Q(\mathbf{x}) = C$ iff $\mathbf{x} \in C$. This mapping is non-ambiguous and always exists.

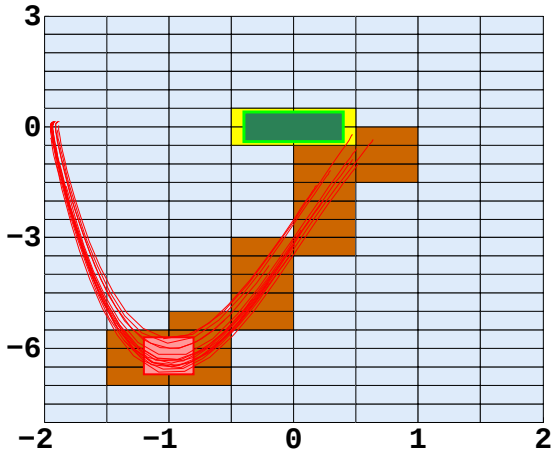

Figure 4.5: A tiling with $\epsilon = 0.5$

Fig. 4.2 shows a tiling of a subset of the state-space for the van der Pol system from Example 4.2.2, with $\epsilon = 0.5$. The meaning of the different colors assigned to the tiles will be explained subsequently.

Tiling as an Equivalence Class. The quantization function induces an equivalence relation, partitioning the state-space into cells, with each cell being a hypercube. This aggregates the states based on the $||\mathbf{x}||_\infty$ norm. Let $\epsilon = 10^{-k}$ for some $k > 0$, then the distance $||\mathbf{x} - \mathbf{y}||_\infty$ between two states $\mathbf{x} \in C$ and $\mathbf{y} \in C$ is upper bounded by ϵ. Let us denote this equivalence relation as $\sim_k$ over $\mathbb{R}^n$, then $\mathbf{x} \sim_k \mathbf{y}$ iff the decimal representation of $\mathbf{x}_i, \mathbf{y}_i$ agree to first k decimal places. We extended it to hybrid state-spaces (with discrete states q) by relating two states $(q_1, \mathbf{x}_1) \sim_k (q_2, \mathbf{x}_2)$ iff they have the same discrete states $q_1 = q_2$ and $\mathbf{x}_1 \sim_k \mathbf{x}_2$. We note that the $\sim_k$ satisfies the requirements of an equivalence relation, i.e., it is reflexive, symmetric and transitive.

As noted earlier, explicitly constructing this tiling is impractical for most systems. The number of cells is infinite if $\mathcal{X}$ is unbounded. Even when $\mathcal{X}$ is bounded, the number of cells is exponential in the dimensionality of $\mathcal{X}$. We reiterate that our technique does not seek to fully construct the tiling, or the abstraction resulting from it.

Abstraction. Given a quantization function Q_ϵ (which induces an ϵ-tiling), we define an existential abstraction using a family of abstract timed parameterized reachability relations $\overset{t}{\rightsquigarrow}$.

An abstract state (or cell) C' is reachable from C, if and only if, there is a witness trajectory segment of time length t beginning from $\mathbf{x}$ and ending at $\mathbf{x}'$ such that $\mathbf{x} \in C$ and $\mathbf{x}' \in C'$. Formally,

$$C \overset{t}{\rightsquigarrow} C' \iff \exists \mathbf{x} \in C.\, \exists \mathbf{x}' \in C'.\, \mathbf{x} \overset{t}{\rightsquigarrow} \mathbf{x}'.$$

This lifting of the reachability relation can be easily extended to systems with inputs.

$$C \overset{t}{\rightsquigarrow} C' \iff \exists \mathbf{x} \in C.\, \exists \mathbf{x}' \in C'.\, \exists u \in \mathcal{U}.\, \mathbf{x} \overset{t,u}{\rightsquigarrow} \mathbf{x}'$$

For a fixed time step t, we represent the relation $\overset{t}{\rightsquigarrow}$ by $\rightsquigarrow$.

Example 4.2.2 Fig. 4.6 shows the trajectories of a van der Pol oscillator whose dynamics are defined by a system of ODEs over $(x_1, x_2) \in \mathbb{R}^2$: $\dot{x}_1 = x_2,\ \dot{x}_2 = -5(x_1^2 - 1)x_2 - x_1$. Attempting 1000 random simulations on the initial set Fig. 4.6(a) yields precisely one trajectory that witnesses the violation. Fig. 4.6(b)

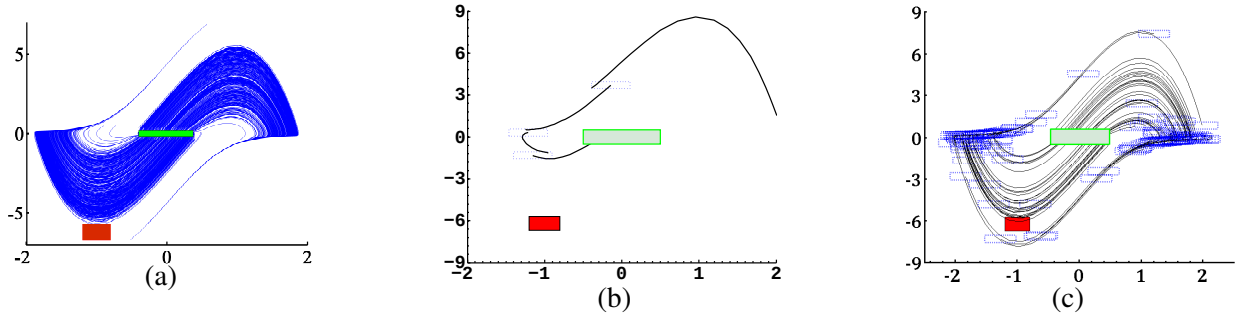

Figure 4.6: (a) Van der Pol ODE trajectories with initial set $\mathcal{X}_0 : [-0.4, 0.4] \times [-0.4, 0.4]$ are shown in green and the unsafe set $[-1.2, -0.8] \times [-6.7, -5.7]$ in red. (b) single segmented trajectory. (c) Randomly simulated segmented trajectories. Blue boxes highlight the gaps between segments.

shows an example of a segmented trajectory, while Fig. 4.6(c) shows a collection of 100 segmented trajectories. Each segmented trajectory in this collection has two segments; the source of the first segment is picked from a random sampling of the initial state set, while the source of the second segment is chosen by adding a random vector to the destination of the first segment.

4.3 Abstraction as a Reachability Graph

The discussed abstraction can be defined as a reachability graph. In this graph, each node represents a cell and two nodes have an edge iff a reachability relation exists between them. A cell is reachable from another cell, if there exists a path in this graph between the nodes representing them. Hence, an abstract violation or counter-example can be found by searching for a path between the initial and unsafe nodes.

Definition 4.3.1 (Abstract State Graph) Let $\Delta > 0$ be a fixed time step. The abstract state graph $\mathcal{H}(\Delta)$ for time step Δ is defined by the set of vertices $\mathcal{C}$, and edges (C, C') whenever $C \overset{\Delta}{\rightsquigarrow} C'$. Let $\mathcal{C}_0$ denote the collection of initial cells in $\mathcal{C}$, i.e., cells C such that $C \cap X_0 \neq \emptyset$. Further, let $\mathcal{C}_u$ denote the set of unsafe cells, or cells C' such that there is a state $\mathbf{x}_j \in C'$ that reaches an unsafe state $\mathbf{y} \in X_f$ within time $0 \leq t_j < \Delta$. The abstraction $\mathcal{H}(\Delta)$ is given by $\left\langle \mathcal{C}, \overset{\Delta}{\rightsquigarrow}, \mathcal{C}_0, \mathcal{C}_u \right\rangle$.

To make this problem tractable in practice, we explore this graph on-the-fly and define **budgets** as additional stopping criteria. Finding a violation involves labeling the initial cells as source nodes and the unsafe cells as sink nodes. The violation is a path in the graph from the source nodes to the sink nodes. A graph search is then conducted to find a path between any of the source and any of the sink nodes. It proceeds by selecting a node and exploring its outgoing edges (relations). Once discovered, they are added to the graph. This continues until the exploration budget is exhausted.

The graph search affects the efficiency of the approach. It can either proceed form the initial states by using a basic breadth-first (BFS) or depth-first (DFS) exploration, or it can use an A^* like algorithm combined with admissible heuristics. However, the search need not be 'sequential' and can be directed by a random procedure which selects cells by sampling them uniformly from the state-space. We use an approach termed **scatter-and-simulate** to accomplish this. It is defined and analyzed later in this section.

Besides the lack of scalability, there are other computational barriers to constructing such an abstract state graph. For instance, we would need a formal procedure to (a) determine if two cells C, C' are connected, and (b) decide if a cell C_k is unsafe in the abstraction. Such tasks require us to perform symbolic reasoning about dynamics of black box (or a complex non-linear) systems, which is assumed infeasible. Therefore, we resort to a simulation-based approach to explore the abstract graph $\mathcal{H}(\Delta)$.

Given a node C, we sample its concrete states $\{\mathbf{x}|\mathbf{x} \in C\}$ uniformly at random. Using numerical simulations SIM, we can then generate trajectory segments beginning from each of these samples and find witnesses to relations $C \overset{\Delta}{\rightsquigarrow} C'$ in the form of $x \overset{\Delta}{\rightsquigarrow} \mathbf{x}'$, where $\mathbf{x} \in C$ and $\mathbf{x}' \in C'$. If the system has inputs, the input space $\mathcal{U}$ can also be sampled to obtain finite samples $\mathbf{u} \in \mathcal{U}$ and combination pairs of $(\mathbf{x}, \mathbf{u})$ can be used to generate relations of the form $\mathbf{x} \overset{\Delta,\mathbf{u}}{\rightsquigarrow} \mathbf{x}'$.

We now formally show that segmented trajectories are paths through an abstraction of the underlying system. A path in the graph involving more than two nodes represents a segmented trajectory. Hence, once an abstract counter-example is found, we try to concretize it by iteratively refining the abstraction. This refinement entails decreasing the cell sizes by increasing the value of ϵ in order to decrease the gaps between segments. As we show later, this might not always converge to a violation.

Example 4.3.1 Fig. 4.7 is a partial depiction of $\mathcal{H}(\Delta)$ for the system from Example 4.2.2. The figure shows $\mathcal{C}_0$, $\mathcal{C}_u$, and a subset of cells reachable from the initial cells. Edges between cells are shown by showing a trajectory between states that belong to the cells.

Abstract Paths Consider a path $P_\pi : C_0 \to C_1 \to \cdots \to C_N$ through the abstract graph $\mathcal{H}(\Delta)$. Corresponding to this path, we define a **witness segmented trajectory** $\mathbf{S}_\pi$ with N segments $\langle \pi_{\tau_0}, \pi_{\tau_1}, \ldots, \pi_{\tau_{N-1}} \rangle$, where $start(\pi_{\tau_i}) \in C_i$, $end(\pi_{\tau_i}) \in C_{i+1}$ and $start(\pi_{\tau_i}) \overset{\Delta,u}{\rightsquigarrow} end(\pi_{\tau_i})$. The existence of this witness $\mathbf{S}_\pi$ follows immediately from the construction of $\mathcal{H}(\Delta)$. Furthermore, since the tiling $\mathcal{C}$ is an ϵ-tiling, we have that each inter-segment gap $d(\mathsf{dest}(\tau_i), \mathsf{src}(\tau_{i+1}))$ is at most ϵ. Therefore, the overall cost is $\text{COST}(\mathbf{S}_\pi) \leq (N-1)\epsilon$. Substituting $N = \lceil \frac{T}{\Delta} \rceil$, we get the below lemma.

Lemma 4.3.1 For every path π through the abstract graph $\mathcal{H}(\Delta)$, there exists a witness segmented trajectory $\mathbf{S}_\pi$, such that $\text{COST}(\mathbf{S}_\pi) \leq \left(\lceil \frac{T}{\Delta} \rceil - 1\right) \epsilon$.

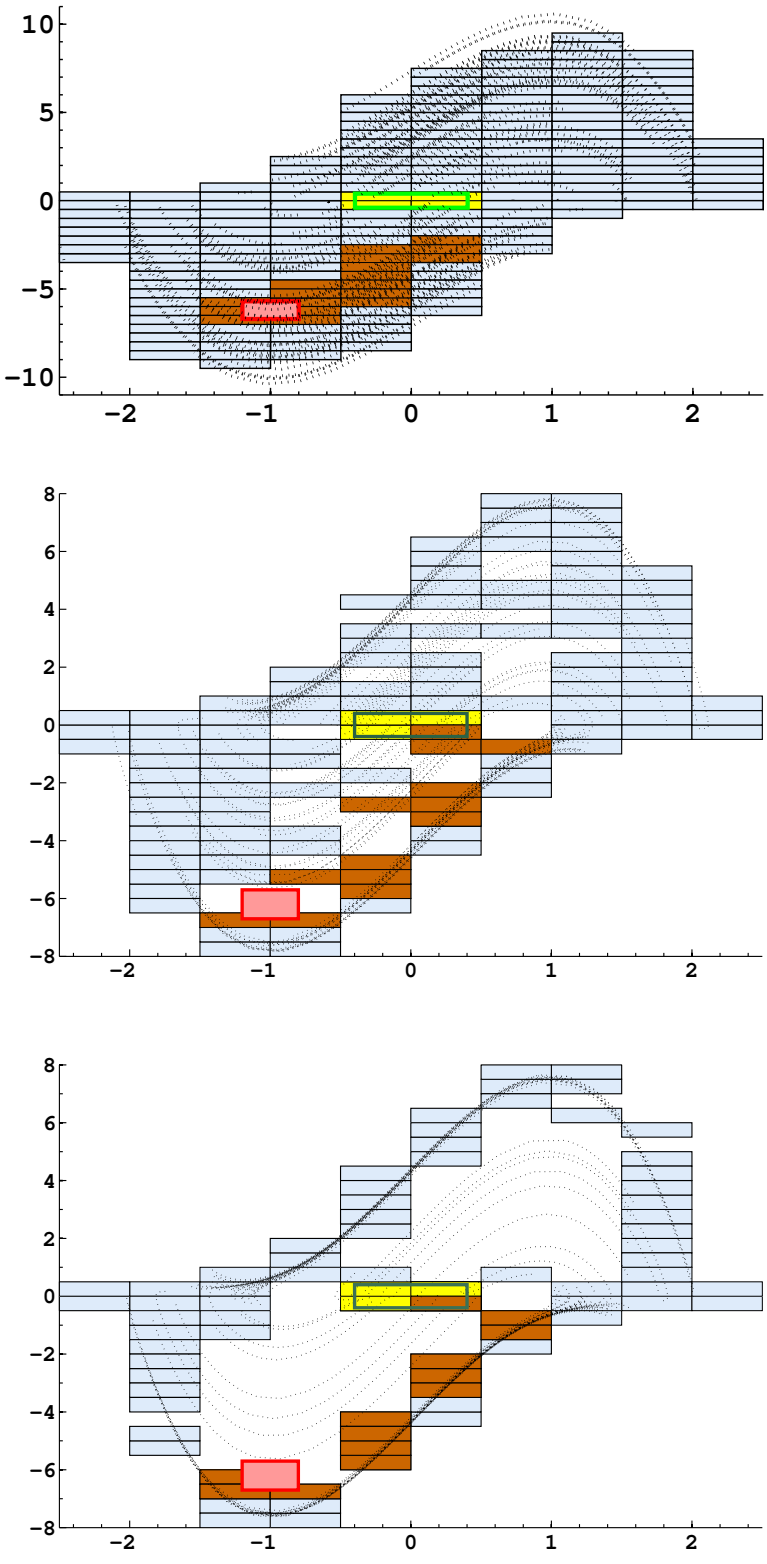

Figure 4.7: Visualization of a subset of $\mathcal{H}(\Delta)$ showing cells reachable from the initial set of states for the van der Pol system. Yellow cells are initial (but not unsafe), cells shaded brown are unsafe and blue cells are neither initial nor known to be unsafe. The dotted trajectory segments represent the edges.

4.4 Parameters of the Abstraction (Δ and ϵ)

The abstraction is clearly parameterized by the ϵ through the quantization function Q_ϵ which decides the size of the tiling, and the time length of the trajectory segments Δ. The effect of ϵ can be mitigated, as it only affects the first abstraction in the complete refinement process. However, it still plays an important role in practice. This is discussed in greater detail in the next section.

Initial Abstraction Size (ϵ). The effect of the size of tiling can be understood as the coarseness or fineness of the resulting abstraction. When only a finite number of cells are to be explored, small size of cells imply more number of cells and consequently, more relations. On the other hand, large cell sizes imply fewer relations and a very coarse picture of the dynamics can be revealed. In the limit, as $\epsilon \to 0$, the abstract states reduce to concrete states, requiring the search to find reachability for points. On the other extreme, with $\epsilon \to \infty$, the abstraction will be described by only one cell. Such a cell will encompass all of the state-space, and will contain both the initial and unsafe states in its interior. This trivially declares the existence of a violation and is of no use in practice.

We now look at Δ which can also be thought of as the **time step** of the resulting discrete abstraction.

Time Step (Δ). The time step decides the length of the trajectory segments. With a large Δ, the relation $\overset{\Delta}{\rightsquigarrow}$ can include complex dynamics, involving multiple mode switches and effects of non-linear dynamics. At the limit $\Delta = T$, constructing the abstraction reduces to the (undecidable) reachability problem: determining if an abstract state is reachable. At the other extreme, as $\Delta \to 0$, every existing cell relation is revealed. As a result, the abstraction becomes too conservative, capturing all the relations present in the original system. We do not consider the case of $\Delta = 0$, where the relation reduces to the identity function and a cell is only connected to itself. We can see the effect of varying Δ for the van der Pol system in Fig. 4.7.

4.5 Search for Abstract Counter-examples

Our search for falsification is based on discovering just enough relations to help us find the violating trajectory. As we cannot find this out a priori, we rely on heuristics. In this section we elaborate on the sampling based search methodology which uses the heuristic: **scatter-and-simulate**.

A sampling based search proceeds by sampling a subset of the state space and simulating the samples using the SIM function for a finite duration in time Δ. We now discuss the various parts of such an approach, namely the sampling process, the simulation and the overall search.

Sampling. To find relations between cells, we need to select K samples from them. A sampling function will assume a particular distribution on the states; a good choice of the distribution will bias the search procedure to quickly discover the relations required to find a violation. A 'perfect' distribution will sample the exact states which lie on the violating trajectory. Clearly, selecting the perfect distribution would require the knowledge of the violation. More practical solutions [54, 95] guess a distribution and then tune it according to some heuristics as the search proceeds. The selection of heuristics is often not clear and instead, most approaches restrict themselves to a uniform random distribution. Similar ideas are applicable to the sampling of inputs when present. The sampling process takes in a cell C and computes a sampled set $sample(C) = \{\mathbf{x} | \mathbf{x} \in C\}$. The other aspect of sampling, is the number of samples K. Clearly, the more the number of samples, the more thorough the search, but also, the more expensive.

Simulations. This step is straightforward and requires computing the end points $\mathbf{x}'$ of the trajectory segments beginning from the sample set $sample(C)$. For every cell, it computes the set $\{\text{SIM}(\mathbf{x}, \Delta) | \mathbf{x} \in sample(C)\}$. Q_ϵ is then used to determine the corresponding reached cell C'.

The search procedure now involves selecting a cell C and calling the sampling and simulation functions to discover reach relations. This is illustrated in Algorithm 1. We now present the complete search procedure.

Algorithm 1: Establish a time parameterized reachability relation.

Input: Q_ϵ, Δ, C_s, K

Output: Set of reach relations $RR = \{C \overset{\Delta}{\rightsquigarrow} C' | C = C_s\}$

1 $\{\mathbf{x}_1, \ldots, \mathbf{x}_K\} = \mathsf{sample}(C_s)$
2 **foreach** $\mathbf{x}$ **in** $\{\mathbf{x}_1, \ldots, \mathbf{x}_K\}$ **do**
3 $\quad \mathbf{x}' = \text{SIM}(\mathbf{x}, \tau)$
4 $\quad C'_s = Q_\epsilon(\mathbf{x}')$
5 $\quad RR = RR \cup \{C \overset{\Delta}{\rightsquigarrow} C'_s\}$

4.5.1 Scatter and Simulate

In this section, we explore the abstract graph $\mathcal{H}(\Delta)$ by sampling a finite subgraph $G(\mathsf{V}, \mathsf{E})$. We call the approach **scatter-and-simulate** to reflect its two main steps: (1) uniformly sample a reachable cell and the input space [2] to obtain pairs of initial states and inputs (2) perform repeated simulations from the obtained states for a fixed time step Δ.

The basic algorithm is shown in Algorithm 2. The two main parameters for the algorithm are the fixed time step Δ and the number of samples to select in each cell $K > 0$. The search is initialized by sampling the initial region $\mathcal{X}_0$, and adding the sampled cells into a work-list (Line 1). For each cell C_j in the work-list, we (uniformly) sample K concrete states in the cell and K inputs from signals $\mathcal{U}$ (Lines 5,6). We then use a numerical simulator to obtain trajectories for Δ seconds (Line 8). We identify the cells corresponding to the end states of the trajectories and add them to workList and V, if previously unseen (Lines 11,12). We also add appropriate edges to E (Line 13). If the simulation starting from $\mathbf{x}_{i,j} \in C_j$ intersects the unsafe set $\mathcal{X}_f$, then we mark the entire cell C_j as unsafe in the abstraction (Line 14). We bound the size of the subgraph G that we wish to explore with the parameter L. We note that the size of the graph G thus obtained is restricted to L vertices and $O(L \times K)$ edges.

The data structure used to implement the workList affects the nature of the search. A guided state-space search A^* using an admissible (under-approximating) heuristic [101] is implemented by using a priority queue for workList. Alternatively, our approach can be modified using motion planning techniques such as RRTs to explore the discrete abstraction in a probabilistically complete fashion.

Maintaining the Time Horizon. Since we are interested in exploring S up to the time horizon T, Algorithm 2 should be restricted to nodes that are reachable within $N = \lceil \frac{T}{\Delta} \rceil$ steps from an initial cell. Therefore, Algorithm 2 is modified to ensure that every node that is popped out of the workList has a shortest path length of at most N.

Identifying Likeliest Abstract Counter-examples. We now explain how we can use the graph G to help search for abstract counter-examples. These are paths in G of length at most $N = \lceil \frac{T}{\Delta} \rceil$ from initial cells

[2] We assume the input space $\mathcal{U}$ to be compact.

Algorithm 2: Scatter-and-Simulate search for exploring $\mathcal{H}(\Delta)$.

Input: Time-bounded Reachability problem $\langle S, \mathcal{X}_0, \mathcal{X}_f, T\rangle$, Scatter amount K, Simulator function SIM_S, size limit L

Output: Subgraph $G(\mathsf{V}, \mathsf{E})$, initial cells V_0 and unsafe cells V_u.

```
workList := sampleInitialSetAndCollectCells(X_0) ;
V_0 := workList, V_u := {}, E := {}, V := V_0 ;
while workList ≠ ∅ and |V| < L do
    C_i := pop(workList) ;
    (x_{1,i}, ..., x_{K,i}) := sampleUniformly(C_i) ;
    (u_1, ..., u_K) := sampleInputSignals(U) ;
    for k ∈ [1, K] do
        x'_{k,i} = SIM_S(x_{k,i}, u_k, Δ) ;
        C'_{k,i} := identifyCellFromConcreteState(x'_{k,i}) ;
        if C'_{k,i} ∉ V then
            workList := push(C'_{k,i}, workList) ;
            V := V ∪ {C'_{k,i}} ;
        E := E ∪ {(C_i, C'_{k,i})} ;
        if x'_{k,i} ∈ X_f then V_u := V_u ∪ {C'_{k,i}} ;
```

V_0 to cells labelled unsafe V_u. In order to prioritize the likeliest counter-examples, we need a notion that associates costs with paths. As each path π is associated with at least one witnessing segmented trajectory σ, we equate the cost of a path with the cost of the minimal cost witnessing segmented trajectory for π.

For a given edge e in G, let $TS(e)$ be a set of trajectory segments defined as the set $\{\tau \mid \mathsf{src}(\tau) \in \mathsf{src}(e) \wedge \mathsf{dest}(\tau) \in \mathsf{dest}(e)\}$, i.e., the collection of all trajectory segments beginning and ending in the source and destination cells of e respectively. Two edges $e_1, e_2 \in \mathsf{E}$ are said to be adjacent iff $\mathsf{dest}(e_1) = \mathsf{src}(e_2)$. Let $\tau_i \in TS(e_1)$ and $\tau_j \in TS(e_2)$, we then define a weight $W(e_1, e_2)$ for edges e_1, e_2 as follows:

$$W(e_1, e_2) = \begin{cases} \min d(\mathsf{dest}(\tau_i), \mathsf{src}(\tau_j)) & \text{if } e_1, e_2 \text{ are adjacent} \\ \infty & \text{otherwise.} \end{cases} \tag{4.1}$$

The cost of path $\pi : e_1 e_2 \ldots e_m$ in G is then defined as $\text{COST}(\pi) = \sum_{j=1}^{m-1} W(e_j, e_{j+1})$; this quantity is finite as each edge e_i in π is adjacent to e_{i+1}.

Even though the cost is defined over pairs of edges rather than edge weights, a simple modification of Dijkstra's shortest path algorithm can be used to compute shortest paths from an initial node to an unsafe node. If no such path exists, our approach re-executes the scatter-and-simulate step (Algorithm 2) with

increased values for the size of the graph L and the scatter amount K.

Fig. 4.7 depicts the scatter-and-simulate algorithm for the van der Pol system in Example 4.2.2, by limiting the number of vertices (L) to 200 and the scatter per cell (K) to 60.

Remarks. We can compute all paths from the initial node to the unsafe node, or have a budget and prioritize the search using the cost function over segmented trajectories. If no such path exists, our approach re-executes the scatter-and-simulate step (Algorithm 2) with increased values for the size of the graph L and the scatter amount K. If a robust path exists from an initial to an unsafe cell in $\mathcal{H}(\Delta)$, then Algorithm 2 will discover it in the limit with probability 1.

4.5.2 Analysis of Scatter and Simulate

Scatter-and-simulate (Algorithm 2) explores the abstract state graph $\mathcal{H}(\Delta)$ in a randomized fashion. In doing so, it suffers from two drawbacks w.r.t. discovering violations: (a) it may miss an edge and (b) it may fail to label a node as unsafe.

For a cell C_j in the ϵ-tiling, let $N(C_j)$ represent its neighbors in $\mathcal{H}(\Delta)$. Algorithm 2 samples a subset of the neighbors from $\mathcal{H}(\Delta)$. Unfortunately, not every neighbor in $N(C_j)$ will be explored by scatter and simulate, even when system has simple constant dynamics as in Example 4.5.1.

Example 4.5.1 Consider a one dimensional autonomous system with dynamics $\dot{x} = 1$ and a cell C defined by the interval $x \in [0, 1]$. Let us fix $\Delta = 1$. Consider the cell D defined by the interval $[2, 3]$. We note that $C \overset{1}{\rightsquigarrow} D$, since $(x = 1) \overset{1}{\rightsquigarrow} (x = 2)$.

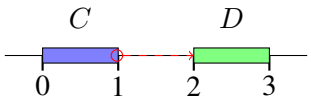

If we sampled the cell C uniformly at random in Algorithm 2, the probability of a single trajectory segment reaching D is zero. This is because, $x = 1$ is the single state in C that can reach D in one time step. Sampling this single state has probability 0.

Consider the function defined by $\textsc{sim}_S(\mathbf{x}_0, u, \Delta)$ for a fixed Δ; let us denote it by Φ. Consider the probability that the edge $e : C \overset{\Delta}{\rightsquigarrow} D$ in $\mathcal{H}(\Delta)$ can be discovered by sampling C, and denote it by $\mathbb{P}(C, D)$.

The probability is well-defined if we assume that Φ is measurable when restricted to cell C. The value of $\mathbb{P}(C, D)$ is a function of the distributions chosen to sample states and inputs. For the purpose of this discussion, let us fix a uniform distribution for sampling the "scatter" states, and also fix the set of inputs to a finite set, and consider a uniform distribution over this set.

Definition 4.5.1 (Robust Edges) An edge $e : (C, D) \in \mathcal{H}(\Delta)$ is robust iff its probability $\mathbb{P}(C, D) > 0$. A path π is robust if each of the edges in the path is robust.

The following shows that if a robust path exists from an initial to an unsafe cell in $\mathcal{H}(\Delta)$, then Algorithm 2 will discover it in the limit with probability 1. As a technicality, we assume that the workList data structure is **fair** (example, a FIFO queue), i.e., every cell placed in it is eventually processed. The result that follows directly from the definition of robust edges, and from the fundamental laws of probability:

Lemma 4.5.1 Let C be a cell reachable from some initial cell C_0 through a robust path π of length at most $\lceil \frac{T}{\Delta} \rceil$. As $L \to \infty, K \to \infty$, the cell C will belong to the graph G explored by Algorithm 2 with probability 1.

Proof 4.5.1 Algorithm 2 will explore each node along π starting with C_0 with some probability $p > 0$. Therefore, as $K \to \infty$, for each node C' in the graph G, every robust edge outgoing from C' is discovered with probability 1. Since $L \to \infty$ and the workList data structure is "fair", we note that every discovered node is eventually processed and therefore every node along π is eventually discovered.

A limitation of our approach is the lack of probabilistic guarantees on its ability to discover non-robust edges in $\mathcal{H}(\Delta)$. However, even for a fixed scatter amount K for each cell, we are not guaranteed to discover all the robust outgoing edges in $N(C_j)$, for a given cell C_j. The choice of value K is thus a crucial tradeoff between scalability and effectiveness. A simple technique is to fix two thresholds p and c to find a value K that guarantees that edges $e : C \overset{\Delta}{\rightsquigarrow} D$ with $\mathbb{P}(C, D) \geq p$ are discovered with a probability of at least c. Assume that Algorithm 2 draws K independent and identically distributed samples for the states and inputs.

Lemma 4.5.2 If $K \geq \frac{\log(1-c)}{\log(1-p)}$ then an edge $e : C \overset{\Delta}{\rightsquigarrow} D$ with $\Pr(C, D) \geq p$ is discovered with probability at least c.

Proof 4.5.2 Consider a sequence of K simulations and let us assume that none of them allowed us to discover the edge e. The probability of this happening is at most $(1-p)^K$. We therefore wish to ensure that this event happens with probability at most $(1-c)$.

$$(1-p)^K \leq (1-c)$$

Therefore, we obtain $K \geq \frac{\log(1-c)}{\log(1-p)}$.

For instance, drawing $K = 59$ or more samples per cell will guarantee that any single outgoing edge with probability 0.05 or more is found more than 95% of the time by our sampling process.

In summary, Algorithm 2 finds robust edges in $\mathcal{H}(\Delta)$, while non-robust edges are discovered **almost never** (with probability 0). Lemma 4.5.1 guarantees if the workList in Algorithm 2 is **fair**, as $K, L \to \infty$, all robust edges in $\mathcal{H}(\Delta)$ are discovered **almost surely** (with probability 1). As a result, all robust paths are also discovered **almost surely**. Next, Lemma 4.5.2 provides bounds on the number of samples per cell K to achieve guarantees on the probabilities of missing an edge.

4.6 Counter-example guided Refinement

Once an abstract counter-example has been obtained, we need to ascertain if it can be concretized as a counter-example of the concrete system. This can be done by refining the abstract states along the abstract counter-example and hence, refining the relations.

We now present a way to refine the abstraction induced by an ϵ-tiling $\mathcal{C}$ by defining the notion of a refined tiling. The basic idea of refinement is to construct a δ-tiling $\mathcal{D}$ where $\delta < \epsilon$, and the cells in $\mathcal{D}$ subdivide those in $\mathcal{C}$. We then wish to check if the abstract counter-examples corresponding to the ϵ-tiling continue to be counter-examples in the δ-tiling. We first formalize the notion of a refined tiling.

Definition 4.6.1 (Refined Tiling) Let $\mathcal{C}$ be an ϵ-tiling of $\mathcal{X}$. A refinement $\mathcal{D}$ of $\mathcal{C}$ is a tiling of $\mathcal{X}$ that satisfies the following:

(1) $\mathcal{D}$ is a δ-tiling for some $\delta < \epsilon$.

(2) For every $D_j \in \mathcal{D}$, there is a unique cell $C_j \in \mathcal{C}$ such that $D_j \subseteq C_j$. D_j is called a **sub-cell** of C_j.

(3) For every $D_j \in \mathcal{D}$ and $C_k \in \mathcal{C}$ if $\mathsf{interior}(D_j) \cap \mathsf{interior}(C_k) \neq \emptyset$ then $D_j \subseteq C_k$.

For an ϵ-tiling, and its corresponding refined δ-tiling, let us denote their respective abstract state graphs (as defined in Def. 4.3.1) by $\mathcal{H}_\epsilon(\Delta)$ and $\mathcal{H}_\delta(\Delta)$.

Our approach performs up to P refinement steps. At each step, a slight modification of scatter-and-simulate algorithm is applied. The resulting graph G is then analyzed to find all abstract counter-examples . The cost of the counter-examples can be used to select the most promising ones. If no counter-examples exist, we declare failure (and possibly restart). Otherwise, we check if any of the abstract paths are concretizable. This step samples initial states from the initial cells for the abstract counter-examples. For each sample, it performs a complete simulation and checks if the concrete simulation results in a violation. If so, the algorithm terminates with a real violation witnessed by a concrete trajectory. Next, we compute a set of abstract counter-example paths (PATHS) to guide the exploration of the refinement in the next step. Finally, the value of ϵ is scaled down for the refinement. We note that the scatter-and-simulate algorithm is modified by providing it a set of PATHS. The set of abstract paths serves to restrict the search for counter-examples in the refinement. We consider two strategies for this restriction.

Likely Initial Cells: In this strategy, we use the initial cells of counter-example paths in PATHS. Here, we replace the RHS of Line 1 of Algorithm 2 by a random sampling of such initial cells.

Refining Abstract Counter-example Paths: In this strategy, we use all cells that belong to some path in PATHS. We explore $\mathcal{H}_\delta(\Delta)$ using Algorithm 2, while restricting our attention to the cells in PATHS. Therefore, Algorithm 2 is modified at line 9 and line 11 to ensure that a cell is added only if it is a sub-cell of a cell in the set PATHS.

Example 4.6.1 Fig. 4.8 shows a series of refinements for the van der Pol system from Example 4.2.2 with decreasing values of ϵ. In each step, we obtain paths in the resulting abstract state graphs, leading from some initial to an unsafe cell. The corresponding segmented trajectories also have costs that decrease in direct proportion to ϵ.

For general hybrid systems, our refinement operation might not converge to a violation. In fact in the complete presentation [165], we provide an example where our refinement procedure can decrease the cost arbitrarily close to zero, without ever converging to a trajectory of the system. The example relies on 'non-robust' behaviors and a careful selection of the initial segmented trajectory which can never be spliced together. This is constructed by letting the trajectory segments lie on either side of a guard surface of measure zero, preventing the splicing. In practice, such a pathological behavior will be hard to observe, and we can exclude them using minimal assumptions to guarantee robust behaviors in the system.

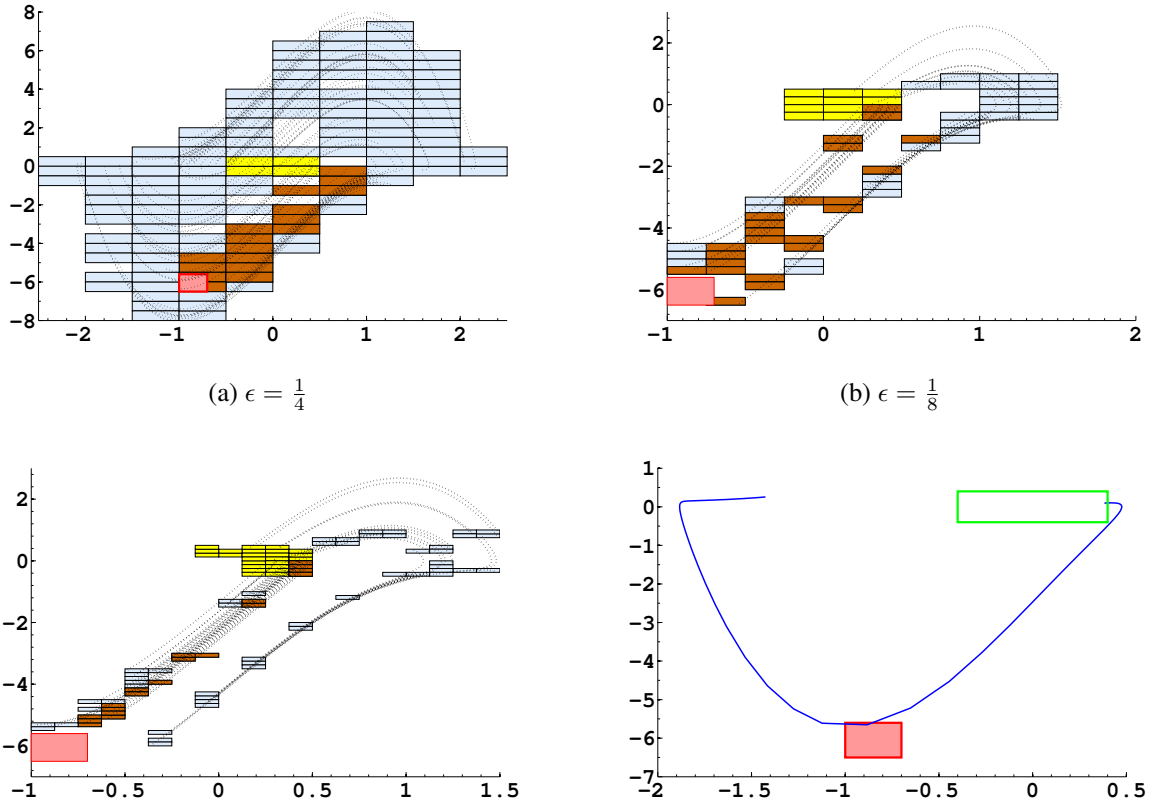

(a) $\epsilon = \frac{1}{4}$

(b) $\epsilon = \frac{1}{8}$

(c) $\epsilon = \frac{1}{16}$

(d) Error Trajectory

Figure 4.8: A series of refinements for the van der Pol system with decreasing values of ϵ. A counter-example path exists in each refinement step, yielding a concrete violation.

4.6.1 Asymptotic Analysis of Refinement

Using the above mentioned strategies to explore the state graph based on a δ-tiling restricts the exploration to regions associated with previously explored abstract states in the ϵ-tiling. As a result, each concrete state obtained by sampling is now clustered within a smaller cell. Let the tiling granularity in the i^{th} refinement step be ϵ_i, and let a witnessing segmented trajectory corresponding to an abstract counter-example path π in $H_{\epsilon_j}(\Delta)$ (if one exists) be denoted σ_j. Then, recalling the result from Lemma 4.3.1, $\textsc{Cost}(\sigma_j) \leq \left(\lceil \frac{T}{\Delta} \rceil - 1\right) \epsilon_j$.

Consider a series of refinement steps, wherein the i^{th} step involves an ϵ_i-tiling $\mathcal{D}_i$, such that $\epsilon_1 > \epsilon_2 > \cdots$ is a strictly decreasing sequence converging to 0 in the limit. Assume that at each refinement step, we obtain an abstract counter-example π_i from an initial cell of $\mathcal{H}_{\epsilon_i}(\Delta)$, the graph at the i^{th} step to an unsafe cell. The costs of the witnessing segmented trajectories converge to zero as well. This could lead us to believe that, in the limit, our approach is guaranteed to find a violation. We show that this is not true.

There can be an infinite sequence of ϵ_1, ϵ_2, $\cdots$, -tilings of a hybrid system and a sequence σ_{ϵ_1}, σ_{ϵ_2}, $\cdots$ of witnessing segmented trajectories from an initial set to an unsafe set in the corresponding abstract state graphs of the tilings such that, $\textsc{cost}(\sigma_{\epsilon_1}) > \textsc{cost}(\sigma_{\epsilon_2}) > \ldots$, and $\lim_{k\to\infty} \textsc{cost}(\sigma_{\epsilon_k}) = 0$, but no concrete trajectory of 0 cost exists in the actual hybrid system. We illustrate this with an example below.

Example 4.6.2 In this example, we show that convergent limits of segmented trajectory may not be a trajectory. For simplicity, we consider a system S with no inputs and two discrete modes q_0 and q_1. Let the dynamics in mode q_0 be the ODEs $\frac{dx}{dt} = 1$, $\frac{dy}{dt} = 2$, and in q_1 be the ODEs $\frac{dx}{dt} = \frac{dy}{dt} = 0$. The system transitions from mode q_0 to q_1 upon hitting the guard set $x + y = 4$. The initial set is taken to be $\mathcal{X}_0 : \{q_0\} \times [0, 0.5] \times [0, 0.5]$ and the unsafe set is taken to be $\mathcal{X}_f : \{q_0\} \times [2, 3] \times [4, 5]$. We note that no behavior can reach $\mathcal{X}_f$, as any trajectory in mode q_0 will hit the switching surface $x + y = 4$, and remain there in mode q_1. Now consider a sequence of segmented trajectories $\sigma_{2\epsilon}$, each with two segments of the form:

$$(0.5 - \epsilon, 0.5 - \epsilon) \xrightarrow{1} (1.5 - \epsilon, 2.5 - \epsilon), (1.5 + \epsilon, 2.5 + \epsilon) \xrightarrow{1} (2.5 + \epsilon, 4.5 + \epsilon)$$

$\textsc{cost}(\sigma_{2\epsilon})$ is 2ϵ with the L_∞ norm. However, as $\epsilon \to 0$, we expect the segments to converge onto the zero

cost "trajectory" $(0.5, 0.5) \xrightarrow{1} (1.5, 2.5) \xrightarrow{1} (2.5, 4.5)$. But the limit is not a valid trajectory as the system switches to the mode q_1 at $(q_0, 1.5, 2.5)$ and never changes state again.

The counter-example above illustrates 'non-robust' behavior that hybrid systems can exhibit. The example relies on the system switching at a precisely defined surface that our segmented trajectories happen to converge to asymptotically. While certainly possible, this behavior is pathological; real-life hybrid systems often exhibit robust behavior such as continuous dependence on initial condition over a small neighborhood. Under the following conditions that guarantee robust counter-examples, a zero cost segmented trajectory in the limit is, in fact, an actual system trajectory:

- Each cell in a counter-example π' in the j^{th} refinement is a sub-cell of a cell in a counter-example π in the i^{th} step for $i \leq j$.
- There is an i such that for all cells in counter-example paths at refinement steps $j > i$, the flow map defined by $\Phi(\mathbf{x}_0, u)$ (i.e., $\text{SIM}_S(\mathbf{x}_0, u, \Delta)$ for a fixed Δ) is continuous over $\mathbf{x}_0$ for each $u \in \mathcal{U}$.

Lemma 4.6.1 A zero cost trajectory segment σ is an actual trajectory of the system.

Proof 4.6.1 As $d(\mathbf{x}, \mathbf{y}) \geq 0$ for all $\mathbf{x}, \mathbf{y}$, $\text{COST}(\sigma) = 0$ implies that for each pair $\mathsf{dest}(\tau_i), \mathsf{src}(\tau_{i+1})$, the distance is 0. Further, $d(\mathsf{dest}(\tau_i), \mathsf{src}(\tau_{i+1})) = 0$ iff $\mathsf{dest}(\tau_i) = \mathsf{src}(\tau_{i+1})$. Thus, σ is an actual system trajectory.

4.7 Summary

In this chapter, we combined the ideas from multiple shooting and CEGAR, to engineer a best effort, sampling based falsification procedure for systems with black box specifications. As we will show in Chapter 6, this approach outperforms the current state-of-the-art and is scalable.

Chapter 5

Analysis of Sampled Data Control Systems

Finally, in this chapter we introduce a methodology to analyze embedded control systems. We combine the analysis of the plant from Chapter 4 with the analysis of the controller. Although, the numerical search is applicable to black boxes and hence, can be directly used for embedded control systems. It is however, more suited towards finding violations in hybrid dynamical systems.

5.1 Overview

As mentioned in Chapter 1, there are several reasons why we would like to treat a software controller separately from a plant (hybrid dynamical systems). Plant models are often created for the purpose of evaluation and testing of specific aspects of the closed-loop system. They are typically unsound approximations of the actual physical environment, which is hard to characterize completely. Therefore, a precise treatment of the controller semantics is a desirable goal in control verification, while a similar precise approach to the plant semantics might not be as useful. Also, it is often prohibitively expensive.

Another reason concerns the analysis itself. Lumping the software controller and the plant (hybrid dynamical systems) as a dynamical system for analysis is not amenable to numerical analysis. A numerical analysis (like the one introduced in Chapter 4) assumes robust behaviors. Moreover, to some extent it relies on the continuous dependence on the initial conditions. Although hybrid dynamical systems in general can exhibit behaviors which violate these assumptions, they are usually rare for physical systems. Software programs (even simple ones) on the other hand, by their very nature, have non-robust and discontinuous behaviors.

5.2 Symbolic-Numeric Methods

We now present how symbolic techniques can be used to capture the behaviors of the software program in conjunction with the plant's analysis. To do this, we extend the CEGAR framework introduced in Chapter 4 to accommodate the symbolic exploration of the controller and enable falsification for a closed loop SDCS. Before formalizing our approach, we give a brief overview of the closed loop abstraction, symbolic analysis and recall the numerical analysis.

Symbolic Analysis for Controller. For finding functional bugs like violations to safety, modeling the software program by its implementation is better than using abstract models commonly accepted by formal reachability analysis tools. Using a dedicated software centric analysis helps us achieve this. We can then model software centric issues such as fixed point arithmetic, overflows, division by zero and buffer overflows. We use symbolic execution to provide a path based coverage on the controller code but the ideas can be extended easily to less precise but efficient methods like interval and affine arithmetic analysis.

Numerical Analysis of Plant. Introduced in the previous chapter, the weak black box assumptions on the plant makes our approach highly applicable to plant models in practice. Also, the analysis uses a CEGAR procedure which can be coupled with most single step controller analysis to provide an analysis for the SDCS.

Closed Loop Exploration of SDCS. Analyzing the controller and the plant together by using a model of the plant dynamics along with precisely handling the controller using symbolic executions, we can assure that bugs found in this process are potentially realizable when deploying the control system. This is often not the case with current approaches (refer Chapter 2) which simplify plant models resulting in false positives.

5.3 Symbolic Execution of Programs

Symbolic execution was first formally proposed in [96]. Since then, with increasingly powerful constraint solvers, it has evolved into an efficient code analysis technique, forming the basis for tools such as CUTE [152], KLEE [27], and Pathcrawler [162]. These tools are usually employed to generate inputs that maximize the coverage of control-flow paths in the program. For large programs, a purely symbolic approach can be quite inefficient, and a modified version of symbolic execution, where concrete states are maintained

alongside symbolic states is usually preferred. This enables program analysis in the presence of complex constraints that the constraint solvers cannot handle, and efficient generation of test cases for path coverage, when 100% coverage is infeasible. Due to their symbolic nature, such techniques can be fused easily with CEGAR-like techniques [33], which we propose in this chapter. Recent surveys on symbolic execution can be found at [28, 29].

5.4 Example: Thermostat-Heater Temperature Controller

Before continuing, we demonstrate the applicability and usefulness of our approach on a simple thermostat-heater SDCS.

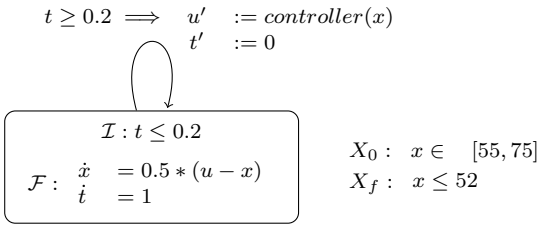

Figure 5.1: The hybrid automaton for the room-heater-thermostat sampled data system with initial set X_0 and unsafe set X_f.

Consider a room heating system regulated by a thermostat that controls the operating mode of the heater. The plant dynamics are modeled as a single-mode hybrid automaton with linear dynamics as shown in Fig. 5.1. The controller action encapsulated inside the reset map of this automaton can be one of three kinds: OFF, REGULAR HEATING, or FAST HEATING. The control software is a `C` program shown in Figure 5.3. This code incorporates extra control logic to prevent the heater from being switched between different modes frequently. The controller is run at 5 Hz (i.e, a controller time-step of 0.2 seconds). Assuming the initial temperature of the room to be $x \in [55, 75]^\circ$ F, we try to find a scenario where the temperature dips too low ($x < 52^\circ$ F) within 10s of system operation.

Using our described approach we can find the violation in a few seconds. We can narrow down the search to initial room temperatures in a small range around $69.9^\circ F$. The cause is determined to be the poorly coded chatter protection, which hinders the functionality of the thermostat. In the case of the uncovered

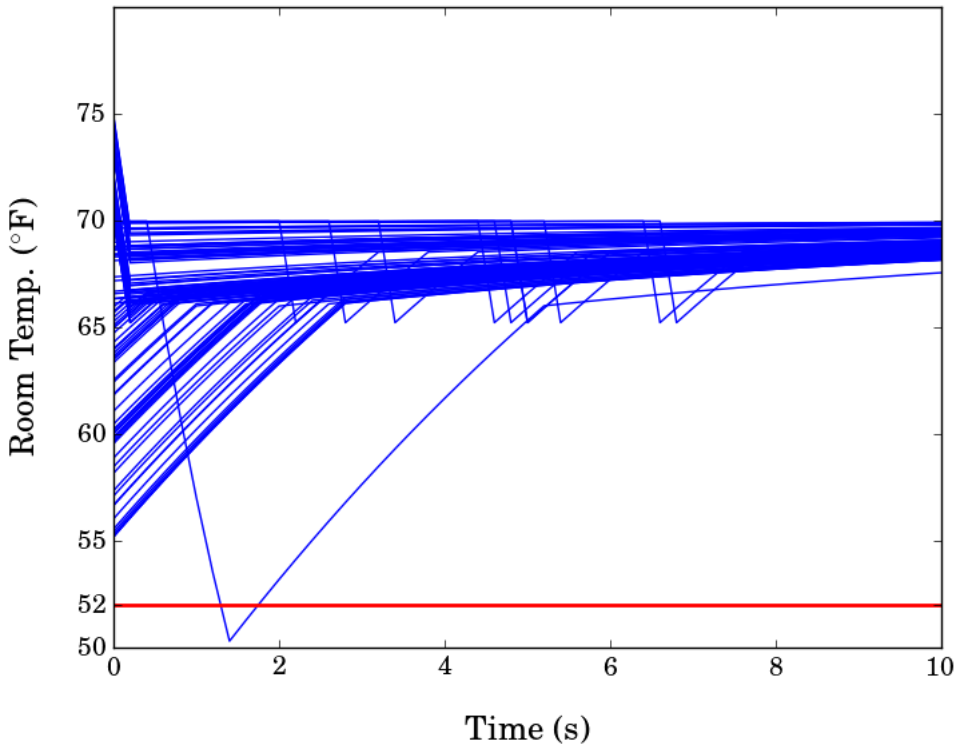

Figure 5.2: A plot showing around 100 biased random simulations with $T = 10s$. The unsafe regions is below red line at $(52°F)$. Biasing towards $x \in [69.9, 70]$ helps magnify the unsafe behaviors.

violation, the system chatters, and the thermostat forces the heater to be non-responsive for too long, causing the room temperature to dip too low. Using 100,000 random simulations running for 20 minutes (about 130x longer than our approach), we find 45 violations, where the temperature dips below 52°F. This corresponds to roughly a 1 in 2000 chance of discovering this violation by Monte Carlo simulations with uniform random sampling of the initial state.

5.5 SDCS Model

We are interested in analyzing closed-loop systems consisting of a **plant** and a **controller**, wherein the plant is a physical process modeled as a dynamical system and the controller is implemented as a set of software tasks that execute repeatedly with a fixed period known as the **sampling period**. We now briefly recap the model definitions.

Definition 5.5.1 (Plant Model) The plant model is described by a set of plant states $\mathcal{X}$, plant inputs $\mathcal{U}$ and plant outputs $\mathcal{Y}$ along with two functions:

- A simulation function $\textsc{sim} : \mathcal{X} \times \mathcal{U} \times \mathbb{R}_{\geq 0} \mapsto \mathcal{X}$, where $\textsc{sim}(\mathbf{x}, \mathbf{u}, \tau)$ maps the current state $\mathbf{x}$ at time t to the next state $\mathbf{x}'$ at time $t + \tau$ (where $\tau \geq 0$) with the assumption that the input signal $u(t)$ is a constant $\mathbf{u} \in \mathcal{U}$ for $t \in [0, \tau)$.
- An observation function $g : \mathcal{X} \mapsto \mathcal{Y}$ that maps the current state $\mathbf{x}$ to the observable output $\mathbf{y} = g(\mathbf{x})$.

The controller samples the output $\mathbf{y}$ of the plant at regular time instants, and updates the control input $\mathbf{u}$ before the next time instant. Controllers are assumed to have an internal state s that is updated by the execution of the controller.

Definition 5.5.2 (Controller Model) A controller is specified in terms of its input space $\mathcal{Y}$, its internal state-space $\mathcal{S}$, and the controller sampling period τ_s. Its semantics are provided by a function $\rho : \mathcal{Y} \times \mathcal{S} \mapsto \mathcal{U} \times \mathcal{S}$, where the function $\rho(\mathbf{y}, s)$ maps the controller input $\mathbf{y}$ (which is the plant output at time t) and internal state s (at time t) to $(s', \mathbf{u})$, where s' and $\mathbf{u}$ are the updated controller state and the input to the plant at time $t + \tau_s$, respectively.

5.6 Software-Centric View of the Controller

So far, we have used a map ρ to describe the controller. In most industrial embedded systems, implementations of controllers use imperative programming languages such as $\mathcal{C}$. For the purpose of our analysis, we present the controller software as a control-flow graph (CFG), a structure that focusses on the organization of the execution paths in the controller software.

In the following presentation, we omit any discussion on features such as function calls, arrays, and pointers, but remark that as our technique uses off-the-shelf analysis tools, such features can be handled by our implementation. On the other hand, a programming language like $\mathcal{C}$, allows dynamic memory allocation, recursive execution without known termination bounds, pointer arithmetic, and complex data structures. Such features are rarely found in real-time embedded control software, and we can safely assume that we do not encounter these in the controllers to be analyzed. We now formalize the control software as a CFG.

Definition 5.6.1 (Control-Flow Graph) A control-flow graph is defined as a tuple $\langle \mathcal{V}, \mathcal{V}_i, \mathcal{V}_o, L, E, \Phi, l_0, l_f \rangle$, where $\mathcal{V}$ is a set of variables, $\mathcal{V}_i \in \mathcal{V}$ and $\mathcal{V}_o \in \mathcal{V}$ are the input and output subset[1] . L is a set of nodes (control locations), l_0, l_f are unique start and end locations, representing entry and exit points of the given program respectively. $E \subseteq l \times l$ is a finite set of directed edges, Φ is a function labeling each $edge(l, l') \in E$ with two kinds of constraints:

- An assignment constraint has the following form:

$$(v_{l'} = e(\mathcal{V}_l)) \ \wedge \bigwedge_{w_l \in \mathcal{V}_l \setminus \{v_l\}} (w_{l'} = w_l).$$

  It arises from an assignment statement $v := e$ in the program, where e is the symbolic expression signifying a function over some subset of variables in $\mathcal{V}$. The constraint itself relates the value of the modified variable v at location l' to the values of the variables at location l through the function e, and asserts that all other variables remain unchanged.

- A conditional constraint has one of the following forms:

$$1.assume(b(\mathcal{V}_l)) \qquad 2.assume(\neg b(\mathcal{V}_l)).$$

[1] Note that some of these variables represent the internal state of the controller.

It arises from a conditional statement of the form `if`(b) `then` l' `else` l''. Here b is a Boolean-valued symbolic expression[2] over the variables. For the $edge(l, l')$, the first label is used, whereas for the $edge(l, l'')$, the second label is used.

Definition 5.6.2 (Control-flow Path) An entry-exit control-flow path $\mathfrak{p}$ is a sequence of nodes, $l_0, \ldots, l_i, \ldots, l_f$, beginning with l_0 and ending in l_f, such that each location pair $(l_i, l_{i+1}) \in E$.

During program execution an $edge(l, l')$ is taken if its label evaluates to **true**. The **conditional** label is assigned the valuation of its expression b or $\neg b$. The sequence of edges naturally partitions a program into a set of paths $\{\mathfrak{p}_1, \ldots, \mathfrak{p}_N\}$. Let each path $\mathfrak{p}_i$ be described by a path constraint $\rho_i(\mathcal{V}_i, \mathcal{V}_o)$ which sequentially composes the constraints along $\mathfrak{p}_i$. The path constraint ρ_i can be understood intuitively as a combination of (a) a path condition $\xi(\mathcal{V}_i)$ on the program inputs which decides if the path is feasible and (b) a path function $f_i(\mathcal{V}_i)$ that describes the updates through the assignment statements along the path.

We can now summarize the program as the union of all possible control-flow paths $\rho = \bigcup_{i=1}^{N} \rho_i$. It can be easily shown that this union of path constraints exhaustively covers the entire set of values for $\mathcal{V}_i$, and thus, $\rho(\mathcal{V}_i, \mathcal{V}_o)$ can be written as a function on program inputs $\mathcal{V}_i := \rho_i(\mathcal{V}_i)$. In the present context, we can formulate the piecewise function which computes the controller move for a controller with N paths as follows:

$$\rho(\mathbf{y}, s) = \begin{cases} f_1(\mathbf{y}, s) & \text{if } \xi_1(\mathbf{y}, s) \\ \ldots & \\ f_N(\mathbf{y}, s) & \text{if } \xi_N(\mathbf{y}, s) \end{cases} \tag{5.1}$$

This is accomplished by using symbolic execution to find the path condition ξ_i and path function f_i for every path $\mathfrak{p}$. In general, a software program might not terminate due to the presence of an infinite path. Additionally, the number of paths in a program can be infinite. It is also non-trivial to determine such cases. Fortunately, best practices in embedded control software discourage the use of jump statements and unbounded loops. Most loops have specified, fixed bounds, and we assume that the same rule is true for the controllers that we encounter. Under this assumption, there is a finite number of finite length control paths in the controller software.

[2] It is assumed that b is side-effect free, i.e., it does not modify the values of the program variables.

We now consider the abstraction of the closed loop system by defining abstractions of the plant and the controller state-spaces.

5.7 Controller Abstraction

Given a CFG with N control-flow paths $\mathfrak{p}_1, \ldots, \mathfrak{p}_N$, recall that we have a set of concrete partial path functions $\rho_1, \ldots, \rho_N$ whose union yields the overall semantics ρ of the program as in Eq. (5.1).

Most real-world controllers use nonlinear expressions and conditions in assignment and conditional statements respectively. Performing analysis over such controller software (e.g. to perform symbolic execution), requires solvers capable of reasoning over such theories. Unfortunately, reasoning about non-polynomial arithmetic (such as transcendentals) is undecidable [144], while reasoning about polynomial arithmetic, while decidable, is computationally expensive. A common approach taken in traditional software verification (such as in abstract interpretation [37]) is to have conservative over-approximation of such operations using efficient logical theories (such as linear arithmetic). In this context, we need to over-approximate each path constraint ρ_i to obtain path constraint $\hat{\rho}_i$ that is expressible using the theory of linear arithmetic.

This is typically formalized using an abstraction function α that maps path constraints ρ_j into abstraction path constraints $\hat{\rho}_j : \alpha(\rho_j)$ that satisfy the following property: $\rho_j(\mathbf{y}, s) \subseteq \hat{\rho}_j(\mathbf{y}, s)$. The overall abstract controller relation $\hat{\rho}$ is simply the union of $\hat{\rho}_j$ for each path $\mathfrak{p}_j$ in the control code. We abuse the notation and use $\hat{\rho}(C^y, \varphi)$ to denote the action of the (abstract) controller on a given cell C^y from the tiling-based plant abstraction, and an abstract set of controller states φ. The result yields a set of control inputs U and updated controller states ψ; we formalize the soundness of the abstraction in the following assumption:

Assumption 5.7.1 (Soundness) Suppose in the abstract semantics, we have $(U, \psi) = \hat{\rho}(C^y, \varphi)$, then for all plant outputs $\mathbf{y} \in C^y$ and all controller states $s \in \varphi$, the concrete values $(\mathbf{u}', s') = \rho(\mathbf{y}, s)$ are contained in their respective abstract states: $\mathbf{u}' \in U$ and $s' \in \psi$.

Having defined an abstraction of the controller semantics, the goal is to compute $(U, \psi) = \hat{\rho}(C^y, \varphi)$. This is achieved through an abstract symbolic execution of the program. One way to achieve this is by

precomputing each relation $\hat{\rho}_j$ for path $\mathfrak{p}_j$ as a tuple of assertions (ξ_j, R_j, T_j), where ξ_j encodes the abstract path condition on C^y and φ, and R_j and T_j are projections of $\hat{\rho}(C^y, \varphi)$ on the controller states and controller outputs (i.e. plant inputs) respectively.

Having defined the plant and controller abstractions, we now explore a series of abstract states to analyze the safety of plant and controller state combinations. The approach presented here can extend to more complex bounded-time temporal logic properties by instrumenting the system with a temporal logic monitor [70, 77, 78], and searching for the reachability of a target state in the monitor.

5.8 Closed Loop Execution

Definition 5.8.1 (Closed Loop Abstract State) The abstract state of the overall closed-loop system is a combination (C, φ), where C is an abstract plant cell and φ is an abstract controller state, i.e., a logical predicate specifying a set of controller states.

The closed-loop system abstraction is explored in two phases:

- We consider an abstract plant move $(C, \varphi) \rightsquigarrow_A (C', \varphi)$ wherein $(C, C') \in E_A$ belongs to the abstract edge relation between cells. The new cell $C' = Q_\epsilon(\mathbf{x}', \mathbf{u})$, is generated using the scatter-and-simulate procedure that samples cell C and performs a concrete simulation using the plant's SIM function.

- Next, we consider a controller move $(C', \varphi) \rightarrow_A (C'', \psi)$ wherein we compute $(U, \psi) = \hat{\rho}(C^y, \varphi)$ and obtain a new cell $C'' = Q_\epsilon(\mathbf{x}', \mathbf{u}')$ for some $\mathbf{x}' \in C'$, and some $\mathbf{u}' \in U$ by quantizing the new control inputs with the plant states. The updated controller states are now represented by ψ. Also, $C^y = Q_\epsilon(g(x'))$.

The two moves combine to give a closed loop move of the system: $(C, \varphi) \xrightarrow{\tau_s}_A (C'', \varphi')$. This can now be used for computing the set of reachable abstract states: $R_{\tau_s} : \{(C'', \varphi') \mid (C, \varphi) \xrightarrow{\tau_s}_A (C'', \varphi')\}$ in one time step ($\tau = \tau_s$). We now present this combined closed loop step as an algorithm.

To compute the plant step, first sample is used to obtain $\mathcal{N}$ state-input pairs which are then supplied to SIM to compute a representative set of next plant states X'_u . The corresponding set of representative plant

Algorithm 3: Closed Loop Execution on Abstract States

Input: Abstract states (C, φ), plant input $\mathbf{u}$, abstract plant output C_y, plant simulator SIM, controller summary ρ

Output: Reachable abstract states R_{τ_s}

$X_u := \{(\mathbf{x}_1, \mathbf{u}_1), \ldots, (\mathbf{x}_\mathcal{N}, \mathbf{u}_\mathcal{N})\} = \mathsf{sample}(C, \mathcal{N})$

$X'_u := \{\mathbf{x}' \mid \mathbf{x}' = \text{SIM}(\mathbf{x}, \mathbf{u}, \tau_s) \wedge\ (\mathbf{x}, \mathbf{u}) \in X_u\}$

$Y := \{C^y \mid C^y = Q_\epsilon(g(\mathbf{x}')) \wedge \mathbf{x}' \in X'_u\}$

$S_{\varphi Y} := \{(U, \psi) \mid (U, \psi) = \hat{\rho}(C^y, \varphi)\ \wedge\ C^y \in Y\}$

$R_{\tau_s} := \{(C'', \psi) \mid C'' = Q_\epsilon(\mathbf{x}', \mathbf{u}') \wedge \mathbf{u}' = sample(U) \wedge (U, \psi) \in S_{\varphi Y} \wedge \mathbf{x}' \in X'_u\}$

outputs are also computed using $g()$ and are then quantized to get Y. Using this set of abstract plant outputs, and controller function $\hat{\rho}$ new abstract controller states and outputs are computed. The controller inputs u are then sampled (using a constraint solver, as discussed in Chapter 6). Finally, R_{τ_s} is built by quantizing plant state-input $(\mathbf{x}', \mathbf{u}')$ pair. This is illustrated in Fig. 5.5.

5.9 Summary

We presented a solution for finding violations of safety properties in SDCS. Unlike the current approaches, which are unable to directly analyze the combination of a hybrid system and control code, we proposed an algorithm to explore the combined set of reachable states. We used a combination of plant abstraction search through a numerical simulation procedure and symbolic execution of the controller code. In doing so, we were able to capture robust plant behaviors along with covering all paths through the controller code. The experimental evaluation discussed in Chapter 6 demonstrates its usefulness and performance.

```c
#define MAX_TEMP (70.0)
#define MIN_TEMP (66.0)
#define CHATTER_LIMIT (2)

int controller(double room_temp){
  //*************************************************
  // on_ctr, off_ctr     :counters to track on/off cycles
  // chatter_detect_ctr :counter to track chattering
  // previous_command    :previous command
  // command             :current command
  // u                   :control input to the heater
  //*************************************************
  static int on_ctr, off_ctr, chatter_detect_ctr;
  static int previous_command, command, u;

  // Compute command to heater based on room temperature
  if(room_temp >= MIN_TEMP && room_temp < MAX_TEMP)
    command = NORMAL_HEAT;
  else if(room_temp >= MAX_TEMP)
    command = NO_HEAT;
  else if(room_temp < MIN_TEMP)
    command = FAST_HEAT;
  else
    command = previous_command;

  // Chattering absent, reset the counter
  if(off_ctr >= 5 || on_ctr >= 5)
    chatter_detect_ctr = 0;

  // New command != previous command. Possible chattering
  if(command != previous_command)
    chatter_detect_ctr++;

  // Chattering detected, hold previous command
  if(chatter_detect_ctr > CHATTER_LIMIT)
    command = previous_command;

  // Increment counters
  if(command == NO_HEAT){
    on_ctr = 0;
    off_ctr++;
  }else{
    on_ctr++;
    off_ctr = 0;
  }

  // Translate command to control input
  if(command == NO_HEAT)      u = 20;
  if(command == FAST_HEAT)    u = 100;
  if(command == NORMAL_HEAT) u = 70;

  return u;
}
```

Figure 5.3: C code for the Thermostat. All initial control states are 0.

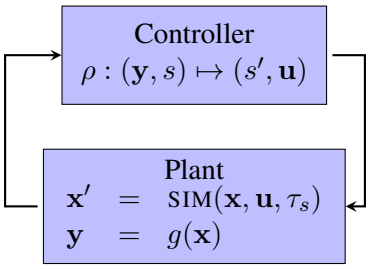

Figure 5.4: Closed loop composition of a plant and a controller model with controller sampling period τ_s.

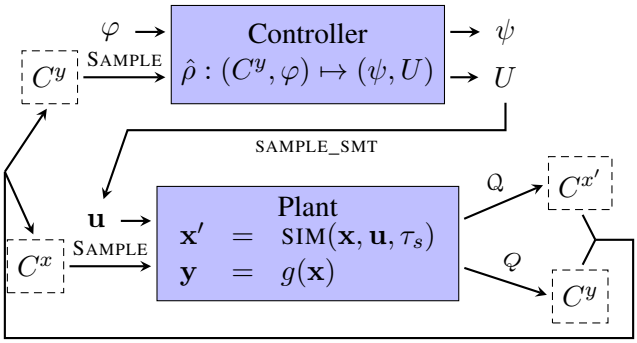

Figure 5.5: Closed loop symbolic execution.

Chapter 6

The Falsification Tool: S3CAM

The ideas presented in the earlier chapters have been implemented as a prototype tool: S3CAM. We have evaluated it on several benchmarks and compared it with other tools: S-TaLiRo [10] and dReach [97]. In this chapter we discuss the details of the implementation, the tool, the benchmarks, and elaborate on the results.

The prototypes were implemented in three stages. S3CAM was the first, wherein we prototyped the numerical search based on trajectory segments and used implicit abstractions. It was extended and released as S3CAM-X by adding symbolic execution (SymEx) of controller code. In the rest of the presentation, we use **S3CAM** to refer to the presented tool and use **S3CAM-X** to explicitly refer to the symbolic execution functionality.

6.1 S3CAM Architecture

Fig. 6.1 provides a structural overview of S3CAM. It takes in the *test description* and the *system description* and outputs the *CEx* (counter-example). The individual components are briefly explained below.

Build Graph explores the abstraction and builds the graph on-the-fly using heuristics. It calls *Rch States* to get the states reachable from the current states. It then adds the state pairs as nodes in the graph, and connects them with edges.

Rch States uses the *concrete simulator* to get concrete reachable plant states and then abstracts them using a quantization function. It also calls the *SymEx* engine to get the reachable states for the controller.

Concrete Simulator generates concrete states using the plant's simulator through the SIM interface. It also executes the controller to get its concrete output.

SymEx is the symbolic execution procedure which takes in the controller paths and uses a constraint solver to determine the reachable states (in constraints form) of the controller.

Constraint Solver is usually an SMT solver, or a similar procedure which can decide the feasibility of the path constraints of programs with floating point arithmetic.

Search Graph. Once the graph is built, it is searched for paths between the initial nodes and the unsafe nodes. Such paths represent the abstract counter-examples.

Concretize tries to find concrete CEx given an abstract counter-example. It outputs CEx when it succeeds, otherwise it calls *Refine*.

Refine. If *Concretize* fails, *Refine* reduces the abstraction's grid size and the process is repeated again.

Pluggable Search Heuristics. The *Build Graph* routine uses the **scatter-and-simulate** algorithm (which uses BFS) to select states for exploration. These selected states are passed down to *Rch States* which computes the new states. These states are added to the graph as nodes along with the edges. To search the abstraction differently, we just need to replace *Build Graph* with a new graph building heuristic.

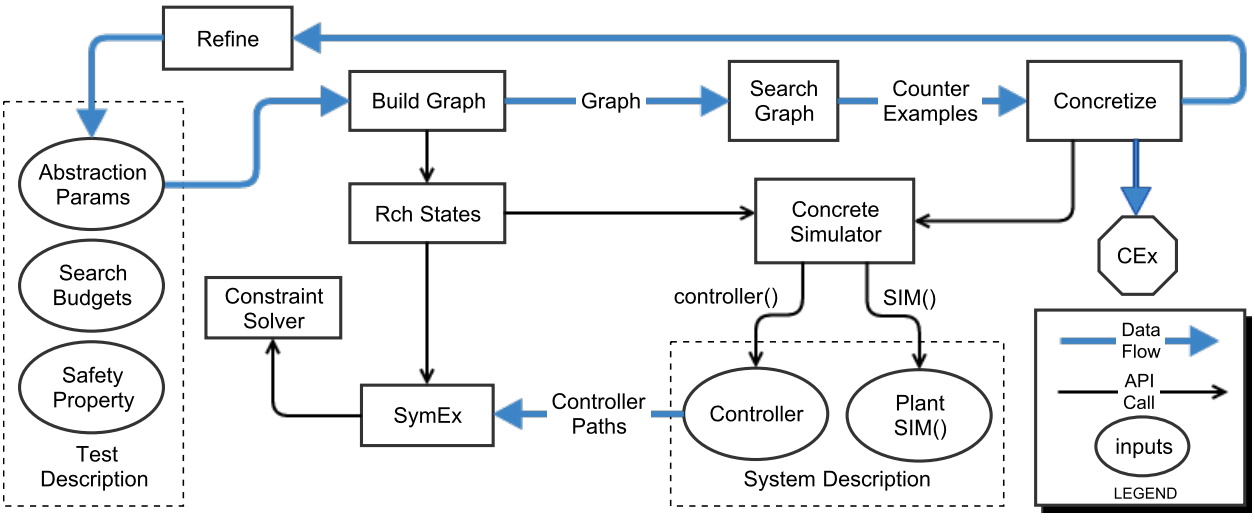

Figure 6.1: S3CAM: Architecture

6.2 Tool Implementation

S3CAM is implemented in Python 2.7, which is an excellent glue language and provides for rapid prototyping [1] . The implementation is self contained, but does use a few open sourced modules obtainable from the Python Package Index (PyPI: `https://pypi.python.org/pypi`).

6.3 Input Description

As mentioned below, S3CAM takes as input the description of the system and the safety property and search parameters. In the next section, we discuss them in detail.

- the description of the black box system: SIM function,
- the controller's description (symbolic and concrete)
- the safety property: initial set, unsafe set, time horizon,
- the abstraction parameters: $\mathcal{N}$, ϵ and Δ ($\Delta = \tau_s$ for SDCS), and
- the various search budgets.

6.3.1 Plant Description

The requirement on the plant's description are in the form of an interface. This provides for easy interfacing of simulators written not only in Python, but also for C /C++, for which multiple interface solutions are available (including the native solution, CFFI, ctypes and Cython). Simulators in other languages can also be accommodated by wrapping them within a layer of Python. In the current version of the prototype, we provide an interface to Matlab® (using its API for Python).

Simulator Interface. The signature of the SIM function is of the form $\mathbf{x}' = \text{SIM}(\mathbf{x}, \mathbf{u}, t)$, with $t, \mathbf{x}, \mathbf{u}, \mathbf{x}'$ as defined. The description can also be provided as a *class* in both Python and Matlab®.

```
int controller(){
    static int var;
    var += 1;
    u = 2*var;
    return u;
}
```

Listing 6.1: Persistent state *var* present.

```
int controller(int *v){ //modify args
    int var = *v; //initialize declaration
    var += 1;
    u = 2*(var);
    *v = var; //return state
    return u;
}
```

Listing 6.2: Persistent state variables changed to local

Figure 6.2: Transforming controller code with persistent state variables.

6.3.2 Controller Description

Control software is usually architected such that there is an entry point function with the signature controller_step(input, output), corresponding to the controller's execution. In our implementation we require that the *input* encapsulates the (a) plant output $\mathbf{y}$, (b) previous controller state s and (c) exogenous controller input $\mathbf{w}$ (disturbances/exogenous inputs). The controller returns a structured *output* consisting of (a) controller's next state and (b) control input (to the plant). This setup is quite generic, and follows a similar format used by Embedded Coder®, Matlab®'s automatic code generation toolbox to generate C code.

We make a special distinction between the persistent ('global') state variables of the controller and 'local' variables that are *reinitialized* each time the controller is invoked. In typical C software, persistent variables are usually easy to identify as their declaration is qualified by **global** or **static**. In a Simulink® model, persistent variables are associated with data-store blocks with dedicated read and write blocks to access their values. Given a control software with persistent states, it can be transformed to one without them by converting the persistent variables into function parameters. The C code snippets in Fig. 6.2 illustrate the transformation of a function with persistent variables to an equivalent function with only local variables.

6.4 Analysis Implementation

We now discuss the implementation of algorithms and the analysis.

[1] Unfortunately, Python programs run slower than the ones written in a high performance general purpose language like C /C++.

6.4.1 Scatter-and-Simulate

Parameters. Our implementation allows a user to customize various system specific parameters within Algorithm 2, such as the initial tiling granularity defined by ϵ, the time step Δ, and the overall time horizon T. A maximum number of switches can also be specified to avoid trajectories with Zeno behavior.

Grid Scaling. Thus far, our definition of tiling subdivides the space uniformly for all variables. However, in practice, different system variables have different ranges and therefore, our implementation treats ϵ as a vector of size n (number of continuous states), with each element defining the tiling size for that particular dimension.

The implementation flowchart is summarized in Fig. 6.4.1. The exploration algorithm is indicated in pink, which illustrates how each reachable cell of the abstraction is explored. The refinement of the abstraction can be carried out using either of two techniques, as explained in Chapter 4. The first refinement technique, illustrated by the green blocks, refines each cell encountered in the previous step. The second refinement technique, illustrated by the purple blocks, refines only the initial cells. The **Likely Initial Cells** approach was used for refining the abstraction and to obtain the presented results.

Failure. Our technique can fail in two ways: (a) failing to find an abstract counterexample path or (b) going beyond the maximum number of refinement steps without finding a concrete violation. Upon such a failure, our implementation restarts the search from the first iteration.

6.4.2 Symbolic Execution

Using symbolic execution, we can extend the current implementation to catch common program bugs in the controller, like **division by zero** and **out of bounds access**. There are two ways a symbolic execution engine could be integrated in our implementation. The analysis could either be performed; (1) statically, by transforming the given controller program into its paths or (2) dynamically, where the symbolic execution is done at every step. The former was selected due to ease of implementation. However, we recommend to explore (2) as it could be more scalable in practice.

Controller Preprocessing. Before beginning the analysis, we transform the controller using a symbolic

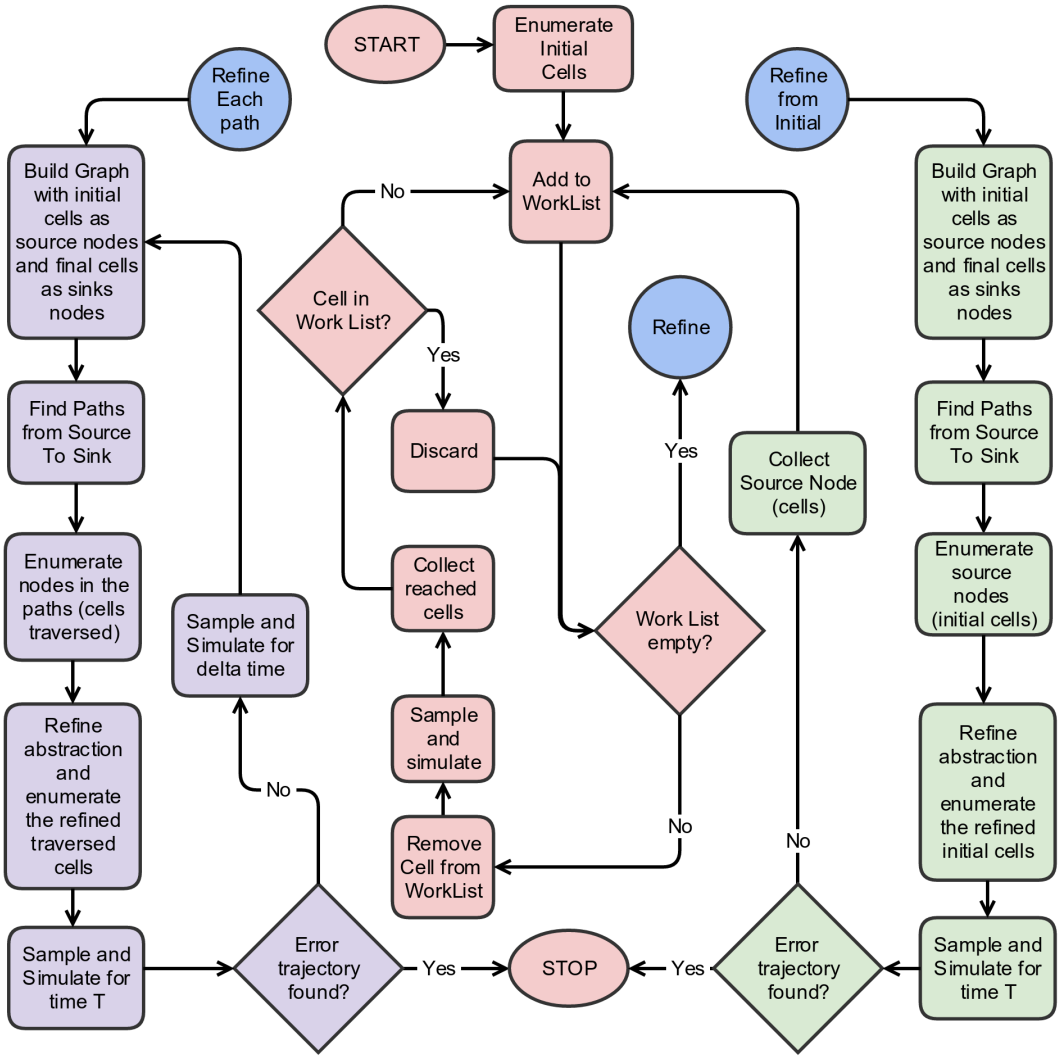

Figure 6.3: Algorithm

execution engine to a set of all possible control-flow paths in the controller. The paths are represented by their associated path constraints and update functions. This enumeration is expensive and carried only once for a given controller. Once pre-processed, a controller move involves checking the feasibility of each path constraint and if feasible, computing the valuations of updated state and output. We use Z3 [44], an SMT solver to check feasibility and compute a concrete satisfying assignment on the controller's input $(\mathbf{y}, s)$. The update function is then used to compute $(s', \mathbf{u})$. Multiple satisfying assignments can be obtained by adding blocking constraints.

SymEx Tools. Several tools for symbolic execution of code exist, but most are research projects. We tried two mature tools, KLEE [27] and Pathcrawler [162]. We preferred the latter, as KLEE uses bitvector theories to model floating point numbers which endures a performance penalty when reasoning about floating point numerical code. Pathcrawler uses ECLiPSe [151] as its constraint solver. During the time of experiments, both Pathcrawler and Z3 did not support the floating points. Instead, theory of reals was used. Presently, both support floating point arithmetic. Although Pathcrawler and Z3 provide for efficient linear constraint solving, they limit the kind of non-linear constraints that can be handled (in the controller).

Constraint Blowup. The symbolic treatment of the controller code has benefits of being precise. But, as in the case with similar methodologies, like bounded model checking, automatic test generation, and more, it suffers from 'constraint blowup'. Each controller move requires an 'unrolling' of the controller in time, tracking the associated constraints. The constraints accumulate with each time step and become very inefficient to solve. Even though SMT solvers are quite efficient, large constraints can make the entire analysis unusable. We address this by providing an option of selecting the 'history depth'. Once the given depth is exceeded, the symbolic controller states are concretized, and the accumulated symbolic constraints (history) are purged. This is done by selecting some representative concrete controller states instead of maintaining complex symbolic representation of all reachable controller states. To clarify, it does not limit the length of the abstract trajectories that can be discovered. For all the presented benchmarks, a depth of 1 was used.

Parallelization. In its current form, S3CAM is not parallelized, but it can be parallelized owing to the

independent nature of plant simulations. In fact, the earlier prototype presented in [165] was parallelized. The reason can be partially attributed to the difficulty of threading in Python. In the future, we plan to explore fine grained lazy approaches to make parallelization more efficient.

6.5 Evaluation and Comparison

We evaluated S3CAM on multiple benchmarks ranging from mathematical systems to representative systems from industry. This included both dynamical systems and SDCS. As S3CAM can accept a black box description of a system, for the case of SDCS we compared the results both with and without symbolic execution.

There are not many falsification tools which can be directly compared to S3CAM/X. Most tools do not accept black box descriptions or SDCS. We compare against uniform random testing and S-TaLiRo. We also compared with dReal/dReach in our publication [165]. The tested version of dReach could not falsify most of the benchmarks.

6.5.1 Setup

S-TaLiRo and S3CAM/X use randomized algorithms. To get consistent results, we run them 10 times on each benchmark, and note down the number of times they can find a violating trajectory. As the tools are best effort and use restarts, we use a $1hr$ timeout to indicate a failed run. For a quantitative comparison, we also collect the avg. time taken. However, because the tools are prototypes and not optimized, the timings should only be qualitatively assessed. Also, S3CAM can execute simulations in parallel while S-TaLiRo can not [2] .

Random Testing. While comparing the tools, the performance of random testing is also noted. Using a uniform random distribution on the search space, we collect 10^5 samples and use them to numerically simulate the benchmark. The generated traces are then examined for being violations. The number of violations found are tabulated alongside the tools' performances. Note that, for some benchmarks, we used random testing to find properties that 'appeared' hard to falsify. This can bias some benchmarks towards

[2] The recent versions of S-TaLiRo can compute in parallel.

properties which are hard to falsify using uniform random sampling. In the future, having a set of curated benchmarks from industry can help alleviate this.

Note: Though S3CAM-X also implements S3CAM's functionality, the results use two different versions of S3CAM's implementation. Hence, the two tables should not be compared directly for timing performances.

Hardware Setup. All the computations were carried out on a machine with a 4 core Intel i7-2820QM 2.30GHz CPU (up to 3.40GHz) and 8GB RAM, running Ubuntu 12.04

6.6 Case Studies for S3CAM (Dynamical Systems)

We evaluated our method on a number of examples, ranging from academic models of nonlinear and hybrid dynamical systems, to models representative of industrial control systems.

6.6.1 Mathematical Dynamical Systems

The first set of benchmarks includes well known examples of complex nonlinear systems such as the Van der Pol oscillator [154], the Brusselator, and the Lorenz reactor [154].

Van der Pol Oscillator

The Van der Pol Oscillator is tested with $\mu = 5$, with both the initial states ranging between $\mathbf{x} \in [-0.4, 0.4]$.

$$\dot{x}_1 = x_2$$

$$\dot{x}_2 = \mu(1 - x_1^2)x_2 - x_1$$

The safety properties are selected based on the difficulty to falsify them using random simulations. The properties P_1, P_2, P_3 have a time horizon = $1s$ and their unsafe set of states $X_f^{P_1}, X_f^{P_2}, X_f^{P_3}$ are shown in Fig. 6.4.

The last property P_4 explicitly specifies the time bound, between which, the unsafe states must be

$$X_f^{P_1} = \begin{cases} x_1 & \in [-1, -0.7] \\ x_2 & \in [-6.5 - 5.8] \end{cases} \quad X_f^{P_2} = \begin{cases} x_1 & \in [-1, -0.7] \\ x_2 & \in [-6.5 - 5.5] \end{cases} \quad X_f^{P_3} = \begin{cases} x_1 & \in [-1, -0.7] \\ x_2 & \in [-6.5 - 5.6] \end{cases}$$

Figure 6.4: Unsafe states.

reached. To check this, we add time as another state with its evolution given by $\dot{t} = 1$.

$$P_4 = \begin{cases} x_1 & \in [-1, -0.7] \\ x_2 & \in [-6.5 - 5.8] \\ t & \in [2.5, 4.5] \end{cases}$$

Lorenz System

The Lorenz system $\sigma = 10$, $\rho = 28$, $\beta = 2.6667$ is described in Fig. 6.5. The time horizon of the property was $10s$.

$$\dot{x} = \sigma(y - x)$$

$$\dot{y} = x(\rho - z) - y$$

$$\dot{z} = xy - \beta z$$

$x \in [-2, 2]$	$x \in [2.5, 3]$
$y \in [-2, 2]$	$y \in [0, 4]$
$z \in [-2, 2]$	$z \in [-\infty\infty]$
Initial states.	Unsafe states.

Figure 6.5: Lorenz System.

Brusselator

The Brusselator [14] models a type of autocatalytic reaction. We have used it with the parameters $a = 1$ and $b = 2.5$ and checked the safety property for a time horizon of $10s$.

$$\dot{x}_1 = 1 + ax_1^2 x_2 - (b+1)x_1$$

$$\dot{x}_2 = bx_1 - ax_1^2 x_2$$

$x_1 \in [0, 1]$	$x_1 \in [2.3, 2.4]$
$x_2 \in [1, 2]$	$x_2 \in [1.2, 1.3]$
Initial states.	Unsafe states.

Figure 6.6: Brusselator.

6.6.2 Hybrid Dynamical Systems

The second set of benchmarks contain hybrid dynamical systems: a 4 state model of a bouncing ball, a variation (B.Ball+S.H.M.) with the ball bouncing on a simple harmonically oscillating platform, and a constrained pendulum [158]. Again, these systems have no formal specification of an unsafe region. We use random testing to synthesize challenging falsification goals by identifying 'hard-to-reach' regions.

The third set of benchmarks consists of a modified instance of navigation benchmark (NAV-30) [164], derived from [61]. These benchmarks describe a particle moving through a 2D grid, with different affine motion dynamics for each cell. The falsification problem is to determine if certain cells are reachable, given the initial position and velocities of the particle.

Bouncing Ball

The bouncing ball hybrid automaton with the safety property is illustrated in Fig. 6.7.

Constrained Pendulum

The benchmark from [158] describes a simple pendulum, constrained using a pin with a parameterized location $x_p \in [1, 1.5]$. The presence of the pin results in hybrid dynamics. It introduces two dynamical modes, one in which the pendulum is swinging unconstrained from the point of suspension and another in which the pin becomes the point of suspension (Fig. 6.8).

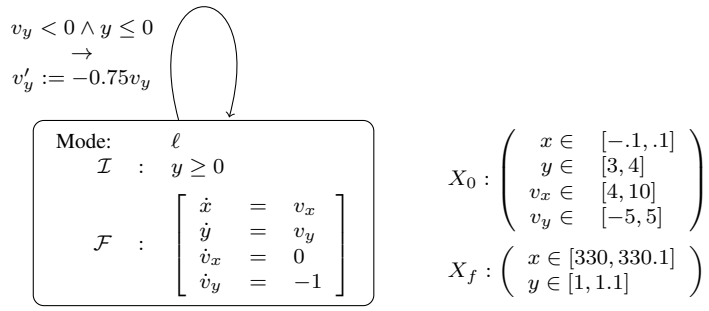

Figure 6.7: The hybrid automaton for a bouncing ball with initial set X_0 and unsafe set X_f. The goal is to find whether a trajectory starting from the initial set X_0 can reach the specified unsafe set X_f within $40s$.

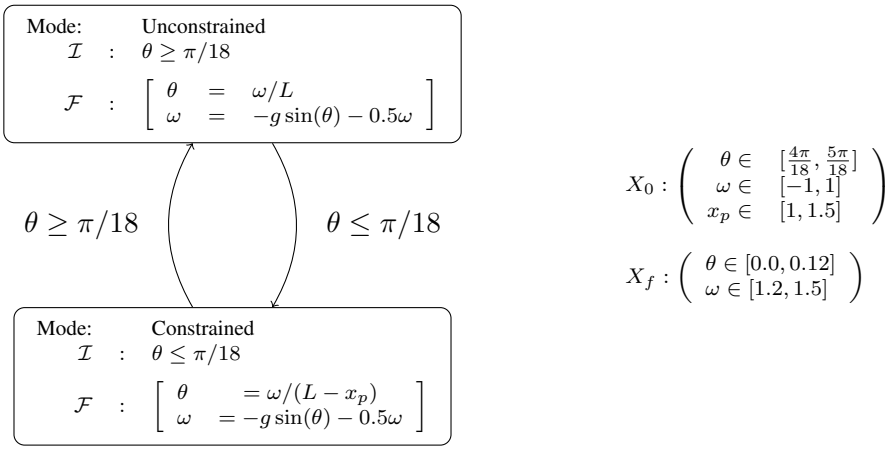

Figure 6.8: Constrained pendulum.

Navigation Benchmarks

NAV benchmarks are state partitioned hybrid systems commonly used to evaluate verification/falsification tools [61]. These benchmarks model a particle traveling on a 2 dimensional grid of cells, each dictating a differing affine continuous dynamics. A transition is taken when the particle crosses over from one cell to its neighbor. All instances of the benchmark designate an initial set of states and an error cell. To test our approach we focus on the largest instance "NAV-30", which has 625 discrete modes and about 2500 possible transitions between them. To make the falsification more challenging, the initial sets modified to $X_0 : \ x \in [4, 5], y \in [21, 22], v_x \in [-1, 1], v_y \in [-1, 1]$. We pick safety properties $\mathcal{P}_P$, $\mathcal{P}_Q$, $\mathcal{P}_R$, $\mathcal{P}_S$, as described in Chapter 3.

6.6.3 Physical Systems

Glucose-Insulin Control with Artificial Pancreas(G-I)

This benchmark is based on work by Fisher [62] and describes an **artificial pancreas** controller to maintain safe levels of plasma blood glucose (pbg) in type I diabetes patients. The insulin-glucose dynamics are modeled using the Bergman minimal model [17]. The plant model uses an exponential glucose absorption sub-model. Using data of 18 different subjects [18] we search for the scenario of hypoglycemia (i.e., $pbg < 3.6$ mmol/L). We incorporate an uncertainty interval for each of the patient parameters in our model. We only report the result for the case (patient ID:1) where we found a violation.

Idle Speed Controller

When a car is stationary, but the engine is running, it is required for the engine speed to be maintained at a certain reference value in the presence of external disturbances such as torque demand (τ_ℓ) (example, due to the A/C system) and the clutch being operated. We use a simplified affine hybrid automaton model of a closed-loop system containing a model of the engine and the powertrain, with a single control input: the throttle plate angle. The controller uses Proportional + Integral (PI) control to maintain the engine speed to 800 ± 35rpm. The aim of the falsifier is to find a simulation trace in the closed-loop model which exceeds this range for time-varying values of $\tau_\ell \in [0, 5] Nm$.

6.7 Case Studies for S3CAM-X (SDCS)

Table 6.1: Summary of benchmarks. Each benchmark mentions the sampling period of the controller τ_s and its description is split into constituent controller and plant. The controller is described by number of **States**, exogenous inputs (**Ex. Ip**), lines of code (**LOC**), symbolic paths in the (**Paths**) and time taken to generate them (**SymEx Time**) in minutes. The plant is described by the language used to implement its model (**Impl.**), number of modes if its a hybrid automaton in Python (Py) or the number of blocks if its a Simulink®(SM) model (**Modes/Blocks**), continuous states (**C. States**)

Benchmark	τ_s(s)	Controller					Plant		
		States	Ex. Ip	LOC	Paths	SymEx Time	Impl.	Modes/Blocks	C. States
SPI	1	0	1	13	3	0	Py	1	1
Heater	0.2	4	0	59	26	0	Py	3	1
Heat	0.5	3	0	37	312	1	Py	6	3
DC Motor	0.02	1	1	29	3	0	Py	0	2
FuzzyC	0.01	0	0	218	208	236	Py	0	3
MRS	1	0	8	29	9	0	Py	0	4
AFC	0.01	7	0	243	120	40	SM	170	12

The benchmarks used for grey box testing are summarized in Table 6.1. Against each system tested, we mention its sampling period τ_s and the controller and plant characteristics. For the former, this includes the number of states, exogenous inputs, lines of code, symbolic controller paths statically discovered by Pathcrawler and the time taken to do so. The plant is characterized by the implementation language for the simulator (Python or Simulink®), the number of discrete modes if the plant is a hybrid system, otherwise the number of Simulink® blocks, and lastly, the number of continuous states. A detailed description for each of the benchmark follows.

Heat Benchmarks

The heat benchmarks proposed in [61], describe a scenario where a limited number of heaters h are being used to heat r rooms, where $h < r$. The control system can shuffle the heaters or turn them on/off in order to maintain a comfortable temperature in all rooms. We are interested in finding scenarios where the controller fails and the temperature of any room dips below a certain threshold. We choose the first instance in the suite of heat benchmarks for case study; this instance has 3 rooms and 1 heater. The controller software has 312 control-flow paths and 3 states tracking each room's temperature. Correspondingly, the plant has 3 continuous states and 6 modes. Each mode is characterized by the heater's location and it's discrete state

(on/off). We try to falsify the property that temperature of the first room does not drop below $17.23°C$. Interestingly, S3CAM-X performs comparably to S3CAM even though the control software has 312 paths. Both tools are faster than S-TaLiRo and finish in a few seconds, where as S-TaLiRo requires a few minutes for falsification.

Sampled Polarity Integrator System (SPI)

The SPI benchmark was used in [49] to highlight the difficulty faced by Markov-chain Monte-Carlo based random testing techniques, and optimization-guided techniques such as RRT-REX and S-TaLiRo. The system has an exogenous input w, and a single continuous state x which after every $\tau_s = 1$ seconds gets reset to either -1, 0, or 1 if the input $w < 0$, $w = 0$ or $w > 0$ respectively. We split this system into a plant and a controller, where the controller computes $u = -1, 0, 1$ based upon its exogenous input w as $u = sign(w)$. The continuous state of the plant evolves as $\dot{x} = u$. We then check the three properties $\mathcal{P}1 : x < 20$, $\mathcal{P}2 : x < 50$ and $\mathcal{P}3 : x < 150$ for time horizons 50, 200, and 500 respectively. For all properties S3CAM takes only a few seconds. S3CAM-X takes a bit longer due to constraint solving, but, S-TaLiRo takes significantly longer and times out for $\mathcal{P}3$. Similar difficulty is faced by RRT-Rex [49]. This example brings out the difference in our iterative approach when compared to directed random search.

Heater

The heater system introduced in Chapter 5 consists of a room, and a heater controlled by a thermostat. The heater has 3 operating modes; **off**, **regular heating**, and **fast heating**. It can be switched between modes by the thermostat in order to reach and maintain a comfortable temperature in the room. Specifically, the thermostat is designed to sense the room temperature after every $\tau_s = 0.2s$ and maintain a temperature of around $70°F$. It also has built-in logic to prevent chattering, i.e., avoiding rapid switching of the heater between modes. The heater is modeled as a hybrid system with linear dynamics, with 1 continuous state and three modes. The thermostat's software controller has 26 control-flow paths with 4 states which keep track of recent mode switchings. The property we seek to falsify is that the room-temperature T_F is always greater than $52°F$. We are able to find the falsification trace, which upon investigation indicates the failure of the chatter-prevention logic in a very narrow range of possible initial settings for the ambient room temperature

(approx.) $T_{F0} \in [69.9, 70.0]$. Though all tools find the falsification in less than half a minute, S3CAM-X is an order of magnitude faster than both S3CAM and S-TaLiRo (for this benchmark).

DC Motor

This example illustrates the search for errors in the presence of controller disturbance. The DC motor is a linear continuous system with armature current i and angular velocity $\dot{\theta}$. It is controlled by a PI controller with saturation which results in 3 control-flow paths. The bounded additive disturbance in the controller induces error in the sensed plant outputs. We parameterize the disturbance as a piecewise constant signal. We wish the system to never enter the following region of the state-space: $i \in [1, 1.2], \dot{\theta} \in [10, 11]$. We choose this set by design; it is designed to be very hard to reach using random simulations. S3CAM-X can, however, find a falsification, demonstrating the effectiveness of symbolic execution in finding a sequence of inputs that lead to a violation. In comparison, S-TaLiRo and our previous technique S3CAM fail to find a violation.

Fuzzy Control of Inverted Pendulum (FuzzyC)

Rule based controllers, such as ones implemented using fuzzy logic, are an interesting challenge for symbolic execution based analyses as they typically have a large number of control-flow paths. We consider an example from [131], where the controller tries to stabilize a nonlinear inverted pendulum balanced on a cart using a 5×5 rule matrix. The $\mathcal{C}$ code [3] has 218 lines describing 208 control-flow paths. The controller is stateless and computes the actuation force by classifying the current plant state (θ and $\dot{\theta}$) and selecting a corresponding control output from a lookup table. The safety property defines bounds on states, which when exceeded, indicate undesirable transients or possible unstable behaviors. S-TaLiRo finds a falsifying trajectory faster than S3CAM-X, but not as fast as S3CAM. This result is nevertheless encouraging as it shows the ability of S3CAM-X to analyze a large number of control-flow paths and yet be successful at finding a falsifying trajectory.

Mode-Specific Reference Selection (MRS)

These are a set of 3 benchmarks from [45, 49]. The benchmarks represent distinctive features from proprietary models of automotive controllers, and they highlight issues faced by optimization-guided methods.

[3] `http://www2.ece.ohio-state.edu/~passino/fuzzycontrol.html`

The systems have simple nonlinear dynamics but complex combinatorial Boolean logic over 8 exogenous inputs. To make the system amenable to S3CAM-X, we split the discrete nonlinear dynamics into a plant, and the rest (linear combinatorial logic) becomes the controller. The controller remains the same across the 3 benchmarks, but the plant varies. The mode selection logic is now part of the controller which takes in 8 inputs $w_1, \ldots, w_8$, where each $w_i \in [0, 100]$ and computes u. The 3 plants have discrete-time nonlinear dynamics where the evolution is governed by $x^+ = f(x, u)$, where $f_i(x, u)$ comprises of polynomials of up to degree 3 and trigonometric functions in x. The falsification can only be found in the mode which is triggered when $\bigwedge_{i \in [1..4]} w_{2i}(t) > 90 \wedge w_{2i-1}(t) < 10$. The probability of triggering the mode is thus a meager 10^{-8}. Such a combinatorial search is not amenable to sampling-based searches, and both S-TaLiRo and S3CAM fail. On the other hand, S3CAM-X can falsify the property in under a minute.

Powertrain Control Benchmark (AFC)

We use the most complex version of the abstract fuel control system benchmark (AFC) presented in [89]. It represents a complex closed loop control system modeling a plant with hybrid dynamics controlled by a PI controller. The original benchmark has both the plant and the controller implemented in Simulink® (Fig. 6.7). To test it using our approach, we use Embedded Coder® to generate $\mathcal{C}$ code for the controller block, which is then hand-tuned to satisfy controller interface requirements. Due to the observability requirement, the plant model is modified by simplifying the variable transport delay block to a first order filter. The property checked is a modified form of the 'Worst-case excursions in the normal mode' property in [89], i.e., we try to falsify $\mu >= 0.02$ while $t \in [0, 1.0]$. The search is over the original parameters: pedal frequency, pedal amplitude and engine speed. Both S3CAM-X and S3CAM take longer than S-TaLiRo to find the falsification due to the inefficient Matlab® interface, as explained below.

6.8 Results

We split the discussion of the results into two sections: black box testing and grey box testing.

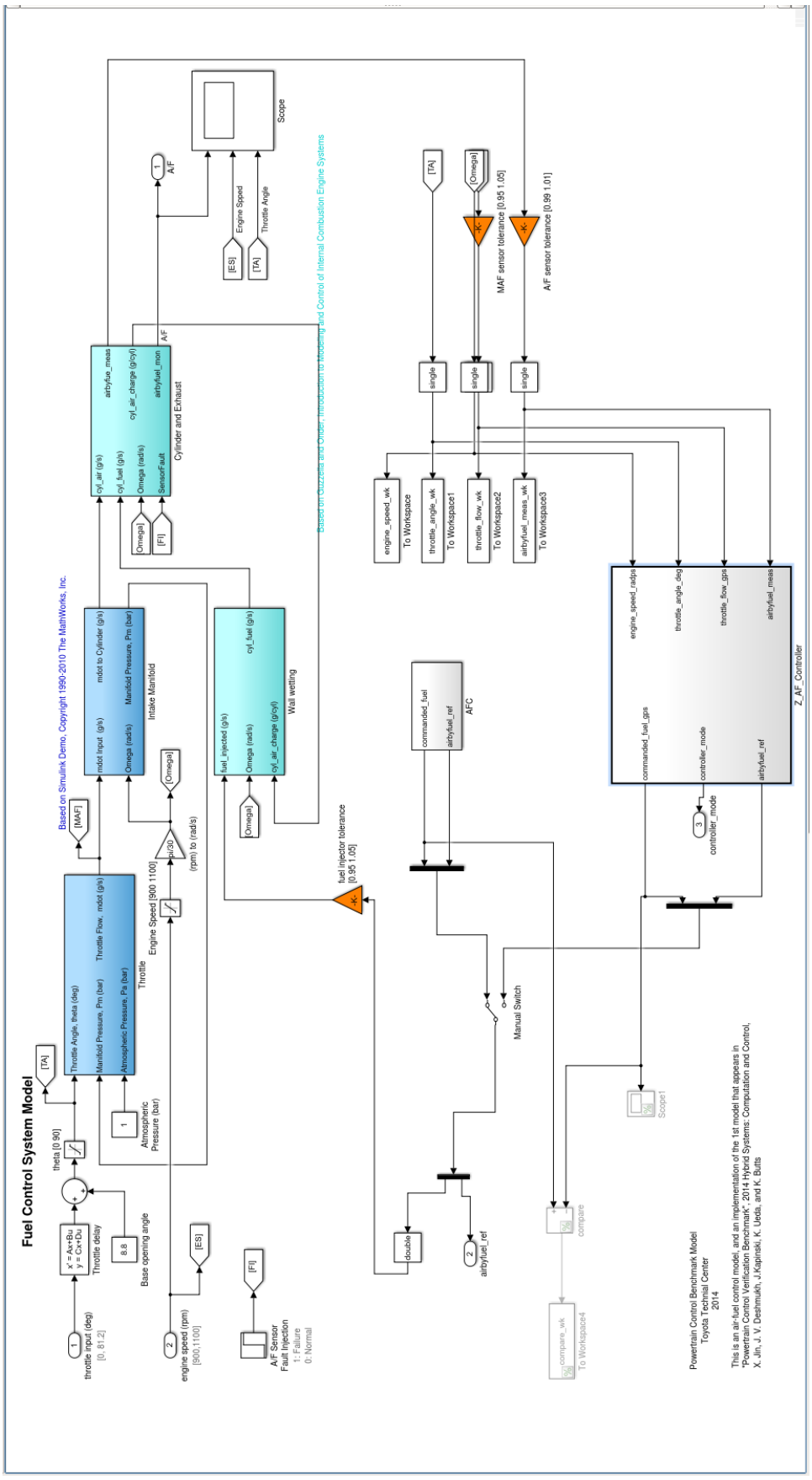

Figure 6.9: Simulink diagram of the powertrain benchmark

Table 6.2: **All times are in minutes**. Mean falsification times (T_{avg}) were computed on only the successful runs out of **10** total runs. Unsuccessful runs indicate a **timeout** ($\geq$ **1hr**). Columns at the left summarize the benchmarks, with the number of continuous states(**S**), inputs(**I**), parameters(**P**) and discrete Modes ('-' implies a purely continuous system). Random simulations (**100,000**) and scatter-and-simulate use **4 threads**, while S-Taliro used a single thread.

Benchmark	S	I	P	Modes	Prop.	Random Testing		S-Taliro		Scatter-Sim	
						Num. Vio.	T (mins.)	Succ. Runs	T_{avg} (mins.)	Succ. Runs	T_{avg} (mins.)
Van der Pol [154]	2	0	0	-	$\mathcal{P}1$	0	10.2	10	0.9	10	0.4
					$\mathcal{P}2$	21	41.9	10	11.8	10	2.9
					$\mathcal{P}3$	19	26.4	10	2.5	10	1.6
					$\mathcal{P}4$	11	42.5	8	18.4	10	6.6
Lorenz [154]	4	0	0	-	$\mathcal{P}$	36	132	3	20.6	10	3.1
Brusselator	2	0	0	-	$\mathcal{P}$	429	22	10	1.1	10	0.2
B.Ball [164]	4	0	0	1	$\mathcal{P}1$	3	20	1	11.0	10	6.5
B.Ball + S.H.M.	5	0	0	1	$\mathcal{P}1$	13k	202	10	0.5	10	0.4
					$\mathcal{P}2$	3k	202	10	1.4	10	0.4
					$\mathcal{P}3$	378	202	10	6.3	10	0.4
Pendulum [158]	3	0	1	2	$\mathcal{P}1$	0	6.6	10	4.7	10	4.7
					$\mathcal{P}2$	0	25	10	5.2	10	1.2
Nav.30 [61, 164]	4	0	0	625	$\mathcal{P}_P$	1	200	3	24.9	10	5.0
					$\mathcal{P}_Q$	7	200	1	48.1	10	5.5
					$\mathcal{P}_R$	1	200	10	23.2	10	17.5
					$\mathcal{P}_S$	108	495	3	33.2	10	20.1
Idle Speed [30]	9	2	0	4	$\mathcal{P}$	70	262	2	7.3	10	7.6
MPC [88]	3	0	0	69	$\mathcal{P}$	1	5.6	10	0.5	10	0.6
G-I [17, 18, 62, 164]	4	0	2	2	$\mathcal{P}$	1	30	10	5.0	10	4.0

6.8.1 Black Box Testing (Dynamical Systems)

The performance comparison of the tools is tabulated in Table 6.2. S3CAM was able to find a falsification in every run, whereas S-TaLiRo failed in some instances. As stated earlier, the times taken should not be directly compared. The S3CAM version (implemented in Matlab®) was parallelized and used 4 threads, which gave it a substantial performance boost (verified by a 2X speedup for the bouncing ball benchmark). This was in contrast with S-TaLiRo's single threaded implementation. Qualitatively, S3CAM's performance is comparable, if not superior to S-TaLiRo. This may be attributed to S-TaLiRo's use of global search on robustness functions, which can be overly dependant on a good distance metric. In comparison, S3CAM is relatively insensitive to distance metrics.

Comparing to random testing, we note that S3CAM can successfully find falsifications where 10^5 random simulations are unable to find any.

Scalability. Our approach scales successfully to some systems with as many as 14 state variables and in some cases systems with hundreds of modes. In general, S3CAM succeeds because of

- relatively inexpensive simulations which can be easily computed in parallel, and
- multiple shooting, which is an efficient way to break down the complexity of the problem, specially in the presence of highly non-linear trajectories.

6.8.2 Grey Box Testing (SDCS Systems)

As before, we compare S3CAM-X (S3CAM + SymEx) in Table 6.3 against S-TaLiRo. We also compare its performance with black box testing without using SymEx, noted as S3CAM in the table. The black box testing accesses the entire composed SDCS as a SIM function. We also provide the performance of random testing using $100,000$ simulations (on most benchmarks except for AFC). Additionally S3CAM-X, S-TaLiRo and random testing were executed using a single thread. If all 10 runs time out, we mention TO as the time taken and 0 as the number of successful runs.

In summary, symbolic execution being an expensive operation, increases the overall time taken for the search. This is evident when comparing the performance of S3CAM and S3CAM-X. At the same time, it

Table 6.3: Current tool **S3CAMX**, compared with **S-Taliro** and our previous tool **S3CAM**. All processes were run as single threaded. **All times are in minutes unless mentioned as seconds(s)**.

Benchmark	Time Horizon	Random Testing		S-Taliro		S3CAM		S3CAMX	
	T (s)	Num. Vio	T	Num. Succ	T_{avg}	Num. Succ	T_{avg}	Num. Succ	T_{avg}
SPI($\mathcal{P}1$)	50	348/100k	17.5	10	0.36	10	0.01	10	0.22
SPI($\mathcal{P}2$)	200	33 /100k	60.9	10	19.59	10	0.03	10	1.31
SPI($\mathcal{P}3$)	500	0 /100k	154.4	0	TO	10	0.08	10	8.39
Heater	2	47 /100k	3.9	10	0.48	10	0.22	10	0.06
Heat	10	156/100k	39.0	10	11.78	10	0.06	10	0.16
DC Motor	1	0 /100k	45.0	0	TO	0	TO	10	0.63
FuzzyC	0.1	6 /100k	10.1	10	0.27	10	0.03	10	1.59
MRS 1	2	0 /100k	0.6	0	TO	0	TO	10	0.18
MRS 2	2	0 /100k	0.4	0	TO	0	TO	10	0.11
MRS 3	2	0 /100k	0.4	0	TO	0	TO	10	0.43
AFC	12	1 /100	238.7	10	0.25	10	16.15	10	13.45

also finds a falsification where S3CAM without SymEx completely fails. As noted from the benchmarks, this happens in cases where the control program has non-robust or marginally robust paths (corner cases, which are hard-to-cover behaviors using a uniform random distribution) leading to the violation. This is overcome by SymEx as it does an exhaustive coverage of all possible control paths for a given set of plant states. It is also not dependant on a distribution for sampling, unlike S3CAM. These cases are found in the DC Motor and MRS benchmarks. When this is not the case, and the controller paths leading to the violation can be covered using uniform random sampling alone, SymEx adds a performance penalty. This is evident by the benchmarks: SPI, Heat and FuzzyC.

6.9 Concluding Remarks and Future Extensions

To conclude, we presented the tool S3CAM, which implements the approaches in the thesis. It also provides a test bed to experiment with additional ideas. We now discuss a few extensions which can improve the tool's performance.

- **Optimizations**: The present implementation of S3CAM is in Python. A re-implementation in C /C++ can provide an immediate performance boost.

- **Compositional Testing**: S3CAM can be easily extended to compositionally reason over systems composed of multiple copies of the plants. For example, systems with non-communicating multiple agents, like satellites. Furthermore, we need to explore compositional reasoning when the plants are different and communicate with each other.

- **Incorporating Heuristics from AI**: The numerical exploration of the plant can be improved by using more sophisticated searches like A^*. Additionally, pattern databases can provide clever ways to build the abstraction.

- **Resource Bounded Exploration**: In practice, it is critical that a tool works with the given set of resources. Instead of terminating unexpectedly, it should be able to work with bounded memory. In the future, we would like to modify the abstraction search to respect resource constraints by using

bounded memory algorithms.

- **Integration of Symbolic Execution**: We would like to integrate symbolic execution in a dynamical fashion. To explain, the present implementation statically computes the symbolic paths of the controller. A dynamic approach, which computes the symbolic states in every iteration can be more scalable.

Chapter 7

Relational Modeling for Falsification

In Chapter 4, we analyzed systems by restricting ourselves to their black box semantics. This enabled us to reason about the state-space reachability of the system without a direct analysis of its structure. Using a coarse abstraction which we searched on-the-fly, we could observe the local dynamics as required. This gave us an efficient procedure to find abstract counter-examples. However, to concretize the counter-examples, a 'closer look' or refinement of the abstraction is required. The grid based state-space abstraction was refined by splitting the relevant cells (abstract states) into smaller ones. As noted previously, due to the curse of dimensionality, such a uniform splitting is an expensive operation, and can not scale to higher dimensions.

In this chapter, we further our exploration of trajectory segment based methods; and explore an alternative approach to overcome the explosion in abstract states. Instead of selectively refining the abstraction, we compute a model of the black box system and use bounded model checking to find a concrete counter-example in the model [1] . We then use this counter-example to guide the search towards a counter-example in the original system.

More specifically, we use regression to quantitatively estimate the discovered relations, which were witnessed by trajectory segments, by affine maps. These maps approximate locally observed behaviors, which are incorporated into the sampled reachability graph as edge annotations. The resulting graph or the Piece-Wise Affine (PWA) relational model can be interpreted as an infinite state discrete transition system and model checked for time bounded safety properties. A counter-example if found, can indicate the presence of a violation in the system.

[1] Due to modeling errors, this might not be reproducible in the original black-box system.

Towards the end of the chapter, we discuss extensions to data driven approaches (instead of simulator driven), where instead of a simulator, a fixed set of data is provided as the behavioral description of the system. Using a combination of relational modeling, and program analysis we outline the future work for falsifying properties of SDCS.

7.1 Overview

We now briefly describe the approach. Given a numerical simulator SIM and an initial abstraction defined by a quantization function Q_ϵ and a time step Δ, we use scatter-and-simulate (parameterized by number of samples n as described in Chapter 4) to explore the abstract graph $\mathcal{H}(\Delta)$. The result is a graph G, which has a finite number of abstract states C (or cells) and edges (C, C') iff $C \overset{\Delta}{\rightsquigarrow} C'$.

Instead of using a CEGAR like loop (as in Chapter 4), we use the generated trajectory segments to learn quantitative models describing the local behavior of the system. These models are defined by a set of relations $R \subseteq \mathcal{X} \times \mathcal{X}$ for each edge of the reachability graph.

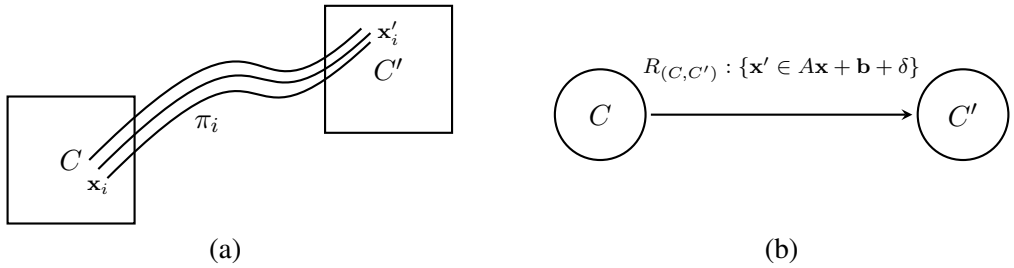

Figure 7.1: (a) Trajectory segments π_i are used to compute the relation $R_{(C,C')}$ that annotates the edge in (b). $R_{(C,C')} : \{\mathbf{x}' \in A\mathbf{x} + \mathbf{b} + \delta\}$ is an interval affine relation defined by an affine map (matrix A and vector $\mathbf{b}$) and an error interval (vector of intervals δ).

Recall that each edge (C, C') of the graph G denotes an observed trajectory segment between the respective cells. The graph abstraction G only states that there exists a state $\mathbf{x} \in C$ from which the system can evolve to a future state $\mathbf{x}' \in C'$. To increase the precision we iteratively refined the abstraction by state splitting. Instead, we now propose an 'enrichment' G^R of G by computing a set of local relations $R_{(C,C')}(\mathbf{x}, \mathbf{x}')$ for every edge (C, C'), which non-deterministically describe relations between $\mathbf{x} \in C$ and $\mathbf{x}' \in C'$. This is illustrated in Fig. 7.1 (compare with Fig. 4.3).

The enriched graph G^R captures the underlying local forward dynamics describing the evolution of the system in each abstract state. We represent the dynamics using an affine model with an interval error. Such a model can either be approximated using learning methods or computed as a sound (over) approximation using reachability set computation methods. Because we assume black box semantics, we only present the former. Using regression analysis on the $start$ and end states of the witnessed trajectory segments between two cells, we compute an approximate discrete map along with an error estimate. Moreover, using the simulation function SIM, additional trajectory segments (or data) can be generated if required. The data can be separated into a training set and testing set to compute the map and the error respectively. The latter case can be explored if the symbolic dynamics of the system are known. A tool like FLOW* [32] can be used to find the reachable set map.

Observe that G^R, a directed reachability graph, is rich enough to search for concrete behaviors in the system. We call it a time parameterized PWA relational abstraction. It can be interpreted as an infinite state discrete transition system, and we can use off-the-shelf bounded model checkers to find concrete violations of a given safety property, and even other temporal properties. We now discuss the background required to present our ideas.

7.2 Background

In this section, we present the basics of relational abstractions and fundamentals of regression analysis.

7.2.1 Relational Abstraction

For general hybrid dynamical systems, algorithmic ways for computing analytical solutions do not exist. Discretization (along with suitable abstractions) is often employed to transform the systems into a discrete transition system. Relational abstractions is one such idea, which abstracts continuous dynamics by discrete relations using appropriate *reachability invariants*. Both time independent and time dependent relations have been proposed; the former captures all reachable states over all time, whereas, the latter explicitly includes time by relating reachable states to time. Thus it can prove timing properties whereas, time independent relational abstractions can not. In both cases, the resulting abstractions can be interpreted

as discrete transition systems and can be analyzed using model checkers. We briefly discuss these two types of abstractions.

Timeless Relational Abstraction

Relational abstractions for hybrid systems were proposed in [149]. For a hybrid automaton model, they can summarize the continuous dynamics of each mode using a binary relation over continuous states. The resulting relations are timeless (independent) and hence valid for all time as long as the mode invariant is satisfied. The relations take the general form of $R(\mathbf{x}, \mathbf{x}') \bowtie 0$, where $\bowtie$ represents one of the relational operators $=, \geq, \leq, <, >$. For example, an abstraction that captures the monotonicity with respect to time for the differential equation $\dot{x} = 2$ is $x' > x$. The abstraction capturing the relation between the set of ODEs: $\dot{x} = 2$, $\dot{y} = 5$, is $5(x' - x) = 2(y' - y)$.

Such relation summaries, discretize the continuous evolution of a given system into an infinite state transition system, in which safety properties can be verified using k-induction, or falsified using bounded model checkers. The relationalization procedure involves finding suitable invariants in a chosen abstract domain, such as affine abstractions, eigen abstractions or box abstractions [149]. For this, different techniques like template based invariant generation [36, 75] can be used.

Timed and Time-Aware Relational Abstractions

As the above discussed relations are timeless, we cannot reason over the timing properties of the original system. Moreover, they are not suitable for time-triggered systems. Timed relational abstractions [166] and time-aware relational abstractions [123] were proposed to overcome these shortcomings by explicitly including time in the relations. In addition, both can be more precise than their timeless counterpart, but unlike it, assume continuous affine dynamics.

To analyze time-triggered systems like an SDCS modeled by an affine hybrid automata [2] , timed relational abstractions can be computed directly from the solutions of the underlying affine ODEs. Recall that the solution of an affine ODE $\dot{\mathbf{x}} = A\mathbf{x}$ can be represented using the matrix exponential as $\mathbf{x}(t) = e^{tA}\mathbf{x}(0)$. This gives us the timed relation $\mathbf{x}' = e^{tA}\mathbf{x}$. Clearly, the relation is non-linear with respect to time. However,

[2] An affine hybrid automata is restricted to the ODEs, resets and guards being affine.

for the case of SDCS with a fixed sampling time period, we obtain linear relations in $\mathbf{x}$. We demonstrated the usefulness of timed relational abstractions for the case of linear systems in [166], and now incorporate the idea to discretize black box dynamical systems.

Similar to timeless relational abstractions, time-aware relational abstractions [123] construct binary relations between the current state $\mathbf{x}$ of the system and any future reachable state $\mathbf{x}'$. The difference lies with the latter also constructing relations between the current time t and any future time t'. This is achieved by a case by case analysis of the eigen structure of the matrix A (of an affine ODE). Separate abstractions are used for the case of linear systems with constant rate, real eigen values and complex eigenvalues.

7.2.2 Learning Dynamics using Simple Linear Regression

Regression Analysis

In statistics, regression is the problem of finding a *predictor*, which can suitably predict the relationship between the given set of observed input $\mathbf{x}$ and output $\mathbf{y}$ vectors. In other words, assuming that $\mathbf{y}$ depends on $\mathbf{x}$, regression strategies find either a parameterized or a non-parameterized prediction function to explain the dependence. We now discuss simple linear regression, which is parametric in nature and searches for an affine predictor. It is also called *ordinary least squares*.

Ordinary Least Squares (OLS)

Let the data set be comprised of N input and output pairs $(\mathbf{x}, y)$, where $\mathbf{x} \in \mathbb{R}^n$ and $y \in \mathbb{R}$. If $N > n$, which is the case in the current context of *finding the best fit*, the problem is over-determined; there are more equations than unknowns. Hence, a single affine function cannot be found which satisfies the equation $\forall i \in \{1 \dots N\}. y_i = \mathbf{a}^T \mathbf{x}_i + b$. Instead, we need to find the 'best' choice for $\mathbf{a}$ and b. This is formally defined using a loss function. For the case of simple linear regression or OLS, the loss function is the sum of squares of the errors in prediction. The task is then to determine the vector of coefficients $\mathbf{a}$ and an offset constant b, such that the least square error of the affine predictor is minimized for the given data set.

$$\underset{\mathbf{a},b}{\operatorname{argmin}} \sum_{i=1}^{N} \left(\mathbf{y}_i - (\mathbf{a}^T \mathbf{x}_i + b)\right)^2 \tag{7.1}$$

To ease the presentation, we can rewrite the above as a homogeneous expression by augmenting $\mathbf{x}$ by $\hat{\mathbf{x}} = \begin{bmatrix} \mathbf{x} \\ 1 \end{bmatrix}$ and replacing $\mathbf{a}$ and b by the vector $\mathbf{ab} = \begin{bmatrix} \mathbf{a} \\ b \end{bmatrix}$. The equation 7.1 now becomes

$$\underset{\mathbf{ab}}{\operatorname{argmin}} \sum_{i=1}^{N} (\mathbf{y}_i - \mathbf{ab}^T \hat{\mathbf{x}}_i)^2$$

The solution of OLS can be analytically computed as

$$Ab = (X^T X)^{-1} X^T \mathbf{y}$$

where X is the matrix representing the horizontal stacking of all $\hat{\mathbf{x}}$. The details can be found in several texts on learning and statistics [67].

Given a time invariant dynamical system $\mathbf{x}' = \text{SIM}(\mathbf{x}, \Delta)$, where $\mathbf{x} \in \mathbb{R}^n$ we can use OLS to approximate its trajectories at fixed time step Δ by a discrete map $\mathbf{x}' = A\mathbf{x} + \mathbf{b}$, where $A = \begin{bmatrix} \mathbf{a}_1^T \\ \vdots \\ \mathbf{a}_n^T \end{bmatrix}$ and $\mathbf{b} = \begin{bmatrix} b_1 \\ \vdots \\ b_n \end{bmatrix}$. This map is a global relational model for the system. The data set for the regression is a set of pairs $\{(\mathbf{x}, \mathbf{x}') | \mathbf{x}' = \text{SIM}(\mathbf{x}, \Delta)\}$ and can be generated on demand. Another set can be generated to compute the error δ as an interval of vectors, where each element is an interval $\delta_i \in [\delta_{min}, \delta_{max}]$.

Affine maps are poor approximations for arbitrary non-linear functions. Hence, we use a collection of affine maps to approximate the local behaviors (in state-space) of the system SIM. This results in a piece wise approximation, as described in the next section.

7.2.3 Piecewise Affine (PWA) Transition System

We define the PWA transition system as a transition system (ref. Sec. 2.2.2) $\rho : \langle L, \mathcal{V}, \mathcal{T}, l_0, \Theta \rangle$ where each transition $\tau \in \mathcal{T}$, is associated with a transition relation of the form

$$\rho_\tau(v, v') \subseteq \{(v, f_\tau(v)) \mid g_\tau(v) \wedge g'_\tau(f_\tau(v))\}$$

where f_τ is an affine map relating the states and g_τ, g'_τ are affine guards (pre and post conditions) on the states. The assertion on the initial states Θ is also affine.

We can now use a PWA transition system ρ to approximate the behavior of a hybrid dynamical system S defined by a simulator SIM_S [3] . Each transition of ρ represents a discrete time step Δ. Let the state-space of S be given by $\mathbf{x} \in \mathcal{X}^n$, then the states of ρ are also given by $\mathbf{x} \in \mathcal{X}^n$. The affine guard predicates g_τ are given by a conjunction of hyper-planes and hence can be represented in matrix form as a polyhedron (defined by m constraints) in the state-space

$$g : C\mathbf{x} - \mathbf{d} \leq 0$$

where C is an $m \times n$ matrix and $\mathbf{d}$ is a vector of length m. The affine maps f_τ can be represented in matrix form as $f : \mathbf{x} \mapsto A\mathbf{x} + \mathbf{b}$. To make f_τ 'richer', we incorporate an error term δ which is defined by a vector of intervals $[\delta_{\min}, \delta_{\max}]$. Hence,

$$f : \mathbf{x} \mapsto A\mathbf{x} + \mathbf{b} + \delta$$

defines a set valued relation of the form $R : \{(\mathbf{x}, \mathbf{x}') \mid \mathbf{x}' \in f_\tau(\mathbf{x})\}$.

We now formalize the PWA affine transition system for a dynamical system.

Definition 7.2.1 (PWA Transition System) Given a hybrid dynamical system over a state-space $\mathcal{X}^n$, a PWA transition system ρ is given by the tuple $\langle L, \mathbf{x}, \mathcal{T}, l_0, \Theta \rangle$, where $\tau \in \mathcal{T}$ are affine transition relations and Θ is an affine predicate over $\mathbf{x}$ and the states $\mathbf{x} \in \mathcal{X}^n$. The transition relation is then defined by $\mathcal{T}$ with n transition relations as follows

$$\mathcal{T} = \begin{cases} g_1(\mathbf{x}) \wedge g'_1(\mathbf{x}') \implies \mathbf{x}' \in f_1(\mathbf{x}) \\ \dots \\ g_n(\mathbf{x}) \wedge g'_n(\mathbf{x}') \implies \mathbf{x}' \in f_n(\mathbf{x}) \end{cases} \tag{7.2}$$

where $f_i : \mathbf{x} \mapsto A_i\mathbf{x} + \mathbf{b}_i + \delta_i$, $g_i(\mathbf{x}) : C_i\mathbf{x} - \mathbf{d}_i \leq 0$, $g'_i(\mathbf{x}') : C'_i\mathbf{x}' - \mathbf{d}'_i \leq 0$ and $\mathbf{x}'$ denotes the next state of the system.

A PWA model is *deterministic*, iff for every state $\mathbf{x} \in \mathcal{X}^n$, a unique guarded affine map is satisfied and all errors δ are singletons. However, in practice such a case rarely exists. A PWA model will be usually

[3] Due to f_τ being restricted to an affine form, we can only approximate general hybrid systems.

non-deterministic, both due to multiple choice of transition relations and the reachable states at the k^{th} time step (or after $k\Delta$ units of time) being a set. Abusing the notation, we denote the set of states reachable in a single step in ρ by $\mathbf{x}' = \rho(\mathbf{x})$.

A PWA transition system is *complete*, iff for every state $\mathbf{x} \in \mathcal{X}^n$, there exists at least one satisfied transition relation $\mathcal{T}$. If this is not the case, the system can deadlock, with no further executions. This usually results from incorrect modeling of SDCS, and from here on, we do not consider such cases.

7.3 Relational Modeling

We now describe how relational models can be computed for a given black box system by enriching the abstract reachability graph obtained by scatter-and-simulate. We first formalize the notion of an enriched graph, and then show how they can be interpreted as a PWA transition system using k-relational modeling.

7.3.1 Abstract Enriched Graph

The existential abstraction relation in Chapter 4 was defined as follows:

$$C \overset{t}{\rightsquigarrow} C' \iff \exists \mathbf{x} \in C.\, \exists \mathbf{x}' \in C'.\, \mathbf{x} \overset{t}{\rightsquigarrow} \mathbf{x}'$$

The abstract relation $\overset{t}{\rightsquigarrow}$ can be enriched by incorporating the affine relation between $\mathbf{x}$ and $\mathbf{x}'$. For an arbitrary dynamical system, such a relation can be rarely represented using an exact affine map. This is due to the presence of non-linear and hybrid behaviors. But, an affine map can always be estimated with an error.

If the system dynamics are completely specified in the form of a white box model, we can use first order approximations to find the affine expressions for the relations. Using a tool like FLOW*, we can obtain sound over-approximate affine maps of the form $A\mathbf{x} + [\mathbf{b}^l, \mathbf{b}^h]$, where $[\mathbf{b}^l, \mathbf{b}^h]$ denotes the interval of vectors, such that, every element b_i of the vector $\mathbf{b}$ is contained in the respective scalar interval $b_i \in [b_i^l, b_i^h]$.

For the case of black box systems, such a sound approximation is not possible. Instead, we rely on a statistical method like simple linear regression to estimate the affine map $f : A\mathbf{x} + \mathbf{b}$. We then estimate the error δ and generalize f to an interval affine map as before $f : A\mathbf{x} + \mathbf{b} + \delta$. Finally, we get an abstraction

with the below relation

$$C \overset{f}{\rightsquigarrow} C' \iff \exists \mathbf{x} \in C.\, \exists \mathbf{x}' \in C'.\, \mathbf{x}' \in A\mathbf{x} + \mathbf{b} \pm \delta.$$

However, in the presence of complex non-linear behavior, using a single affine map can lead to a poor approximation. To increase the precision, one can use more than one affine map. Let us denote this set as $R_{(C,C')}$ (ref. Sec. 7.1).

$$R_{(C,C')}(\mathbf{x}, \mathbf{x}') : \{f_i \mid \exists \mathbf{x} \in C.\, \exists \mathbf{x}' \in C'.\, \mathbf{x}' \in f_i(\mathbf{x})\}$$

Figure 7.2: Using OLS, G^R is computed by determining the appropriate $R_{(C,C')}$ for each edge of G.

As shown in Fig. 7.2, we use OLS to compute an enrichment of the abstraction graph G. For every edge $(C, C') \in edges(G)$, the set of relations $R_{(C,C')}(\mathbf{x}, \mathbf{x}')$ is computed. The semantics of the enriched edge are clearly non-deterministic. Form a state $\mathbf{x} \in C$, any $f_i \in R_{(C,C')}$ can be taken as long as $\mathbf{x}' \in C$' is satisfied. This interpretation results in an infinite state transition system. We now detail the construction of the set $R_{(C,C')}$ using k-relational modeling.

7.3.2 k - Relational Modeling

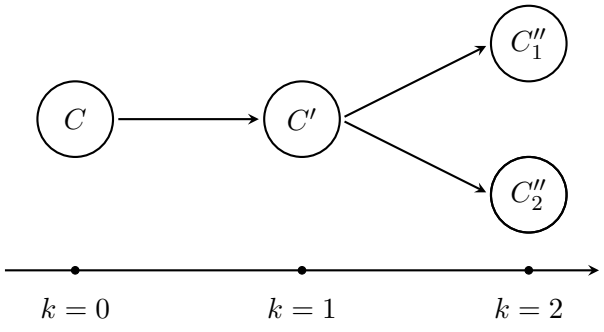

Figure 7.3: Nodes/Cells of G shown along with increasing values of k.

Given a G, when computing the set of relations for an edge R, we consider only the set of abstract states reachable at a specific time step. Intuitively, one might consider the states reachable in one time step Δ. However, such a process can be generalized by looking at the states reachable at $0\Delta, 1\Delta, \ldots, k\Delta$ time steps.

Using Fig. 7.3, we illustrate this notion. To compute $R_{(C,C')}$, we split the data set $D(C, C')$ consisting of trajectory segments (of time lengths $k\Delta$) as follows. We observe the local behavior of the system by noting the evolution of the system S from a state $\mathbf{x}(t) \in C$ for a time length dependant on k. For

- $k = 0$: we observe all trajectory segments of length Δ.
- $k = 1$: we observe trajectory segments of length Δ, which satisfy $\mathbf{x}(t + \Delta) \in C'$.
- $k = 2$: we observe trajectory segments of length 2Δ, and split them in two sets (a) and (b) on the basis of the cells reached at time $(t + \Delta)$ and $(t + 2\Delta)$.

  (a) $\mathbf{x}(t + \Delta) \in C' \wedge \mathbf{x}(t + 2\Delta) \in C''_1$

  (b) $\mathbf{x}(t + \Delta) \in C' \wedge \mathbf{x}(t + 2\Delta) \in C''_2$

- $k = n$: we observe trajectory segments of length $n\Delta$, and split them in to multiple sets on the basis of the cells reached at time $(t + \Delta),\ (t + 2\Delta),\ \ldots,\ (t + n\Delta)$.

k-relational modeling can be understood as a heuristic, which uses the underlying abstraction to differentiate behaviors of the system which 'diverge' (or are revealed to be 'distinct' at a future time). Such a heuristic can be useful in increasing the precision of the learnt affine maps. We now formalize this notion for $k = 0$, 1, and n and illustrate using examples.

0-Relational Model

When $k = 0$, the 0-relational model is a PWA transition system which only defines the evolution of states $\mathbf{x}$, and does not specify the reachable cell. The guard predicates of the relations are defined over cells: $g_i(\mathbf{x}) : \mathbf{x} \in C_i$ while $g'_i(\mathbf{x}') : True$.

We use regression to estimate the dynamics for the outgoing trajectory segments form a cell C. Hence, the data set $\mathcal{D}$ for the regression includes all trajectory segments beginning from the same cell

$$\mathcal{D} = \{\pi_t | start(\pi_t) \in C\}.$$

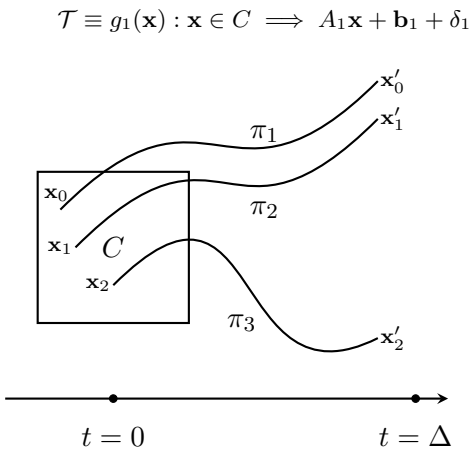

Figure 7.4: All the trajectory segments will be used to construct the model; $\mathcal{D} = \{\pi_1, \pi_2, \pi_3\}$.

This includes trajectory segments ending in different cells, as shown in Fig. 7.4. For N cells, this results in a ρ with N transition relations.

$$\mathcal{T} = \begin{cases} g_1(\mathbf{x}) : \mathbf{x} \in C_1 \implies A_1\mathbf{x} + \mathbf{b}_1 + \delta_1 \\ \dots \\ g_n(\mathbf{x}) : \mathbf{x} \in C_n \implies A_n\mathbf{x} + \mathbf{b}_n + \delta_n \end{cases}$$

Note that this can be quite imprecise when the cells are big, containing regions of state-space with complex dynamics. This is true for both non-linear systems and hybrid dynamical system, where a cell can contain two or more modes with differing continuous dynamics.

1**-Relational Model**

$$\mathcal{T} = \begin{cases} g_1(\mathbf{x}) : \mathbf{x} \in C \wedge g'_1(\mathbf{x}) : \mathbf{x} \in C'_1 \implies A_1\mathbf{x} + \mathbf{b}_1 + \delta_1 \\ g_2(\mathbf{x}) : \mathbf{x} \in C \wedge g'_2(\mathbf{x}) : \mathbf{x} \in C'_2 \implies A_2\mathbf{x} + \mathbf{b}_2 + \delta_2 \end{cases}$$

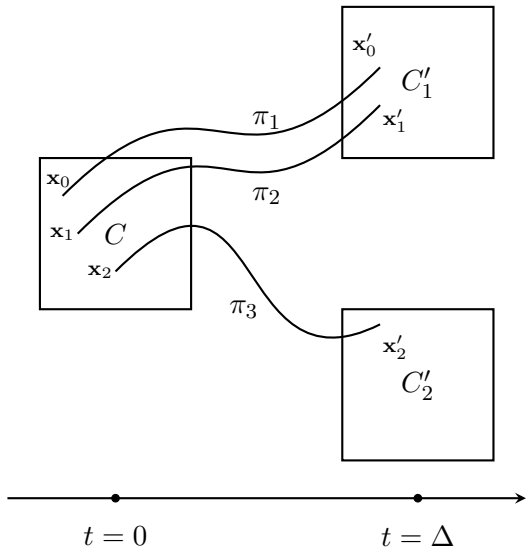

Figure 7.5: The data gets split into two sets $\mathcal{D}_1 = \{\pi_1, \pi_2\}$ and $\mathcal{D}_2 = \{\pi_3\}$ and two relations: $R_{(C,C'_1)}$ and $R_{(C,C'_2)}$, each with one affine map, are constructed.

To improve the preciseness of learnt dynamics, we include the reachability relation in the regression. For every relation $C \overset{t}{\rightsquigarrow} C'$, the data set $\mathcal{D}$ is comprised only of trajectory segments π_t which start and end in the same set of cells.

$$\mathcal{D} = \{\pi_t | start(\pi_t) \in C \wedge end(\pi_t) \in C'\}.$$

For N edges in G, 1-relationalization results in a ρ with N transition relations.

Fig. 7.5 illustrates the $k = 1$ refinement of the case shown in Fig. 7.4. The data set $\mathcal{D}$ is split into two data sets $\mathcal{D}_1 = \{\pi_1, \pi_2\}$ and $\mathcal{D}_2 = \{\pi_3\}$, using which, two relations are constructed. The resulting 1-relational model is at least as precise as the corresponding 0-relational model.

k-Relational Model

$$\mathcal{T} = \begin{cases} g_1(\mathbf{x}) : \mathbf{x} \in C \wedge g'_1(\mathbf{x}) : \mathbf{x} \in C'_1 \implies A_1\mathbf{x} + \mathbf{b}_1 + \delta_1 \\ g_1(\mathbf{x}) : \mathbf{x} \in C \wedge g'_1(\mathbf{x}) : \mathbf{x} \in C'_1 \implies A_2\mathbf{x} + \mathbf{b}_2 + \delta_2 \end{cases}$$

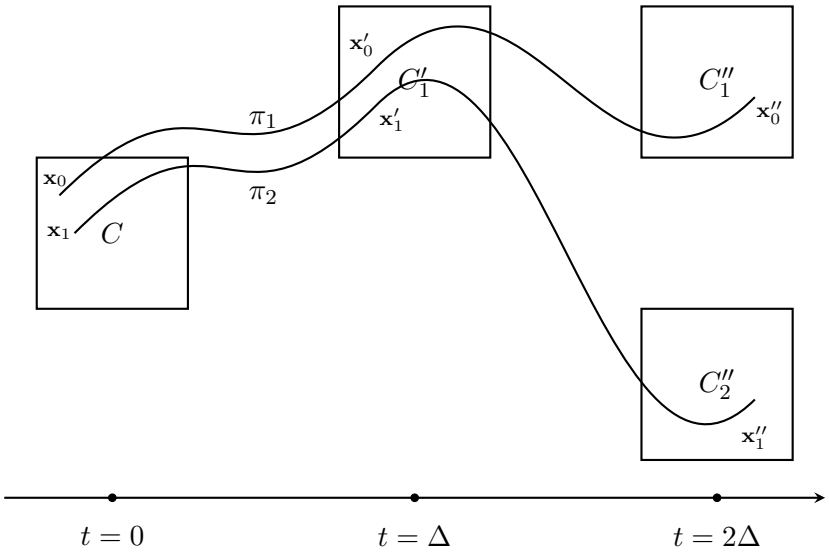

Figure 7.6: The $k = 2$ refinement further splits the data set $\mathcal{D}_1$ into two sets $\mathcal{D}_{11} = \{\pi_1\}$ and $\mathcal{D}_{12} = \{\pi_2\}$ and $R_{(C,C'_1)}$ now has two affine maps, non-deterministically defining the system behavior.

Finally, we generalize the relational models to k-relational PWA models. A k-relational model is constructed by using k length *connected* segmented trajectories. A segmented trajectory $\mathbf{S}_\pi$ is *connected* iff its cost $\text{COST}(\mathbf{S}_\pi) = 0$.

Two $\mathbf{S}_\pi : \langle \pi_{t_1}, \ldots, \pi_{t_k} \rangle$ and $\mathbf{S}'_\pi : \langle \pi'_{t_1}, \ldots, \pi'_{t_k} \rangle$ are *similar* if their trajectory segments have the same sequence of cell traversals $\langle C_1, C_2, \ldots, C_k \rangle$, i.e.

$$\forall i \in \{1 \ldots k\}. start(\pi_{t_i}) \in C_i \wedge start(\pi'_{t_i}) \in C_i \wedge end(\pi_{t_i}) \in C_{i+1} \wedge end(\pi'_{t_i}) \in C_{i+1}$$

For every cell C in the reachability graph, we construct a data set $\mathcal{D}$ by collecting π_{t_i}, such that they are the first segment of k length *connected* and *similar* segmented trajectories.

Fig. 7.6 illustrates the $k = 2$ refinement on Fig. 7.5.

7.4 Bounded Model Checking Black Box Systems

We now describe the entire procedure in three steps.

(1) Given a black box system S specified by SIM_S, we use scatter-and-simulate with (Δ-length) trajectory segments to sample a finite reachability graph $\mathcal{H}(\Delta)$.

(2) Using regression, we enrich the graph relations and annotate the edges with the estimated affine maps.

(3) Interpreting the directed reachability graph as a transition system, we use a bounded model checker to find fixed length violations to safety properties.

7.5 An Example: Van der Pol Oscillator

We now describe the above using the Van der Pol oscillator benchmark presented in Sec. 6.6.1. Simulations generated using uniformly random samples are shown in Fig. 7.5. We want to check the property P_3, indicated by the red box, given the initial set indicated by the green box. The abstraction is defined by $Q_{0.2}(\mathbf{x})$, which results in an evenly gridded state-space, where each cell is of size 0.2×0.2 units. Scatter-and-simulate is then used to construct the abstract graph G, using 2 samples per cell and the time step $\Delta = 0.1s$. The complete process follows.

(1) **Abstract** Consider an implicit abstraction induced by the quantization function $Q_\epsilon(\mathbf{x})$. The corresponding reachability graph $\mathcal{H}(\Delta)$ (with time step Δ) is given by $\left\langle \mathcal{C}, \overset{\Delta}{\rightsquigarrow}, \mathcal{C}_0, \mathcal{C}_u \right\rangle$.

(2) **Discover**: Using scatter-and-simulate, enumerate a finite number of cells (vertices) and the relations (edges) of the graph $\mathcal{H}(\Delta)$. Associate the set of generated trajectory segments with their respective originating cells using a map $D : C \mapsto \{\pi | start(\pi) \in C\}$. The discovered abstraction is show in Fig. 7.5. As mentioned, red cells are unsafe and green cells are initial cells.

(3) **Relationalize** For each cell C, perform regression analysis on the respective set of trajectory segments $D(C)$, and compute a set of affine relations $R_{C,C'}(\mathbf{x}, \mathbf{x}')$ between $\mathbf{x} \in C$ and $\mathbf{x}' \in C'$ s.t., edge$(C, C') \in \mathcal{H}(\Delta)$. Annotate each edge in the graph $\mathcal{H}(\Delta)$ with the respective relation.

Fig. 7.5 shows the cells and the trajectory segments which are part of the data sets constructed using the 1-relational modeling. Against each cell, its unique identifier (integer co-ordinate) is mentioned. Finally, Fig. 7.5 and Table 7.1 show the enriched graph G^R with its transition relations. Note that self loops result when an observed trajectory segment has its $start$ and end states in the same cell.

(4) **Model Check** The graph $\mathcal{H}(\Delta)$ can now be viewed as a transition system $\langle C, \mathbf{x}, \mathcal{T}, C_0, \mathcal{X}_0 \rangle$, where $C \in vertices(\mathcal{H}(\Delta))$ and $\mathbf{x} \in \mathcal{X}$. A transition $\tau \in \mathcal{T}$ is of the form $\langle C, C', \rho_\tau \rangle$, where $\rho_\tau(\mathbf{x}, \mathbf{x}') \subseteq \{R_{(C,C')}(\mathbf{x}, \mathbf{x}') | (C, C') \in edge(\mathcal{H}(\Delta))\}$.

(5) **Check Counter-example** The infinite state (but finite location) transition system can be model checked to find a concrete counter-example, which if exists, can indicate the existence of a similar trace in the original black-box system S. The latter check is carried out as before, using the numerical simulation function SIM. For the given example, the model checker is unable to find a counter-example.

7.5.1 Search Parameters

The search parameters for S3CAM-R include the parameters of S3CAM: N, ϵ and Δ. Additionally, they also include the maximum error budget δ_{max} for OLS and the maximum length of segmented trajectory for building k-relational models.

We have already discussed the effects of N, ϵ and Δ on S3CAM's performance. However, they also have an effect on relational modeling. A finer grid with small cells produces more accurate models than a coarser grid with large cells. Similarly, small time length trajectory segments result in more accurate modeling.

Maximum Model Error ($\boldsymbol{\delta_{\max}}$) . Given a δ_{max}, we keep increasing k during the k-relational modeling

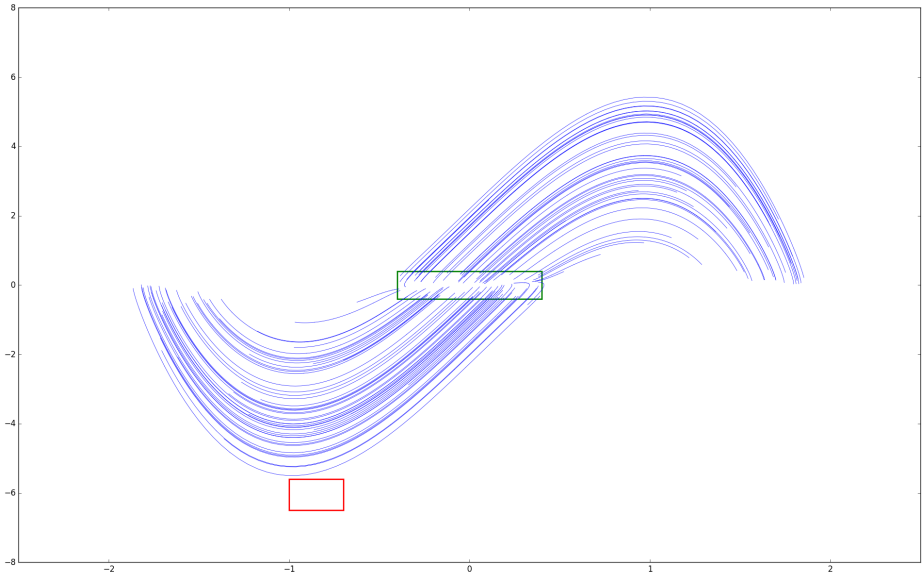

Figure 7.7: Van der Pol: continuous trajectories. Red and green boxes indicate unsafe and initial sets.

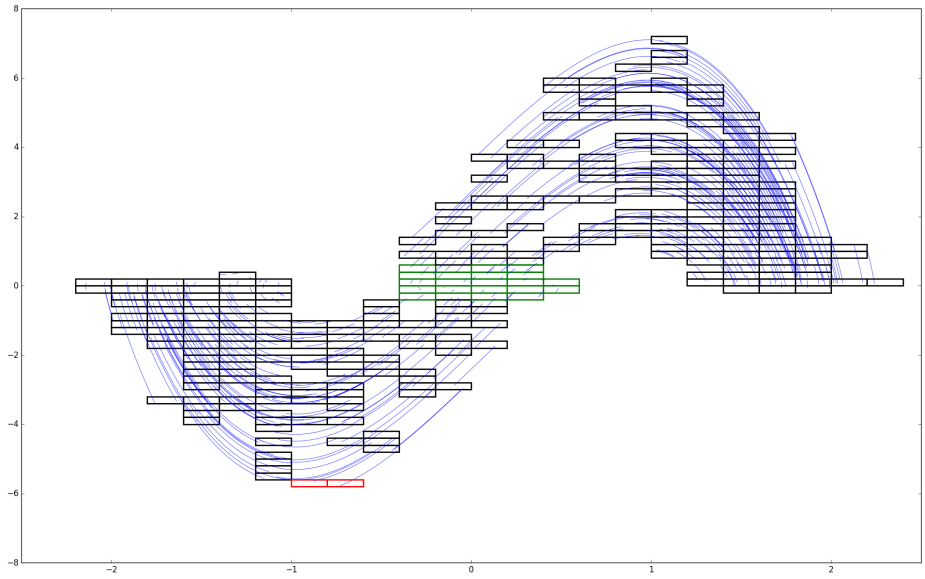

Figure 7.8: The discovered abstraction $\mathcal{H}(0.1)$. Red cells are unsafe cells and green cells are initial cells.

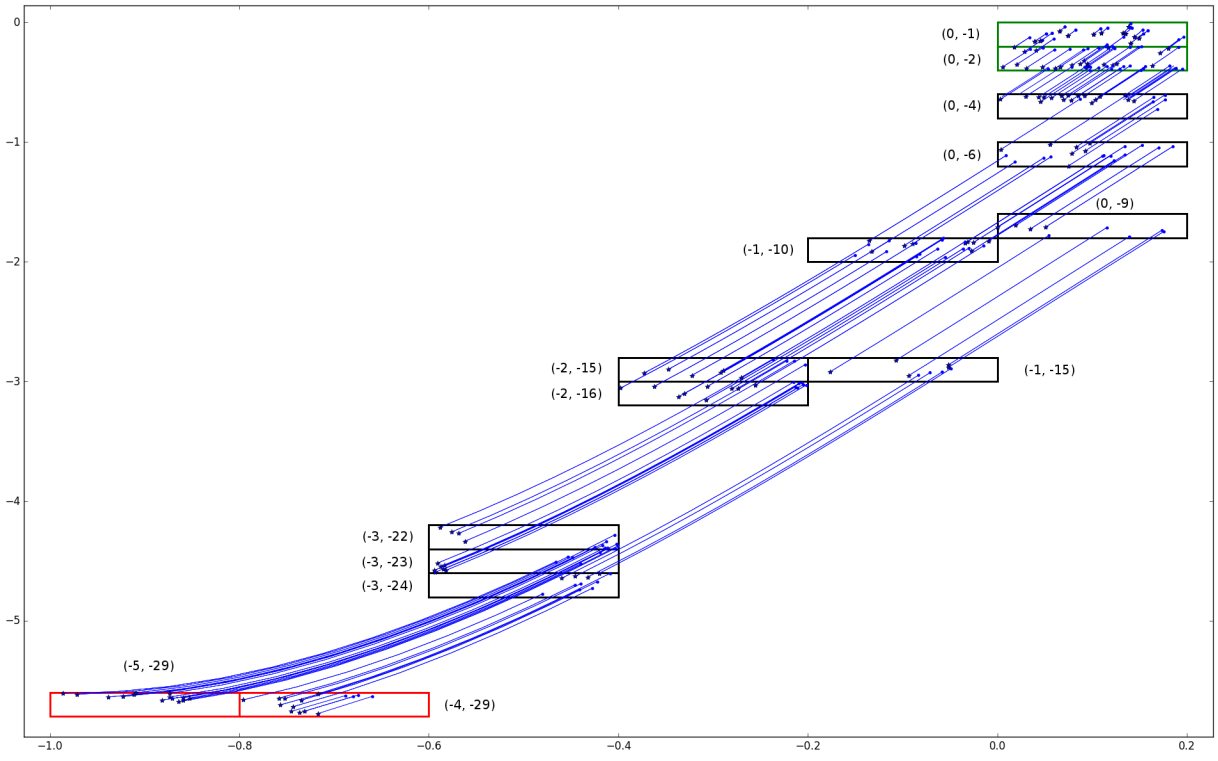

Figure 7.9: Cells and trajectory segments used by 1-relational modeling.

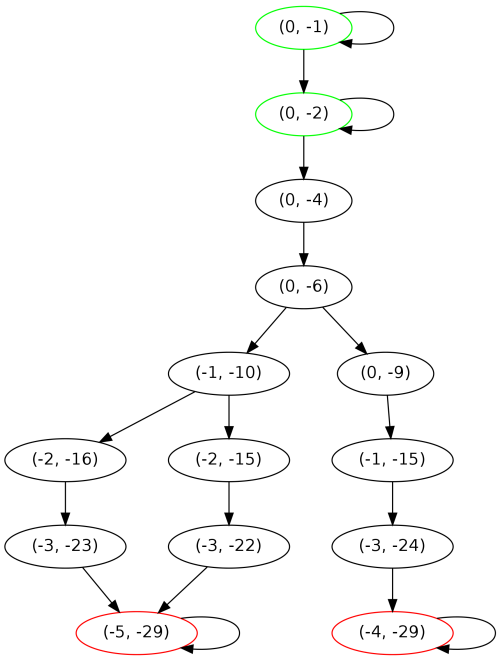

Figure 7.10: Enriched graph G^R. The affine maps f for the transition relations are show in Table 7.1.

Table 7.1: PWA model computed using OLS. The affine model for each edge (C, C') in the graph Fig. 7.5 is given by $x' \in Ax + b + \delta$, where δ is a vector of intervals.

C	C'	A	b	δ
(0, -1)	(0, -1)	$\begin{bmatrix} 0.99 & 0.12 \\ -0.12 & 1.63 \end{bmatrix}$	$\begin{bmatrix} 0 \\ 0 \end{bmatrix}$	$\begin{bmatrix} [0,0] \\ [0,0] \end{bmatrix}$
(0, -1)	(0, -2)	$\begin{bmatrix} 0.99 & 0.12 \\ -0.10 & 1.63 \end{bmatrix}$	$\begin{bmatrix} 0 \\ 0 \end{bmatrix}$	$\begin{bmatrix} [0,0] \\ [0,0] \end{bmatrix}$
(0, -2)	(0, -2)	$\begin{bmatrix} 0.99 & 0.12 \\ -0.09 & 1.63 \end{bmatrix}$	$\begin{bmatrix} 0 \\ 0 \end{bmatrix}$	$\begin{bmatrix} [0,0] \\ [0,0] \end{bmatrix}$
(0, -2)	(0, -4)	$\begin{bmatrix} 0.99 & 0.12 \\ -0.07 & 1.62 \end{bmatrix}$	$\begin{bmatrix} 0 \\ 0 \end{bmatrix}$	$\begin{bmatrix} [0,0] \\ [0,0] \end{bmatrix}$
(0, -9)	(-1, -15)	$\begin{bmatrix} 0.99 & 0.12 \\ -0.09 & 1.61 \end{bmatrix}$	$\begin{bmatrix} 0 \\ -0.04 \end{bmatrix}$	$\begin{bmatrix} [0,0] \\ [0,0.01] \end{bmatrix}$
(-1, -15)	(-3, -24)	$\begin{bmatrix} 0.95 & 0.12 \\ -1.29 & 1.47 \end{bmatrix}$	$\begin{bmatrix} -0.01 \\ -0.41 \end{bmatrix}$	$\begin{bmatrix} [0,0] \\ [0,0.01] \end{bmatrix}$
(-3, -24)	(-4, -29)	$\begin{bmatrix} 1.11 & -0.17 \\ -1.71 & 0.66 \end{bmatrix}$	$\begin{bmatrix} -1.07 \\ -3.31 \end{bmatrix}$	$\begin{bmatrix} [-0.04,0.04] \\ [-0.07,0.09] \end{bmatrix}$
(-4, -29)	(-4, -29)	$\begin{bmatrix} 0.99 & 0.01 \\ -0.41 & 1.02 \end{bmatrix}$	$\begin{bmatrix} 0 \\ -0.28 \end{bmatrix}$	$\begin{bmatrix} [0,0] \\ [0,0] \end{bmatrix}$
(-1, -10)	(-2, -16)	$\begin{bmatrix} 0.97 & 0.12 \\ -0.71 & 1.56 \end{bmatrix}$	$\begin{bmatrix} 0 \\ -0.11 \end{bmatrix}$	$\begin{bmatrix} [0,0] \\ [0,0.01] \end{bmatrix}$
(-1, -10)	(-2, -15)	$\begin{bmatrix} 0.97 & 0.12 \\ -0.70 & 1.58 \end{bmatrix}$	$\begin{bmatrix} 0 \\ -0.08 \end{bmatrix}$	$\begin{bmatrix} [0,0] \\ [0,0.01] \end{bmatrix}$
(-2, -16)	(-3, -23)	$\begin{bmatrix} 0.92 & 0.12 \\ -1.84 & 1.39 \end{bmatrix}$	$\begin{bmatrix} -0.02 \\ -0.73 \end{bmatrix}$	$\begin{bmatrix} [0,0] \\ [0,0] \end{bmatrix}$
(-3, -23)	(-5, -29)	$\begin{bmatrix} 3.14 & -0.81 \\ -0.96 & 0.23 \end{bmatrix}$	$\begin{bmatrix} -3.13 \\ -4.99 \end{bmatrix}$	$\begin{bmatrix} [-0.04,0.03] \\ [-0.03,0.04] \end{bmatrix}$
(-2, -15)	(-3, -22)	$\begin{bmatrix} 0.93 & 0.12 \\ -1.75 & 1.40 \end{bmatrix}$	$\begin{bmatrix} -0.02 \\ -0.68 \end{bmatrix}$	$\begin{bmatrix} [0,0] \\ [0,0] \end{bmatrix}$
(-3, -22)	(-5, -29)	$\begin{bmatrix} 3.08 & -0.72 \\ -1.69 & 0.40 \end{bmatrix}$	$\begin{bmatrix} -2.77 \\ -4.57 \end{bmatrix}$	$\begin{bmatrix} [-0.02,0.02] \\ [-0.01,0.02] \end{bmatrix}$

process till $\delta_i \leq \delta_{max}$ is satisfied. A k_{max} is introduced to bound the longest segmented trajectory which can be considered.

7.5.2 Reasons for Failure

The approach can fail to find a counter-example, even when it exists, in one of three ways.

- **S3CAM Fails** No abstract counter-example is found by S3CAM. We can remedy it by increasing search budgets and/or restarting.
- **BMC Fails** An abstract counter-example is found, but the BMC fails to find a concrete counter-example in the PWA relational model. The failure can be attributed to either (a) a spurious abstract counter-examples or (b) a poorly estimated model. The former can be addressed by restarting but the latter requires that the maximum model error δ_{max} be decreased.
- **Inaccurate PWA Modeling** An abstract counter-example is found, and it is successfully concretized in the PWA relational model by the BMC. However, it is not reproducible in the black box system. This happens when the PWA relational model is not precise enough.

7.6 Implementation and Evaluation

The implementation was prototyped as S3CAM-R, an extension to our previously mentioned tool S3CAM (Chapter 6). OLS regression routines were used from Scikit-learn [132], a Python module for machine learning. SAL [146] with Yices2 [51] was the model checker and the SMT solver.

We used S3CAM to discover the abstraction graph G, which was then trimmed of the nodes which did not contribute to the error search (nodes from which error nodes were not reachable). In our experiments we used 1-relational modeling to create the transition system from G. Using SAL, we checked for the given safety property. If a concrete trace was obtained from the BMC, it was further checked for validity by simulating using SIM to see if it was indeed an error trace. If not, 100 samples from its associated abstract state was sampled to check the presence of a counter-example in it neighborhood. This can be further extended by obtaining different discrete sequences or discrete trace sequences from the model checker.

We tabulate our preliminary evaluation in Table 7.2. We used few of the benchmarks described in Chapter 6, including the Van der Pol oscillator, Brusselator, Lorenz attractor and the Navigation benchmark. As before, we ran S3CAM-R 10 times with different seeds and averaged the results. We tabulate both the total time taken and the time taken by SAL to compute the counter-example and compare against a newer implementation of S3CAM. Note that different abstraction parameters are used for S3CAM and S3CAM-R, due to the differences in which they operate.

Table 7.2: Avg. timings for benchmarks. The **BMC** column lists time taken by the BMC engine. The total time in seconds (rounded off to an integer) is noted under **S3CAM-R** and **S3CAM**. TO signifies time $> 5hr$, after which the search was killed.

Benchmark	BMC	S3CAM-R	S3CAM
Van der Pol ($\mathcal{P}_3$)	<1	130	24
Brusselator	<1	4	2
Lorenz	<1	122	35
Nav ($\mathcal{P}_P$)	5862	11520	603
Nav ($\mathcal{P}_Q$)	2216	6847	546
Nav ($\mathcal{P}_R$)	-	TO	2003
Nav ($\mathcal{P}_S$)	-	TO	2100
Bouncing Ball	-	TO	450

The results show promise, but clearly S3CAM performs better. Also, S3CAM-R timed out on some benchmarks like Nav $\mathcal{P}_R$, Nav $\mathcal{P}_S$ and the bouncing ball. However, we need to explore more benchmarks to be conclusive. S3CAM-R's performance can be explained by the difficulty in finding a good abstraction Q_ϵ, which needs to be fine enough, to obtain good prediction models but coarse enough, to be manageable by the current SMT solvers. Specifically, to obtain a good quality counter-example from the model checker (and avoid false positives), the transition system should be created from models with high accuracy, for which a finer abstraction is required. However, the exploration of a finer abstraction is exponentially more complex and results in a much bigger transition system, which the current state of the art bounded model checkers (which use SMT solvers) can not handle under reasonable resources.

7.7 Conclusion and Future Work

We have presented another methodology to find falsifications in black box dynamical systems. Combining the ideas from abstraction based search (Chapter 4), with our previous relational abstractions [166], we proposed k-relational modeling to compute richer abstractions. Simple linear regression can be used to estimate the local dynamics of the trajectory segments and compute PWA relational models which can be interpreted as a transition system. These can then be checked for safety violations using an off-the-shelf bounded model checker. Finally, we implemented the ideas as a tool S3CAM-R and demonstrated its performance on a few examples.

7.7.1 Improvements

The approach seems promising as it avoids an expensive refinement step. But, before it can be applied to more complex systems, we need to overcome its shortcomings. As a future extension, we are investigating ideas to improve the performance of the underlying three main sub-processes, namely, abstraction, modeling, and BMC. We detail these below.

(1) **Abstraction** The abstract domain we have used, has been confined to the interval or rectangular domain. Such a domain is very coarse when compared to more general polyhedral domains, using which, we can gain better precision. Due to polyhedral domains being computational expensive, their integration in S3CAM needs to be explored thoroughly.

(2) **Modeling** We have used k-relational modeling to increase the precision of the enriched abstractions, however, there are several other refinement strategies that remain to be explored. This includes refining the abstract states by using guard predicates (similar to predicate abstraction), using non-linear templates in parametric regression to compute more precise quadratic relations, and using an adaptive time step instead of a fixed one to address the non-linearities due to a long time horizon.

(3) **Model Checking** As of now, we use SMT solvers to search for concrete counter-examples. Although they are very efficient, owing to extensive engineering effort, reachability of transition systems result-

ing from dynamical systems remains a difficult problem. As the time horizon of the safety property increases, the possible combinations of discrete transitions increase exponentially. Hence, to find a counterexample which is a sequence of discrete transitions over a 'long' time horizon is not tractable for most, but the simplest of dynamical systems. Instead, we can use linear programming solvers, by enumerating each path in the graph G^R. Note that the constraints are all linear (conjunctions) along an abstract path. However, in the worst case, the number of paths in a graph can be of the order $n!$ where n is the number of vertices of a graph. Hence, this will not be feasible, unless, we can prioritize paths by using a triage process similar to one used by S3CAM and using a budget on the maximum number of paths.

Another approach to address the issue would be to use an adaptive time discretization technique, where relations over both shorter and longer time steps are computed, and the SMT solver can 'select' the time step precise enough to find a counter-example.

(4) **SMT Solvers** One major impediment to our approach is the fact that SMT solvers use the theory of reals with **exact precision**. This is important for verification approaches, but can be relaxed for the problem of falsification. An SMT solver which uses approximate reasoning but returns robust counter-examples will be as useful, and perhaps more efficient.

7.7.2 Data Driven Analysis

Finally, we would like to mention that our approach is 'simulation' driven. It can be easily modified to be 'data driven', by working with a fixed set of data. Given a data set, we then need to automatically find a good abstraction and a high fidelity PWA transition system using which, we can summarize the black box hybrid dynamical system. Apart from model checking the transition system, one can extend it to the analysis of SDCS. More specifically, by combining the transition system model of a plant with the control software, a model checker like CBMC [100] can be used to do a closed loop symbolic analysis of the SDCS. This can be an alternative to S3CAM-X.

Chapter 8

Conclusions

In conclusion, we presented techniques for finding safety violations in cyber-physical systems (CPS). We put forth a combination of symbolic and numerical analysis to automatically analyze sampled-data control systems. The numerical analysis is specialized for the exploration of behaviors of a dynamical system. Moreover, it requires only the numerical simulation function as the definition for the system and makes minimal assumptions. On the other hand, the symbolic analysis is software specific and rigorously explores all paths of the software. Using the two together results in a highly applicable and scalable approach.

We demonstrated the approach by implementing it as a tool: S3CAM, which we tested on several benchmarks. S3CAM's performance is shown to be as good, if not better, than the currently available tools. It is able to find falsifications even when the other tools fail.

There are several aspects of our approach which can be improved upon; and there are many more unexplored avenues which can enable the widespread acceptance of automatic falsification methods. We discuss them below.

MTL Properties

We have focused on falsifying simple safety properties. Many important properties of systems are temporal in nature, and expressible in temporal logics like LTL/MTL/STL. We can extend our techniques to handle temporal properties by using monitors [116–118]. However, done naively, it might not yield acceptable performance in practice. Hence, efficient methods must be explored.

Compositional Analysis

In practice, systems are often specified as compositions of sub-systems. Engineering and development tools like Simulink®, encourage 'block' based compositional methodologies. A complex system block is created by specifying simpler sub-system blocks and defining their interactions. A similar notion is true for software, where natural slices or partitions in the program can exist. Program slicing has been explored in [3, 43, 98, 153, 155, 159]. Exploring compositional analyses can increase our applicability; and also give us efficient procedures to analyze large systems by decomposing them into smaller ones.

Input Output Relationalization

A limitation of the current numerical exploration of the plant is the requirement of state observability. This is often restrictive in practice. An exploration into the space of *input output relational abstractions* seems natural. We would like to explore reduced order modeling techniques [143, 150] and relational abstractions of the plants in order to obtain simpler models. This can tremendously improve the scalability of our current approaches by reducing the state-space dimensionality. PWA relational abstractions constructed through machine learning techniques (Chapter 7), highlight our first steps in this direction.

Specialization to Control Software

Using an off-the-shelf symbolic executor for analyzing the control software has its limitations. The symbolic executor is engineered for general purpose software and misses out on the optimizations which are specific to the domain of control software. Also, it does not provide domain specific functionality, like dimensional analysis [129], which can be very useful. Another extension would be to introduce relaxations, like concolic executions, which can improve the scalability of the overall analysis.

Tool Improvements

Finally, we would like to improve our tool S3CAM. We would like to address implementation aspects like, memory and run time optimizations, extension to various input formats used in the industry and automatic parameter selection.

Bibliography

[1] Houssam Abbas, Georgios Fainekos, Sriram Sankaranarayanan, Franjo Ivancic, and Aarti Gupta. Probabilistic temporal logic falsification of cyber-physical systems. Trans. on Embedded Computing Systems (TECS), 12(2s):95, 2012.

[2] Houssam Abbas, Andrew Winn, Georgios Fainekos, and A Agung Julius. Functional gradient descent method for metric temporal logic specifications. In 2014 American Control Conference, pages 2312–2317. IEEE, 2014.

[3] Hiralal Agrawal and Joseph R Horgan. Dynamic program slicing. In ACM SIGPLAN Notices, volume 25, pages 246–256. ACM, 1990.

[4] Rajeev Alur. Formal verification of hybrid systems. In Embedded Software (EMSOFT), 2011 Proceedings of the International Conference on, pages 273–278. IEEE, 2011.

[5] Rajeev Alur. Principles of cyber-physical systems. MIT Press, 2015.

[6] Rajeev Alur, Costas Courcoubetis, Nicolas Halbwachs, P.-H. Ho Thomas A. Henzinger, Xavier Nicollin, Alfredo Olivero, Joseph Sifakis, and Sergio Yovine. The algorithmic analysis of hybrid systems. Theoretical computer science, 138(1):3–34, 1995.

[7] Rajeev Alur, Thao Dang, and Franjo Ivančić. Counter-example guided predicate abstraction of hybrid systems. In TACAS, volume 2619 of LNCS, pages 208–223. Springer, 2003.

[8] Rajeev Alur, Thomas A. Henzinger, G. Lafferriere, and George Pappas. Discrete abstractions of hybrid systems. Proc. of IEEE, 88(7):971–984, 2000.

[9] Rajeev Alur, Thomas A Henzinger, Gerardo Lafferriere, and George J Pappas. Discrete abstractions of hybrid systems. Proceedings of the IEEE, 88(7):971–984, 2000.

[10] Yashwanth Annpureddy, Che Liu, Georgios Fainekos, and Sriram Sankaranarayanan. S-taliro: A tool for temporal logic falsification for hybrid systems. Springer, 2011.

[11] Eugene Asarin, Thao Dang, and Antoine Girard. Hybridization methods for the analysis of nonlinear systems. Acta Informatica, 43:451—476, 2007.

[12] Uri M Ascher, Robert MM Mattheij, and Robert D Russell. Numerical solution of boundary value problems for ordinary differential equations, volume 13. Siam, 1994.

[13] J-P Aubin, John Lygeros, Marc Quincampoix, Shankar Sastry, and Nicolas Seube. Impulse differential inclusions: a viability approach to hybrid systems. Automatic Control, IEEE Transactions on, 47(1):2–20, 2002.

[14] Shaun Ault and Erik Holmgreen. Dynamics of the brusselator. Math 715 Projects (Autumn 2002), page 2, 2003.

[15] Gerd Behrmann, Alexandre David, and Kim G. Larsen. A tutorial on UPPAAL. In SFM-RT 200 (Revised Lectures), volume 3185 of LNCS, pages 200–237. Springer Verlag, 2004.

[16] Luca Benvenuti, Davide Bresolin, Alberto Casagrande, Pieter Collins, Alberto Ferrari, Emanuele Mazzi, Alberto Sangiovanni-Vincentelli, and Riziano Villa. Reachability computation for hybrid systems with Ariadne. In Proc. the 17th IFAC World Congress, 2008.

[17] Richard N Bergman. Toward physiological understanding of glucose tolerance: minimal-model approach. Diabetes, 38(12):1512–1527, 1989.

[18] Richard N Bergman, Lawrence S Phillips, and Claudio Cobelli. Physiologic evaluation of factors controlling glucose tolerance in man: measurement of insulin sensitivity and beta-cell glucose sensitivity from the response to intravenous glucose. Journal of Clinical Investigation, 68(6):1456, 1981.

[19] Martin Berz and Kyoko Makino. Verified integration of odes and flows using differential algebraic methods on high-order taylor models. Reliable Computing, 4(4):361–369, 1998.

[20] Martin Berz and Kyoko Makino. Performance of Taylor model methods for validated integration of ODEs. LNCS, 3732:65–74, 2005.

[21] John T Betts. Survey of numerical methods for trajectory optimization. Journal of guidance, control, and dynamics, 21(2):193–207, 1998.

[22] John T Betts. Practical methods for optimal control and estimation using nonlinear programming, volume 19. Siam, 2010.

[23] Amit Bhatia and Emilio Frazzoli. Incremental search methods for reachability analysis of continuous and hybrid systems. Proc. of HSCC, page 451–471, 2004.

[24] Hans Georg Bock and Karl-Josef Plitt. A multiple shooting algorithm for direct solution of optimal control problems. 1983.

[25] M. Branicky, M. Curtiss, J. Levine, and S. Morgan. Sampling-based planning, control and verification of hybrid systems. IEE Proc.-Control Theory Appl., 153(5):575–590, 2006.

[26] Michael S Branicky. Introduction to hybrid systems. In Handbook of Networked and Embedded Control Systems, pages 91–116. Springer, 2005.

[27] Cristian Cadar, Daniel Dunbar, and Dawson R Engler. Klee: Unassisted and automatic generation of high-coverage tests for complex systems programs. In OSDI, volume 8, pages 209–224, 2008.

[28] Cristian Cadar, Patrice Godefroid, Sarfraz Khurshid, Corina S Păsăreanu, Koushik Sen, Nikolai Tillmann, and Willem Visser. Symbolic execution for software testing in practice: preliminary assessment. In Proceedings of the 33rd International Conference on Software Engineering, pages 1066–1071. ACM, 2011.

[29] Cristian Cadar and Koushik Sen. Symbolic execution for software testing: three decades later. Communications of the ACM, 56(2):82–90, 2013.

[30] Alberto Casagrande, Andrea Balluchi, Luca Benvenuti, Alberto Policriti, Tiziano Villa, and AL Sangiovanni-Vincentelli. A new algorithm for reachability analysis of hybrid automata. Technical report, Citeseer.

[31] Xin Chen, Erika Abrahám, and Sriram Sankaranarayanan. Taylor model flowpipe construction for non-linear hybrid systems. In Real-Time Systems Symposium (RTSS), pages 183–192. IEEE, 2012.

[32] Xin Chen, Erika Ábrahám, and Sriram Sankaranarayanan. Flow*: An analyzer for non-linear hybrid systems. In Computer Aided Verification, pages 258–263. Springer, 2013.

[33] Edmund Clarke, Ansgar Fehnker, Zhi Han, Bruce Krogh, Joël Ouaknine, Olaf Stursberg, and Michael Theobald. Abstraction and counterexample-guided refinement in model checking of hybrid systems. International Journal of Foundations of Computer Science, 14(04):583–604, 2003.

[34] Edmund M. Clarke, Orna Grumberg, Somesh Jha, Yuan Lu, and Helmut Veith. Counterexample-guided abstraction refinement for symbolic model checking. J. ACM, 50(5):752–794, 2003.

[35] Edmund M. Clarke, Orna Grumberg, and Doron A. Peled. Model Checking. MIT Press, 1999.

[36] Michael Colón, Sriram Sankaranarayanan, and Henny Sipma. Linear invariant generation using non-linear constraint solving. In CAV, volume 2725 of LNCS, pages 420–433. Springer, July 2003.

[37] P. Cousot and R. Cousot. Abstract interpretation: a unified lattice model for static analysis of programs by construction or approximation of fixpoints. In Conference Record of the Fourth Annual ACM SIGPLAN-SIGACT Symposium on Principles of Programming Languages, pages 238–252, Los Angeles, California, 1977. ACM Press, New York, NY.

[38] T. Dang, A. Donze, O. Maler, and N. Shalev. Sensitive state-space exploration. In Proc. of the 47th IEEE CDC, pages 4049–4054, Dec. 2008.

[39] Thao Dang, Alexandre Donzé, Oded Maler, and Noa Shalev. Sensitive state-space exploration. In Decision and Control, 2008. CDC 2008. 47th IEEE Conference on, pages 4049–4054. IEEE, 2008.

[40] Thao Dang, Oded Maler, and Romain Testylier. Accurate hybridization of nonlinear systems. In HSCC '10, pages 11–20. ACM, 2010.

[41] Thao Dang and Tarik Nahhal. Coverage-guided test generation for continuous and hybrid systems. Formal Methods in System Design, 34(2):183–213, 2009.

[42] Thao Dang and Tarik Nahhal. Coverage-guided test generation for continuous and hybrid systems. Formal Methods in System Design, 34(2):183–213, 2009.

[43] Andrea De Lucia et al. Program slicing: Methods and applications. In scam, pages 144–151, 2001.

[44] Leonardo De Moura and Nikolaj Bjørner. Z3: An efficient smt solver. In Tools and Algorithms for the Construction and Analysis of Systems, pages 337–340. Springer, 2008.

[45] Jyotirmoy Deshmukh, Xiaoqing Jin, James Kapinski, and Oded Maler. Stochastic local search for falsification of hybrid systems. In Automated Technology for Verification and Analysis, pages 500–517. Springer, 2015.

[46] A. Donzé and O. Maler. Robust satisfaction of temporal logic over real-valued signals. In Proc. FORMATS, pages 92–106, 2010.

[47] Alexandre Donzé. Breach, a toolbox for verification and parameter synthesis of hybrid systems. In Proc. CAV, pages 167–170, 2010.

[48] Alexandre Donzé and Oded Maler. Systematic simulation using sensitivity analysis. In Hybrid Systems: Computation and Control, pages 174–189. Springer, 2007.

[49] Tommaso Dreossi, Thao Dang, Alexandre Donzé, James Kapinski, Xiaoqing Jin, and Jyotirmoy V Deshmukh. Efficient guiding strategies for testing of temporal properties of hybrid systems. In NASA Formal Methods, pages 127–142. Springer, 2015.

[50] Parasara Sridhar Duggirala and Sayan Mitra. Abstraction refinement for stability. In Cyber-Physical Systems (ICCPS), 2011 IEEE/ACM International Conference on, pages 22–31. IEEE, 2011.

[51] Bruno Dutertre. Yices 2.2. In International Conference on Computer Aided Verification, pages 737–744. Springer, 2014.

[52] Bruno Dutertre and Leonardo De Moura. The yices smt solver. Tool paper at http://yices. csl. sri. com/tool-paper. pdf, 2:2, 2006.

[53] Joel M. Esposito, Jongwoo Kim, and Vijay Kumar. Adaptive rrts for validating hybrid robotic control systems. In Workshop on Algorithmic Foundations of Robotics, pages 107–132, 2004.

[54] Joel M. Esposito, Jongwoo Kim, and Vijay Kumar. Adaptive RRTs for validating hybrid robotic control systems. In Proceedings of the International Workshop on the Algorithmic Foundations of Robotics, 2004.

[55] Joel M Esposito, Jongwoo Kim, and Vijay Kumar. Adaptive rrts for validating hybrid robotic control systems. In Algorithmic Foundations of Robotics VI, pages 107–121. Springer, 2005.

[56] Georgios Fainekos and George J. Pappas. Robustness of temporal logic specifications for continuous-time signals. Theoretical Computer Science, 410:4262–4291, 2009.

[57] Georgios E. Fainekos. Robustness of Temporal Logic Specifications. PhD thesis, Department of Computer and Information Science, University of Pennsylvania, 2008.

[58] Georgios E. Fainekos, Antoine Girard, and George J. Pappas. Temporal logic verification using simulation. In FORMATS, volume 4202 of LNCS, pages 171–186. Springer, 2006.

[59] Georgios E Fainekos and George J Pappas. Robustness of temporal logic specifications for finite state sequences in metric spaces. Technical report, Technical Report MS-CIS-06-05, Dept. of CIS, Univ. of Pennsylvania, 2006.

[60] Georgios E Fainekos and George J Pappas. Robust sampling for mitl specifications. In Formal Modeling and Analysis of Timed Systems, pages 147–162. Springer, 2007.

[61] Ansgar Fehnker and Franjo Ivanĉić. Benchmarks for hybrid systems verification. In HSCC, volume 2993 of LNCS, pages 326–341. Springer, 2004.

[62] Michael E Fisher. A semiclosed-loop algorithm for the control of blood glucose levels in diabetics. Biomedical Engineering, IEEE Transactions on, 38(1):57–61, 1991.

[63] Martin Fränzle and Christian Herde. Hysat: An efficient proof engine for bounded model checking of hybrid systems. Formal Methods in System Design, 30(3):179–198, 2007.

[64] Goran Frehse. PHAVer: Algorithmic Verification of Hybrid Systems Past HyTech. STTT, 10(3), June 2008.

[65] Goran Frehse, Colas Le Guernic, Alexandre Donzé, Scott Cotton, Rajarshi Ray, Olivier Lebeltel, Rodolfo Ripado, Antoine Girard, Thao Dang, and Oded Maler. Spaceex: Scalable verification of hybrid systems. In Computer Aided Verification, pages 379–395. Springer, 2011.

[66] Goran Frehse, Colas Le Guernic, Alexandre Donzé, Scott Cotton, Rajarshi Ray, Olivier Lebeltel, Rodolfo Ripado, Antoine Girard, Thao Dang, and Oded Maler. Spaceex: Scalable verification of hybrid systems. In Proc. CAV, LNCS. Springer, 2011.

[67] Jerome Friedman, Trevor Hastie, and Robert Tibshirani. The elements of statistical learning, volume 1. Springer series in statistics Springer, Berlin, 2001.

[68] Sicun Gao, Soonho Kong, and Edmund M Clarke. dreal: An smt solver for nonlinear theories over the reals. In Automated Deduction–CADE-24, pages 208–214. Springer, 2013.

[69] Sicun Gao, Soonho Kong, and Edmund M Clarke. Satisfiability modulo odes. In Formal Methods in Computer-Aided Design (FMCAD), 2013, pages 105–112, 2013.

[70] Dimitra Giannakopoulou and Klaus Havelund. Automata-based verification of temporal properties on running programs. In Automated Software Engineering, 2001.(ASE 2001). Proceedings. 16th Annual International Conference on, pages 412–416. IEEE, 2001.

[71] Antoine Girard. Reachability of uncertain linear systems using zonotopes. In HSCC, volume 3414 of LNCS, pages 291–305. Springer, 2005.

[72] Antoine Girard and George J Pappas. Approximation metrics for discrete and continuous systems. 2005.

[73] Rafal Goebel, Ricardo G Sanfelice, and Andrew R Teel. Hybrid Dynamical Systems: modeling, stability, and robustness. Princeton University Press, 2012.

[74] Colas Le Guernic and Antoine Girard. Reachability analysis of linear systems using support functions. Nonlinear Analysis: Hybrid Systems, 4(2):250 – 262, 2010.

[75] Sumit Gulwani and Ashish Tiwari. Constraint-based approach for hybrid systems. In CAV, volume 5123 of LNCS, pages 190–203, 2008.

[76] Charles R Hargraves and SW Paris. Direct trajectory optimization using nonlinear programming and collocation. Journal of Guidance, Control, and Dynamics, 10(4):338–342, 1987.

[77] Klaus Havelund and Grigore Roşu. Monitoring programs using rewriting. In Automated Software Engineering, 2001.(ASE 2001). Proceedings. 16th Annual International Conference on, pages 135–143. IEEE, 2001.

[78] Klaus Havelund and Grigore Roşu. Synthesizing monitors for safety properties. In Tools and Algorithms for the Construction and Analysis of Systems, pages 342–356. Springer, 2002.

[79] Thomas A. Henzinger. The theory of hybrid automata. In LICS'96, pages 278–292. IEEE, 1996.

[80] Thomas A Henzinger, Pei-Hsin Ho, and Howard Wong-Toi. Hytech: the next generation. In Real-Time Systems Symposium, 1995. Proceedings., 16th IEEE, pages 56–65. IEEE, 1995.

[81] Thomas A. Henzinger, Pei-Hsin Ho, and Howard Wong-Toi. Algorithmic analysis of nonlinear hybrid systems. IEEE Transactions on Automatic Control, 43:540–554, 1998.

[82] Thomas A Henzinger, Peter W Kopke, Anuj Puri, and Pravin Varaiya. What's decidable about hybrid automata? In Proceedings of the twenty-seventh annual ACM symposium on Theory of computing, pages 373–382. ACM, 1995.

[83] Thomas A Henzinger, Marius Minea, and Vinayak Prabhu. Assume-guarantee reasoning for hierarchical hybrid systems. In International Workshop on Hybrid Systems: Computation and Control, pages 275–290. Springer, 2001.

[84] Thomas A Henzinger, Shaz Qadeer, and Sriram K Rajamani. You assume, we guarantee: Methodology and case studies. In International Conference on Computer Aided Verification, pages 440–451. Springer, 1998.

[85] C. Herde, A. Eggers, and T. Franzle, M. Teige. Analysis of hybrid systems using HySAT. In Third International Conference on Systems, 2008. ICONS 08., pages 13–18. IEEE, 2008.

[86] Chieh Su Hsu. Cell-to-cell mapping: a method of global analysis for nonlinear systems, volume 64. Springer Science & Business Media, 2013.

[87] CS Hsu and RS Guttalu. An unravelling algorithm for global analysis of dynamical systems: an application of cell-to-cell mappings. Journal of Applied Mechanics, 47(4):940–948, 1980.

[88] Mike Huang, Hayato Nakada, Srinivas Polavarapu, Richard Choroszucha, Ken Butts, and Ilya Kolmanovsky. Towards combining nonlinear and predictive control of diesel engines. In American Control Conference, 2013. Proceedings of the 2004, pages 2852–2859. IEEE, 2013.

[89] Xiaoqing Jin, Jyotirmoy V Deshmukh, James Kapinski, Koichi Ueda, and Ken Butts. Powertrain control verification benchmark. In Proceedings of the 17th international conference on Hybrid systems: computation and control, pages 253–262. ACM, 2014.

[90] A Agung Julius, Georgios E Fainekos, Madhukar Anand, Insup Lee, and George J Pappas. Robust test generation and coverage for hybrid systems. In Hybrid Systems: Computation and Control, pages 329–342. Springer, 2007.

[91] Aditya Kanade, Rajeev Alur, Franjo Ivančić, S. Ramesh, Sriram Sankaranarayanan, and K.C. Sashidhar. Generating and analyzing symbolic traces of Simulink/Stateflow models. In Computer-aided Verification (CAV), volume 5643 of LNCS, pages 430–445, 2009.

[92] Aditya Kanade, Rajeev Alur, Franjo Ivančić, S Ramesh, Sriram Sankaranarayanan, and KC Shashidhar. Generating and analyzing symbolic traces of simulink/stateflow models. In Computer Aided Verification, pages 430–445. Springer, 2009.

[93] Jim Kapinski, Bruce H. Krogh, Oded Maler, and Olaf Stursberg. On systematic simulation of open continuous systems. In HSCC, volume 2623 of LNCS, pages 283–297. Springer, 2003.

[94] Jongwoo Kim, Joel M. Esposito, and Vijay Kumar. An RRT-based algorithm for testing and validating multi-robot controllers. Technical report, DTIC Document, 2005.

[95] Jongwoo Kim, Joel M Esposito, and Vijay Kumar. An rrt-based algorithm for testing and validating multi-robot controllers. Technical report, DTIC Document, 2005.

[96] James C King. Symbolic execution and program testing. Communications of the ACM, 19(7):385–394, 1976.

[97] Soonho Kong, Sicun Gao, Wei Chen, and Edmund Clarke. dreach: Delta-reachability analysis for hybrid systems. In Tools and Algorithms for the Construction and Analysis of Systems, 2015.

[98] Bogdan Korel and Janusz Laski. Dynamic program slicing. Information Processing Letters, 29(3):155–163, 1988.

[99] Ron Koymans. Specifying real-time properties with metric temporal logic. Real-time systems, 2(4):255–299, 1990.

[100] Daniel Kroening and Michael Tautschnig. Cbmc–c bounded model checker. In International Conference on Tools and Algorithms for the Construction and Analysis of Systems, pages 389–391. Springer, 2014.

[101] Sebastian Kupferschmid, Jörg Hoffmann, Henning Dierks, and Gerd Behrmann. Adapting an AI planning heuristic for directed model checking. In Proc. of SPIN, pages 35–52, 2006.

[102] Jan Kuřátko and Stefan Ratschan. Combined global and local search for the falsification of hybrid systems. In International Conference on Formal Modeling and Analysis of Timed Systems, pages 146–160. Springer, 2014.

[103] Jan Kuratko and Stefan Ratschan. Solving underdetermined boundary value problems by sequential quadratic programming. arXiv preprint arXiv:1512.09078, 2015.

[104] Alexander B. Kurzhanski and Pravin Varaiya. Ellipsoidal techniques for reachability analysis. In HSCC, volume 1790 of LNCS, pages 202–214. Springer, 2000.

[105] A. A. Kurzhanskiy and P. Varaiya. Ellipsoidal toolbox. Technical Report UCB/EECS-2006-46, EECS Department, University of California, Berkeley, May 2006.

[106] Steven M LaValle. Rapidly-exploring random trees a new tool for path planning. 1998.

[107] Steven M LaValle and James J Kuffner Jr. Randomized kinodynamic planning. In Proc. ICRA, volume 1, pages 473–479. IEEE, 1999.

[108] Edward Ashford Lee and Sanjit Arunkumar Seshia. Introduction to embedded systems: A cyber-physical systems approach. Lee & Seshia, 2011.

[109] Flavio Lerda, James Kapinski, Edmund Clarke, and Bruce Krogh. Verification of supervisory control software using state proximity and merging. Hybrid Systems: Computation and Control, pages 344–357, 2008.

[110] Flavio Lerda, James Kapinski, Hitashyam Maka, Edmund M Clarke, and Bruce H Krogh. Model checking in-the-loop: Finding counterexamples by systematic simulation. In American Control Conference, 2008, pages 2734–2740. IEEE, 2008.

[111] Jan Lunze and Françoise Lamnabhi-Lagarrigue. Handbook of hybrid systems control: theory, tools, applications. Cambridge University Press, 2009.

[112] John Lygeros. Lecture notes on hybrid systems. In Notes for an ENSIETA workshop, 2004.

[113] Rupak Majumdar, Indranil Saha, KC Shashidhar, and Zilong Wang. Clse: Closed-loop symbolic execution. In NASA Formal Methods, pages 356–370. Springer, 2012.

[114] Oded Maler. A unified approach for studying discrete and continuous dynamical systems. In Decision and Control, 1998. Proceedings of the 37th IEEE Conference on, volume 2, pages 2083–2088. IEEE, 1998.

[115] Oded Maler. Algorithmic verification of continuous and hybrid systems. arXiv preprint arXiv:1403.0952, 2014.

[116] Oded Maler and Dejan Nickovic. Monitoring temporal properties of continuous signals. In Formal Techniques, Modelling and Analysis of Timed and Fault-Tolerant Systems, pages 152–166. Springer, 2004.

[117] Oded Maler, Dejan Nickovic, and Amir Pnueli. From mitl to timed automata. In International Conference on Formal Modeling and Analysis of Timed Systems, pages 274–289. Springer, 2006.

[118] Oded Maler, Dejan Nickovic, and Amir Pnueli. Checking temporal properties of discrete, timed and continuous behaviors. In Pillars of computer science, pages 475–505. Springer, 2008.

[119] Zohar Manna and Amir Pnueli. Temporal Verification of Reactive Systems: Safety. Springer, New York, 1995.

[120] James D. Meiss. Differential Dynamical Systems. SIAM publishers, 2007.

[121] Ian Mitchell and Claire J Tomlin. Level set methods for computation in hybrid systems. In Hybrid Systems: Computation and Control, pages 310–323. Springer, 2000.

[122] Ian M Mitchell, Alexandre M Bayen, and Claire J Tomlin. A time-dependent hamilton-jacobi formulation of reachable sets for continuous dynamic games. Automatic Control, IEEE Transactions on, 50(7):947–957, 2005.

[123] Sergio Mover, Alessandro Cimatti, Ashish Tiwari, and Stefano Tonetta. Time-aware relational abstractions for hybrid systems. In Embedded Software (EMSOFT), 2013 Proceedings of the International Conference on, pages 1–10. IEEE, 2013.

[124] Tadao Murata. Petri nets: Properties, analysis and applications. Proceedings of the IEEE, 77(4):541–580, 1989.

[125] Tarik Nahhal and Thao Dang. Test coverage for continuous and hybrid systems. In Computer Aided Verification, page 449–462, 2007.

[126] N. S. Nedialkov and M. von Mohrenschildt. Rigorous simulation of hybrid dynamic systems with symbolic and interval methods. In Proc. of ACC, pages 140–146. IEEE, 2002.

[127] Truong Nghiem, Sriram Sankaranarayanan, Georgios Fainekos, Franjo Ivancić, Aarti Gupta, and George J Pappas. Monte-carlo techniques for falsification of temporal properties of non-linear hybrid systems. In Proceedings of the 13th ACM international conference on Hybrid systems: computation and control, pages 211–220. ACM, 2010.

[128] Truong Nghiem, Sriram Sankaranarayanan, Georgios E. Fainekos, Franjo Ivančić, Aarti Gupta, and George J. Pappas. Monte-carlo techniques for falsification of temporal properties of non-linear hybrid systems. In Hybrid Systems: Computation and Control, pages 211–220. ACM Press, 2010.

[129] Sam Owre, Indranil Saha, and Natarajan Shankar. Automatic dimensional analysis of cyber-physical systems. In International Symposium on Formal Methods, pages 356–371. Springer, 2012.

[130] Corina S Păsăreanu, Matthew B Dwyer, and Michael Huth. Assume-guarantee model checking of software: A comparative case study. In International SPIN Workshop on Model Checking of Software, pages 168–183. Springer, 1999.

[131] Kevin M Passino, Stephen Yurkovich, and Michael Reinfrank. Fuzzy control, volume 42. Citeseer, 1998.

[132] Fabian Pedregosa, Gaël Varoquaux, Alexandre Gramfort, Vincent Michel, Bertrand Thirion, Olivier Grisel, Mathieu Blondel, Peter Prettenhofer, Ron Weiss, Vincent Dubourg, et al. Scikit-learn: Machine learning in python. Journal of Machine Learning Research, 12(Oct):2825–2830, 2011.

[133] James Lyle Peterson. Petri Net Theory and the Modeling of Systems. Prentice Hall, 1981.

[134] Erion Plaku, Lydia Kavraki, and Moshe Vardi. Falsification of LTL safety properties in hybrid systems. Proc. TACAS, page 368–382, 2009.

[135] André Platzer. Differential dynamic logic for hybrid systems. Journal of Automated Reasoning, 41(2):143–189, 2008.

[136] André Platzer. Logical analysis of hybrid systems: proving theorems for complex dynamics. Springer, 2010.

[137] André Platzer and Jan-David Quesel. Keymaera: A hybrid theorem prover for hybrid systems (system description). In Automated Reasoning, pages 171–178. Springer, 2008.

[138] Pavithra Prabhakar and Miriam Garcia Soto. Abstraction based model-checking of stability of hybrid systems. In International Conference on Computer Aided Verification, pages 280–295. Springer, 2013.

[139] Pavithra Prabhakar and Miriam García Soto. Counterexample guided abstraction refinement for stability analysis. In International Conference on Computer Aided Verification, pages 495–512. Springer, 2016.

[140] Stephen Prajna and Ali Jadbabaie. Safety verification of hybrid systems using barrier certificates. In Hybrid Systems: Computation and Control, pages 477–492. Springer, 2004.

[141] Stefan Ratschan and Zhikun She. Safety verification of hybrid systems by constraint propagation based abstraction refinement. In HSCC, volume 3414 of LNCS, pages 573–589. Springer, 2005.

[142] Stefan Ratschan and Zhikun She. Safety verification of hybrid systems by constraint propagation based abstraction refinement. In Hybrid Systems: Computation and Control, pages 573–589. Springer, 2005.

[143] Michal Rewienski and Jacob White. A trajectory piecewise-linear approach to model order reduction and fast simulation of nonlinear circuits and micromachined devices. IEEE Transactions on computer-aided design of integrated circuits and systems, 22(2):155–170, 2003.

[144] Julia Robinson. The collected works of Julia Robinson, volume 6. American Mathematical Soc., 1996.

[145] Hendrik Roehm, Jens Oehlerking, Matthias Woehrle, and Matthias Althoff. Reachset conformance testing of hybrid automata. In Proceedings of the 19th International Conference on Hybrid Systems: Computation and Control, pages 277–286. ACM, 2016.

[146] John Rushby, Patrick Lincoln, Sam Owre, Natrajan Shankar, and Ashish Tiwari. Symbolic analysis laboratory (sal). Cf. `http://www.csl.sri.com/projects/sal/`.

[147] Sriram Sankaranarayanan, Thao Dang, and Franjo Ivančić. Symbolic model checking of hybrid systems using template polyhedra. In TACAS, volume 4963 of LNCS, pages 188–202. Springer, 2008.

[148] Sriram Sankaranarayanan, Henny Sipma, and Zohar Manna. Constructing invariants for hybrid systems. Formal Methods in System Design, 32(1):25–55, 2008.

[149] Sriram Sankaranarayanan and Ashish Tiwari. Relational abstractions for continuous and hybrid systems. In CAV, volume 6806 of LNCS, pages 686–702. Springer, 2011.

[150] Wilhelmus HA Schilders, Henk A Van der Vorst, and Joost Rommes. Model order reduction: theory, research aspects and applications, volume 13. Springer, 2008.

[151] Joachim Schimpf and Kish Shen. Ecl i ps e–from lp to clp. Theory and Practice of Logic Programming, 12(1-2):127–156, 2012.

[152] Koushik Sen, Darko Marinov, and Gul Agha. CUTE: a concolic unit testing engine for C, volume 30. ACM, 2005.

[153] Josep Silva. A vocabulary of program slicing-based techniques. ACM computing surveys (CSUR), 44(3):12, 2012.

[154] Steven H. Strogatz. Nonlinear Dynamics And Chaos. Perseus Books Group, 1 edition, 1994.

[155] Frank Tip. A survey of program slicing techniques. Journal of programming languages, 3(3):121–189, 1995.

[156] Ashish Tiwari. Abstractions for hybrid systems. Formal Methods in Systems Design, 32:57–83, 2008.

[157] Ashish Tiwari. Hybridsal relational abstracter. In Computer Aided Verification, CAV'12, pages 725–731. Springer-Verlag, 2012.

[158] Arjan J Van Der Schaft and Johannes Maria Schumacher. An introduction to hybrid dynamical systems, volume 251. Springer London, 2000.

[159] Mark Weiser. Program slicing. In Proceedings of the 5th international conference on Software engineering, pages 439–449. IEEE Press, 1981.

[160] Jan C Willems. The behavioral approach to modeling and control of dynamical systems. In AICHE SYMPOSIUM SERIES, pages 97–108. New York; American Institute of Chemical Engineers; 1998, 2002.

[161] Jan C Willems and Jan W Polderman. Introduction to mathematical systems theory: a behavioral approach, volume 26. Springer Science & Business Media, 2013.

[162] Nicky Williams, Bruno Marre, Patricia Mouy, and Muriel Roger. Pathcrawler: Automatic generation of path tests by combining static and dynamic analysis. In Dependable Computing-EDCC 5, pages 281–292. Springer, 2005.

[163] Aditya Zutshi, Sriram Sankaranarayanan, Jyotirmoy V Deshmukh, and Xiaoqing Jin. Symbolic-numeric reachability analysis of closed-loop control software. In Proceedings of the 19th International Conference on Hybrid Systems: Computation and Control, pages 135–144. ACM, 2016.

[164] Aditya Zutshi, Sriram Sankaranarayanan, Jyotirmoy V Deshmukh, and James Kapinski. A trajectory splicing approach to concretizing counterexamples for hybrid systems. In IEEE Conf. on Decision and Control (CDC). IEEE Press, 2013.

[165] Aditya Zutshi, Sriram Sankaranarayanan, Jyotirmoy V Deshmukh, and James Kapinski. Multiple shooting, cegar-based falsification for hybrid systems. In Proceedings of the 14th International Conference on Embedded Software, page 5. ACM, 2014.

[166] Aditya Zutshi, Sriram Sankaranarayanan, and Ashish Tiwari. Timed relational abstractions for sampled data control systems. In Computer Aided Verification, pages 343–361. Springer, 2012.